REPORT DOCUMENTATION PAGE

Public reporting burden for this collection of information is estimated to average 1 hour per response, including the time for reviewing instructions, searching existing data sources, gathering and maintaining the data needed, and completing and reviewing the collection of information. Send comments regarding this burden estimate or any other aspect of this collection of information, including suggestions for reducing this burden, to Washington Headquarters Services, Directorate for Information Operations and Reports, 1215 Jefferson Davis Highway, Suite 1204, Arlington, VA 22202-4302, and to the Office of Management and Budget, Paperwork Reduction Project (0704-0188), Washington, DC 20503.

1. AGENCY USE ONLY (Leave blank)	2. REPORT DATE 6/18/97	3. REPORT TYPE AND DATES COVERED Final – 1/15/94–01/14/97

4. TITLE AND SUBTITLE

Film Cooling by A Pulsating Wall Jet

5. FUNDING NUMBERS

F49620-94-1-0131

AFOSR-TR-97
0357

6. AUTHOR(S)

Israel J. Wygnanski, Alfonso Ortega, and Hermann Fasel

7. PERFORMING ORGANIZATION NAME(S) AND ADDRESS(ES)

Department of Aerospace and Mechanical Engineering
The College of Engineering and Mines
The University of Arizona
Tucson, AZ 85721

8. PERFORMING ORGANIZATION REPORT NUMBER

9. SPONSORING/MONITORING AGENCY NAME(S) AND ADDRESS(ES)

AFOSR/
110 Duncan Avenue, Room B115
Bolling AFB, DC 20332-8080

N/A

10. SPONSORING/MONITORING AGENCY REPORT NUMBER

F49620-94-1-0131

11. SUPPLEMENTARY NOTES

12a. DISTRIBUTION/AVAILABILITY STATEMENT

Approved for Public Release
Distribution is Unlimited

12b. DISTRIBUTION CODE

13. ABSTRACT

This report summarizes the results of an experimental, numerical, and theoretical project that was initiated in 1994 with funding under AFOSR Contract Number F49620-94-1-0131. The objective of the work was to perform a fundamental exploration of the heat transfer and fluid mechanics in a wall jet with emphasis on applying passive techniques to control or manipulate the rates of heat transfer. After constructing the apparatus, developing the instrumentation, and developing the computer codes for the numerical simulation and the models for the theoretical investigations, we proceeded to study the effects of heating and cooling on the steady laminar wall jet. We examined the evolution of small-amplitude perturbations which were externally introduced into the flow. The amplitudes of the disturbances were significantly increased in the second stage of the investigation and their effect on the flow and temperature field was analyzed. The primary finding suggests that Reynolds analogy is not as universally applicable as we were lead to believe primarily when the mean velocity profile and the mean temperature profile are different or when the flow is periodic.

14. SUBJECT TERMS

15. NUMBER OF PAGES 135

16. PRICE CODE

17. SECURITY CLASSIFICATION OF REPORT	18. SECURITY CLASSIFICATION OF THIS PAGE	19. SECURITY CLASSIFICATION OF ABSTRACT	20. LIMITATION OF ABSTRACT
UNCLASSIFIED	UNCLASSIFIED	UNCLASSIFIED	UNLIMITED

NSN 7540-01-280-5500

Standard Form 298 (Rev. 2-89)
Prescribed by ANSI Std. Z39-18

FILM COOLING BY A PULSATING WALL JET
Experiments, Numerical Simulation, and Stability Theory

by

I. Wygnanski, A. Ortega, H. Fasel

FINAL REPORT

Department of Aerospace and Mechanical Engineering
The University of Arizona
Tucson, AZ 85721

June 1997   DTIC QUALITY INSPECTED 3

19971006 007

FILM COOLING BY A PULSATING WALL JET

Experiments, Numerical Simulation, and Stability theory

FINAL REPORT
AFOSR CONTRACT NO. F49620-94-1-1310

By
I. Wygnanski, A. Ortega, H. Fasel

Department of Aerospace and Mechanical Engineering
The University of Arizona
Tucson, AZ 85721

ABSTRACT

This report summarizes the results of an experimental, numerical, and theoretical project that was initiated in 1994 with funding under AFOSR Contract Number F49620-94-1-1310. A detailed description of the work performed is described in the appended manuscripts. The objective of the work was to perform a fundamental exploration of the heat transfer and fluid mechanics in a wall jet with emphasis on applying passive techniques to control or manipulate the rates of heat transfer. Previous explorations of the turbulent wall jet, under AFOSR sponsorship, showed that small amplitude forcing, at selected frequencies, could dramatically reduce the local time-mean skin friction. We embarked upon a study to determine if similar effects could be observed on the heat transfer. After constructing the apparatus, developing the instrumentatation, and developing the computer codes for the numerical simulation and the models for the theoretical investigations, we proceeded to study the effects of heating and cooling on the steady laminar wall jet. We examined the evolution of small- amplitude perturbations which were externally introduced into the flow. The amplitudes of the disturbances were significantly increased in the second stage of the investigation and their effect on the flow and temperature field was analyzed. Preliminary measurements in turbulent flow were also made and simple turbulence models predicting the mean base-flow were considered. The primary finding suggests that Reynolds analogy is not as universally applicable as we were lead to believe primarily when the mean velocity profile and the mean temperature profile are different or when the flow is periodic. Experiments indicate that perturbations in velocity and temperature are affected by the steady temperature differential across the flow. Thus, the mean velocity and temperature distributions as well as the temporal oscillations in both quantities are interdependent. The independence of the temperature and velocity field, so often assumed in solving convective heat transfer problems, appears to be the exception rather than the rule. Selective forcing of the flow at dominant modes produced profound effects on the velocity and temperature fields and hence on the time-averaged shear stress and heat transfer. Excitation of the inner (viscous) mode at an initial amplitude of 2% resulted in a *reduction* of the maximum skin friction by as much as 65% and in a concomitant *increase* in the maximum wall heat flux of 45%. The ability to control the transport rates by exploiting the instabilities of the strong laminar wall jet were demonstrated as well as the strong coupling existing between the temperature gradient and velocity gradients.

TABLE OF CONTENTS

1. INTRODUCTION

By turning on the defroster in our car and directing the flow to the interior of the windshield we activate a most common yet profound convective heat transfer process. The flow along the windshield is a jet which adheres to the surface and is thus referred to as a wall-jet. It transmits heat to the surface in some applications (the windshield defroster) and it provides cooling and protection in others (film cooling on turbine blades or on quartz windows in high speed vehicles or warheads). Wall jets occur extensively in boundary layer control applications such as slotted flaps or blown flaps and they possess a peculiar tendency of adhering to highly convex surfaces, such as a circular cylinder, and turning around them and changing their direction in the process (the Coanda effect). It was therefore quite a surprise to discover that such a practically relevant flow is not well understood even under isothermal conditions.

A wall jet represents a source of momentum and a source (or a sink) of heat irrespective of the manner in which it originated. It may be embedded in a decelerating or accelerating external stream as in flaps or turbine-blades. The upstream flow may be steady and uniform or a highly agitated, thick, turbulent boundary layer. It may originate from a slot (a line source) or from series of holes inclined to the wall. The surface itself might be smooth and carefully machined, as it is in aeronautical applications, or highly corrugated and rough as it occurs in electronic cooling applications. All these factors add to the complexity of the flow which, in most engineering applications, is highly turbulent. Out of the broad spectrum of eddies contained in such flows, the largest ones are coherent and responsible for most of the cross stream transport of either mass, momentum, or heat. Understanding the genesis and evolution of these eddies may lead to improvements in the design criteria which use the wall jet for controlling the cross-flow transport processes.

We realized long ago that most of the mass and momentum transport across the wall jet (i.e. the entrainment of the ambient fluid) is controlled by the coherent structures which, in turn may be manipulated and modified by external excitation. This is so because the large coherent structures in fully turbulent shear flows (such as the wall-jet, the wake, and the mixing layer) were identified as being the predominant instability modes of these flows. Thus a small external perturbation, which naturally destabilizes the flow may yield a large effect on the entire flow field. This was used very effectively to delay the "stall" of airfoils and to enhance the maximum

lift generated by them (Seifert èt al 1993, 1996). Since the large, coherent eddies also transport heat and mass (in heat transfer and chemical reaction applications) they can be manipulated to alter either of those processes. The findings of this research will allow investigations of the relationship between the large eddies and of the scalar transport and the possibility of altering the heat transfer from the surface regardless of whether it is heated or cooled by the flow.

2. BRIEF BACKGROUND AND LITERATURE REVIEW

In a steady laminar boundary layer there is a precise relation between the skin friction $C_f = \dfrac{\tau_w}{\frac{1}{2}\rho U_\infty^2}$, the Reynolds Number $Re = \dfrac{U_\infty l}{v}$ and the Nusselt number describing the convective heat transfer from the surface:

$$Nu = \tfrac{1}{2} C_f R_e f(x/l, P_r)$$

where $f(x/l, P_r)$ is a universal function representing the distance from some predetermined origin and $Pr = v/a$, is the Prandtl number representing the ratio of viscosity to thermal diffusivity. This equation, was derived by Reynolds and established the first link between skin friction and thermal convection. It eventually evolved into one of the cornerstones of turbulent convective heat transfer, commonly referred to as the **Reynolds analogy,** which relates forced convection of heat with the momentum exchange occurring across a turbulent shear flow. It takes advantage of the similarity between the mean energy and the mean momentum equations in a turbulent, compressible boundary layer. Since neither equation can be solved (the turbulent closure problem for time-averaged equations of motion), models have to be proposed and the simplest ones make the turbulent shear stress proportional to the mean velocity gradient. The proportionality constant is often called the "eddy viscosity" or the eddy diffusivity for momentum, ε_m. This definition is expressed by:

$$\overline{u'v'} = -\varepsilon_m \frac{\partial \bar{u}}{\partial y}$$

Similarly, the thermal eddy diffusivity, ε_H, is related to the heat flux by:

$$\overline{v't'} = \varepsilon_H \frac{\partial \bar{t}}{\partial y}$$

4

The ratio of these two quantities defines the turbulent Prandtl number:

$$\Pr_t = \frac{\varepsilon_m}{\varepsilon_H} = \frac{\overline{u'v'}\,\dfrac{\partial \bar{t}}{\partial y}}{\overline{v't'}\,\dfrac{\partial \bar{u}}{\partial y}}$$

and Reynolds analogy suggests that the fluxes of heat and momentum in turbulent, or in time dependent flows are identical, i.e. that:

$$\varepsilon_m = \varepsilon_H \quad \text{or} \quad \Pr_t = 1$$

The approximate validity of the analogy is supported by a large body of experimental results obtained in the canonical turbulent shear flows. In the turbulent boundary layer, for instance [Kays and Crawford, 1993], $\Pr_t$ is approximately constant of order unity in the logarithmic region of the flow. In the viscous sublayer, which is notoriously unsteady, the turbulent Prandtl number, is generally larger.

When significant reductions in the skin friction were observed in the periodically excited wall jet (Katz, Horev and Wygnanski, 1991) one could anticipate a corresponding reduction in heat transfer or a definite proof of failure of a long surviving concept--the Reynolds analogy. The exploration of either possibility was a key objective of the present study.

Very few experiments determined the heat transfer resulting from a wall-jet blowing over a surface and none explored the applicability of Reynolds analogy. Myers et al. (1963) and Nagano and Tagawa (1987) investigated heat transfer from two-dimensional wall jets while MacArthur (1986) studied the heat transfer resulting from an impinging circular wall jet. Quasi-steady heat and momentum transfer coefficients were assumed although the flow investigated was highly turbulent and the heat transfer coefficient and adiabatic wall temperature were solely dependent on the jet fluid dynamics. Recent work in an unforced turbulent wall jet, Holmberg and Pestian (1996), involving simultaneous measurement of the fluctuating velocities, $<u'>$ and $<v'>$, and temperature $<t'>$, along with instantaneous wall heat flux, $<q'>$, showed that in the presence of high free stream turbulence, the wall heat flux is largely controlled by the penetration of large scale eddies deep into the boundary layer. This was evidenced by the strong coherence

of the fluctuating wall heat flux and the fluctuating streamwise component, $<u'>$. It was suggested therefore that Stanton number, both mean and fluctuating, is more appropriately scaled with the fluctuating velocity field than with any mean flow descriptor such as jet Reynolds number.

Work on heat transfer due to a pulsating wall-jet or a pulsating free-jet injected into a steady, infinite stream is even more scarce. Indeed, knowledge of heat transfer in the presence of oscillating or unsteady mean flows is meager. There has been a good deal of interest recently in pulsed combustion and the unsteady heat transfer problem that arises in the combustor tailpipe, as described by Arpaci et al. (1992), and in pulsating impinging jets. The data and analysis for pulsating turbulent pipe flows elucidate some of these issues. Many attempts have been made to model heat transfer in oscillatory flows by use of steady or quasi-steady assumptions in which the flow at any instant in time is assumed to behave as if it were steady at the instantaneous velocity. Obviously, such crude models would only apply to the lowest range of pulsation frequencies. If one applies the steady heat transfer correlation instantaneously and integrates over a cycle to obtain a cycle-averaged heat transfer coefficient, one obtains a modification of the steady correlation that predicts enhancement of the heat transfer coefficient, independent of frequency (Hanby, 1969).

Dec and Keller (1990) refuted the applicability of the Reynolds analogy for unsteady flows in pipes based on the dissimilarity of the momentum and thermal boundary conditions in the oscillating flow. Arpaci et al. (1992) developed a simple model assuming that Kolmogorov's microscales for velocity fluctuations and temperature fluctuations are identical. The few experimental data available corroborate Arpaci's model reasonably well over a fair range of amplitudes and frequencies. However, there are too few detailed measurements of temperature and velocity to provide insight into the convective mechanisms. For example, the empirical constants used, are derived from a simple curve-fitting to the data, an unsatisfactory approach. A main result of the model suggests that the heat transfer coefficient is always enhanced above its steady value.

It is clear, from examination of the sparse results available in the literature, that the detailed mechanisms controlling the transport of thermal energy to or from a surface in an unsteady flow are not well understood. There was conflicting evidence as to the applicability of

6

the Reynolds analogy and there is no known attempt to control film cooling by periodic forcing. The reduction in skin friction in the pulsating wall jet indicated the possibility that the convective heat transfer may be similarly controlled in this class of flows. It seemed apparent that either enhancement or degradation of heat transfer is a likely outcome of forcing the wall-jet and that its regime may depend on the frequency and amplitude of the pulsations. In either case, the possibility of dramatically altering the steady flow behavior, perhaps with minimum energy expenditure, has important fundamental and technological applications.

3. WORK PERFORMED AND HIGHLIGHTS OF THE PROGRESS MADE WITH AFOSR FUNDING

3.1 Experimental and Theoretical

We were committed to examine the problem experimentally, theoretically, and numerically and we made some interesting observations in all three categories of the investigation. Since a few journal articles (in various stages of completion) are provided in the appendix, only some highlights of the investigation are provided in the following sections. It is evident that the task undertaken is very ambitious and it could not have been completed during the initial three years.

The first article describes the linear stability properties of the laminar wall jet with heat transfer. For this purpose the mean flow had to be predicted first and the prediction compared with experiment. The self-similar velocity and temperature distributions across the flow were calculated for a variety of Prandtl numbers (to allow for different origins of heat and momentum) and a characteristic non-dimensional temperature difference. It was shown that the non-dimensional velocity and temperature profiles differ only slightly from the Glauert's solution even when the physical properties of the gas are not constant and the representative temperature difference is large (fig. 1a). When the scales chosen to normalize these distributions were compared to those used for isothermal flow, the differences became apparent, indicating that a hot surface enhances the lateral rate of spread of the wall jet for a prescribed momentum loss. The effect of the unheated starting length was also addressed by using an artificial Prandtl number that describes the ratio between the thermal and the hydrodynamic boundary layer thicknesses.

7

Three sets of experiments were carried out, corresponding to three different values of wall temperature: cooling with $\Theta = -0.0174$, heating with $\Theta = 0.0275$ and the neutral case in which the wall-jet, the surface and free stream temperatures are identical (the Glauert case). The non-dimensional temperature is defined as: $\Theta = (T_w - T_0)/T_0$. Throughout the experiments, the jet exit Reynolds number was maintained constant. The normalized mean profiles of the streamwise velocity measured for the three cases mentioned are shown in figure 2. Full velocity profiles for all cases are plotted above, while the inner region is shown in more detail for the cooling, Glauert, and heating cases respectively. The symbols represent the experiments while the solid line corresponds to the theoretical prediction. The agreement between the experiments and the theory is good except in the inner region where the velocity gradient of the experimental data is higher due to the relatively high turbulence level of 0.5% associated with the present apparatus. As can be seen, when cooling is applied, the inner velocity gradient is the highest and the maximum velocity is shifted closer to the surface, while the heated flow has opposite trend. This result is in agreement with the theoretical predictions. It is important to note that the wall temperature, at these low levels, has a mild affect on the velocity but a potentially large effect on the stability of the flow.

The streamwise development of the hydrodynamic and the thermal boundary layers is plotted in figure 3, where δ_t is defined as the distance from the wall to the place where the normalized temperature is also equal to 0.5. Figure 3a presents the dimensional form, while figure 3b displays the boundary layer thickness normalized by the first measurement point. As can be seen from figure 3a, the hydrodynamic boundary layer thickness is not affected by heating or cooling while the thermal one is. On the other hand, the wall boundary condition affects somewhat the rate of growth of the hydrodynamic thickness while it has no effect on the thermal one (fig. 3b). The thermal entry length affects the growth rate of the thermal boundary layer which is greater than the hydrodynamic boundary layer (fig. 3b).

The stability characteristics of the laminar wall jet flowing over cold or hot surfaces were computed and compared with experiment. Initial computations encompassed a much larger range of temperature difference than was actually measured to date in order to assess the various effects of the temperature gradient on the stability of the flow. The calculated curves representing the

neutral stability ($\alpha_i = 0$) for different values of the dimensionless temperature $\Theta = (T_w - T_0)/T_0$ are shown in figure 4a & b. At low Re there is one unstable solution which at high values of ω (i.e. near the upper branch of the neutral stability diagram) possesses a maximum amplitude of the streamwise velocity component, $\tilde{u}|_{max}$, near the surface (curve A) and is thus dominated by the conditions near the wall. The instabilities near the lower branch of the neutral stability curve are dominated by the inflection point in the outer part of the velocity profile and have their maximum amplitude in that region (B). Both amplitude distributions (A & B) are affected by viscosity due to the no-slip conditions at the surface. A cool surface has a stronger effect on the upper branch of the neutral stability diagram than a hot surface. The cool surface dampens most of the high frequency perturbations while the hot surface destabilizes them. Cooling has little effect on the critical Re which remains around $Re_{crit} \approx 60$ provided $\Theta \geq -0.2$. Heating has no effect whatsoever.

At high Reynolds numbers (e.g. $Re > 430$ for $\Theta = 0$), the wall-jet possesses two, distinctly different unstable regions which are overlapping in the mid-range of the unstable frequencies. The region of overlap depends mostly on Re but it is also dependent on the temperature of the surface; a cold surface shifts the region of overlap towards higher values of ω. Even in the region of overlap the sensitivity of each mode to viscosity (i.e. mainly to the "no slip" boundary condition at the surface) differs. The two amplitude distributions of the streamwise perturbations across the flow (corresponding to point C in figure 4a) reflect the dependence of the two modes on viscosity. The outer mode, C_{out}, which is mostly inviscid, contains a secondary peak in amplitude close to the wall while the inner mode, C_{in}, contains a secondary peak close to the inflection point. There is also a disparity in scales between the two modes because each one propagates at its characteristic phase-velocity. The second, independently unstable mode, starts at $Re_{crit.II} \approx 440$ for all $\Theta > -0.2$. Reducing the relative temperature of the plate below $\Theta = -0.2$ makes the inner layer even more stable and increases $Re_{crit.II}$ further. Consequently cooling between $0 > \Theta \geq -0.2$ increases only the frequency corresponding to $Re_{crit.II}$. At $Re < Re_{crit.II}$, there is an inner stable region which is completely contained within the unstable zone provided $\Theta > -0.175$. The size of this region in the Re-ω plane increases with decreasing Θ and for $\Theta < -0.175$ it joins with the stable zone existing above the upper branch of the main neutral curve. The existence of a small, stable, inner-region in the isothermal wall jet was reported previously by several authors (Chun & Schwarz, 1967, Tsuji et al 1977, Mele et al 1986, and Zhou et al. 1992),

and it is marked by a shaded zone on Fig. 4a. The larger neutral zones caused by cooling are represented by hatched areas in figure 4a. The separation of the two modes at $\Theta < -0.175$ in the vicinity of $\omega = 1$ and Re=230 becomes thus clear.

The neutral stability diagrams for the flow over a heated wall (fig. 4b) are similar to the ones in the isothermal case except that the upper branches of the outer, neutrally stable modes are shifted toward higher frequency while the lower branches are unaffected. The broadening of the unstable region to higher frequencies at moderately low Re implies that heating destabilizes the wall layer without affecting the outer flow. In this aspect the wall jet behaves like a heated laminar boundary layer in air. The first critical Reynolds number is not altered by the heating because it is dominated by the inviscid mode, but $Re_{crit.II}$ shifts towards higher values of *Re and lower* ω with increasing Θ.

The measured amplitude distributions of velocity and temperature agree well with the linear prediction when the imposed excitation amplitude is small (e.g. 0.3%). The relative significance of the inner and outer modes is apparent in figure 5 when the imposed frequency was doubled and the measurements of the fluctuating velocity were made at the same distance from the nozzle. The amplitude distribution of the temperature fluctuations measured with a cold wire are shown in figure 6. The appearance of an inflection point in the inner region is consistent with the inflection point in the mean temperature profile and is due to the evolution of non-linear mechanisms such as the counter-rotating vorticies mentioned earlier. The amplitude of the phase-locked, normal fluctuations $<v'>$ could not be measured in the inner region of the jet because of probe resolution problems, however it can be calculated from $<u'>$ by using continuity and assuming that the coherent fluctuations are two-dimensional.

High amplitude excitation at low frequency affects the rate of spread of the laminar wall jet but does not distort the shape of the mean velocity profile. High frequency forcing at similar amplitudes results in a broader inner region and distorts the form of the velocity profile. It thus affects the mean gradient of the velocity at the surface (fig. 7) resulting in a reduction in skin friction C_f. A 1% amplitude perturbation may reduce the skin friction by 35% at x/d=20 provided the oscillations trigger the inner mode of instability. A similar amplitude of excitation at lower frequency, triggering the outer mode of instability only, generates a much smaller reduction in C_f amounting to 7% only. ***The 35% reduction in C_f was accompanied by a 25% increase in***

the heat flux from the wall irrespective of the sign of the temperature gradient, i.e. for both heating or cooling the wall. This is observed in figure 8. The total heat flux from the surface and the total skin friction with the surface were computed for various amplitudes and frequencies of forcing (fig. 9) and the oscillations always reduced the drag while increasing the heat flux. Higher amplitudes of forcing distort the mean temperature profile (fig. 10) while only increasing the rate of spread of the mean velocity field (fig. 11). The distortion in the mean temperature is due to the dominance of the coherent eddies which augment the unsteady temperature field and hence the scalar transport as evidenced by the distortion in $<t'>$ shown in figure 6. A similar observation was made in a mixing layer generated between two streams of different temperature and velocity which was excited by fairly high amplitude oscillations. There are many additional observations to be made from the present data and are discussed in detail in the manuscripts, but the primary finding suggests that *Reynolds analogy does not apply when the mean velocity profile and the mean temperature profile are different. Secondly, there is no reason to believe that the analogy holds in the time mean of an unsteady flow such as the forced wall jet.*

Experiments in the laminar flow indicated that even small, finite amplitude perturbations in velocity and in temperature are affected by the steady temperature differential across the flow. Thus, the mean velocity and temperature distributions as well as the temporal oscillations in both quantities are *interdependent.* The independence of the temperature and velocity field, which is often assumed in solving convective heat transfer problems, appears to be the exception rather than the rule. The effects of heating or cooling the surface are first and foremost felt in the inner layer where the wall jet is sensitive to the high frequency, periodic perturbations. In most instances, heating the surface in air destabilizes the region near the wall while cooling stabilizes it. However, since the first critical Reynolds number is determined by the instability of the outer region, only the flow at very low Reynolds numbers is insensitive to the temperature differential prevailing across the jet.

Linear stability theory is used to chart the leading non linear interactions causing further amplification of disturbances and generating new ones. This can also provide the basis for secondary instabilities and resonant interactions between plane and oblique waves (Craik, 1971) or between different plane waves. We investigated the possible effect of Θ on the plane, inter modal resonance mechanism and thus far, proved its existence experimentally for $\Theta = 0$ (see

appendix). This enabled energy to be extracted from the mean flow to the three coherent waves involved in the triad resonance resulting in a concomitant loss of normalized, mean momentum in the jet but hardly an increase in its displacement thickness.

3.2 Computational

In parallel to the experimental and theoretical investigations, numerical simulations were performed based on the complete Navier-Stokes equations. Towards this end, computer codes had to be developed first. For developing these codes we could rely on Navier-Stokes Codes that we had developed for investigating transition in boundary layers, both for compressible and incompressible flows. Both codes had to be modified and adapted to the wall geometry. This task was more involved than originally anticipated, especially for the compressible code. However, modification and adaptation of the codes is fully completed. Both codes (compressible and incompressible) were also extensively tested by comparison calculations with linear stability theory. These calculations showed that the codes are efficient and reliable. We are convinced that simulations using these codes will be very valuable for understanding the dynamical phenomena observed in experiments. In particular, the simulations with these codes will be an indispensable tool for uncovering the nonlinear mechanisms, as our numerical model does not impose any restriction on the amplitude of the perturbations. In the following, a few typical results from the numerical simulations will be presented.

In the compressible simulations, the complete Navier-Stokes equations, the energy equation, and the continuity equation are solved in conservative formulation. The fluid is modeled as a calorically perfect gas and Sutherlands Law is used to calculate the viscosity from the temperature. The time integration is performed using a 4th-order Runge-Kutta method, for the spatial discretization a 4th order upwind-downwind "splitting" scheme is used. For the results shown here, an equidistant grid in the x- and y-direction was used. In the spanwise direction, a pseudo-spectral approach was chosen.

A sketch of the integration domain is shown in figure 12. Disturbances are introduced into the flow field by periodic blowing and suction through a slot (fig. 12) near the inflow boundary. For this forcing, the stream wise distribution of the disturbance velocity is such that the net mass flux is zero, therefore, vorticity disturbances of a specified frequency are predominantly introduced. For calculating the base flow, the similarity solution for the

12

appropriate nondimensional temperature difference between wall and ambient, Θ, is used as initial condition. Using pseudo-time stepping, the calculation is continued until a given convergence criterion is satisfied. Using these base flows, numerous unsteady simulations were performed for an isothermal and cooled wall jet. All calculations were done for a global Mach number of M=0.3, based on the maximum velocity at the inflow and the speed of sound in the ambient fluid. This Mach number allows for reasonably large time steps and ensures that compressibility effects are still negligible. This is shown in figure 13, where the neutral curves (as obtained form Linear Stability Theory) of the isothermal wall jet are plotted for the incompressible case and for the compressible case at M=0.3.

The results of one validation run are shown in figure 14. The graph shows a comparison of the maximum u-velocity amplitudes as a function of downstream location for the isothermal case. The stream wise locations shown cover the region close to the second branch of the neutral curve of the boundary layer mode (inner mode). The agreement between the compressible and incompressible simulations, which are described in detail later in this report, is excellent. However, there is a slight deviation from the results obtained from Linear Stability Theory. This difference is due to the fact that Linear Stability Theory can only take local effects into account, whereas our simulations follow the development of the disturbances downstream of the blowing and suction slot. In this particular case, the slot was located upstream of the unstable region of the shear layer mode (outer mode), so that this mode was amplified first. Although it is damped in the region shown, it still has a certain amplitude and it takes some downstream distance until its influence on the velocity maximum is negligible compared to the boundary layer mode. From this point on, the agreement of the results from the numerical simulations and Linear Stability Theory is excellent.

We also performed small amplitude (linear) and large amplitude (nonlinear) calculations for a case with strong wall cooling (Θ =-0.1). The comparison of the results for the small amplitude case with results from Linear Stability Theory shows very good agreement (verified by comparison of the location of the neutral points, fig. 15). Disturbing the flow with large amplitude perturbations (~200 times larger than for the linear calculations), we observed a shift of the mean flow maximum away from the wall, accompanied by a decrease in wall shear. Figure 16 shows a

13

comparison of the mean flow profiles with and without disturbances. These results are in good qualitative agreement with our experimental findings.

For a detailed comparison with the ongoing laboratory experiments, a new set of simulations was started for the case with weak wall cooling ($\Theta = -0.0174$). The calculated temperature base flow profiles showed a significant difference from the temperature profiles found in the experiments, where the thermal "boundary layer" thickness was much smaller in the experiments. We were able to attribute this phenomenon to the effects of the unheated starting length in the experimental apparatus. To account for the unheated starting length in the calculations, the concept of the effective or artificial Prandtl number, discussed earlier in this report, was utilized and we were able to obtain very good agreement of the experimental and computational mean flow profiles. Using a base flow calculated with this Prandtl number, calculations with small amplitude disturbances were performed. The u-velocity, v-velocity, and temperature eigenfunctions from the numerical simulations are in good agreement with the results obtained from Linear Stability Theory (fig. 17). Calculations with nonlinear disturbance levels are currently under way.

In addition to the calculations with the compressible code we carried out numerous simulations using the incompressible code to explore in detail the nonlinear phenomena seen in the experiments for the isothermal wall jet. In these incompressible simulations the incompressible vorticity transport equations and velocity Poisson equations are solved in disturbance flow formulation. As a baseflow, Glauert's similarity solution was chosen. Within our integration domain disturbance flow computations using Glauert's similarity solution as a baseflow gave virtually the same result as computations using a baseflow that satisfies the Navier-Stokes equations exactly. In the disturbance flow calculations the wall jet was periodically forced by blowing and suction through a slot in the wall close to the inflow boundary in the same manner as in the compressible calculations.

When forced with large amplitudes we observed a distortion of the meanflow that results in an increased spreading rate of the wall jet, a decreased velocity maximum, and a decreased wall shear stress. This meanflow distortion can be directly attributed to nonlinear interactions of the fundamental disturbance with itself. Figure 18 shows at one streamwise location the percentile decrease of the meanflow velocity maximum, the increase of its wall-normal location, and the

decrease of the wall shear stress over the fundamental Fourier amplitude of the local streamwise disturbance velocity. As expected for nonlinear interactions of sinusoidal traveling waves, an increase of the local streamwise disturbance velocity by one order of magnitude results in a change of the meanflow distortion by two orders of magnitude. Our DNS results are in good agreement with experiments for a forced transitional wall jet by Zhou and Wygnanski in 1993.

From our simulations we found a second important nonlinear phenomenon: a two-dimensional subharmonic resonance that occurs for large amplitude forcing (two-dimensional secondary instability). A manifestation of this subharmonic resonance is an apparent merging of subsequent vorticity concentrations ("vortex pairing") within the traveling disturbance waves which has been observed in experiments by Bajura and Catalano in 1975 and recently also by Amitay in 1994. In our numerical simulations, the subharmonic resonance led to a surprising phenomenon during the startup of the computations: the ejection of mushroom shaped vortices. Detailed results of these simulations are presented in the enclosed paper "Numerical Simulation of Wall Jets", that will be presented at the 3rd International Symposium on Engineering Turbulence Modeling and Measurements in May 1996 in Greece.

In addition to the two-dimensional subharmonic resonance, three-dimensional resonances can occur during the transition process, similar to the secondary instability of a flat plate boundary layer. For our three-dimensional simulations of this boundary layer type secondary instability, we forced the flow by small amplitude blowing and suction with the first spanwise mode in addition to the large amplitude two-dimensional blowing and suction. This results in a slight spanwise modulation of the blowing and suction velocity that generates pairs of small oblique disturbance waves in addition to the large two-dimensional disturbance wave. Until now, we have investigated two types of secondary instability, fundamental resonance and subharmonic resonance. Figure 19, for example, shows results for the case of a fundamental resonance where the flow was disturbed by two-dimensional blowing and suction at a large amplitude with a small spanwise modulation of the same frequency. Shown are iso-surfaces of spanwise vorticity over two spanwise wavelengths. For the leftportion of the plot (when looking in streamwise direction) the top layer of negative vorticity has been removed to expose the layer of positive vorticity below. The flow develops in streamwise direction from a purely two-dimensional to a strongly three-dimensional behavior. A strong steady streamwise structure can be observed in the outer

region that is periodic in spanwise direction. This structure is associated with Fourier mode [0,1][1] and is characteristic for fundamental resonance. For the subharmonic resonance shown in figure 20, small three-dimensional (oblique) disturbances at half the frequency of the large two-dimensional disturbance are introduced. Our calculations have shown that subharmonic resonance occurs at lower amplitudes than fundamental resonance. At this lower amplitude level, Fourier mode [0,1] and the associated longitudinal vortices are not yet generated by the subharmonic resonance. Rather, we observe staggered three-dimensional structures. While maximum amplification for the fundamental resonance occurs when streamwise and spanwise wave numbers are about equal, maximum amplification for the subharmonic resonance occurs when the streamwise wave number is approximately twice the spanwise wave number. Our simulations (so far with up to 10 spanwise modes) indicate that three-dimensional subharmonic resonance is a very likely mechanism to induce transition.

In the experiments by Amitay 1994 at lower Reynolds numbers the transition process was dominated by a series of "vortex pairings" with the ejection of mushroom shaped vortices. However, at higher Reynolds numbers this phenomenon was not observed. Further investigations are planned to determine if and how the shear layer-type two-dimensional subharmonic resonance competes with the boundary layer-type three-dimensional subharmonic resonance and how the competition can be exploited to modify the mean flow. Currently, we are also working on the implementation of the energy equation in the incompressible code. This will give us, in conjunction with the compressible code, the unique opportunity to have two independent codes for investigating the effects of temperature on the stability of the wall jet, for both the linear, but more importantly for the nonlinear regime.

For investigations of turbulent wall jets, we are developing codes for compressible and incompressible Large Eddy Simulations (LES). The incompressible code is currently being tested for the calculation of transitional and turbulent flat plate boundary layers with zero and strong adverse pressure gradients. The flat plate geometry was chosen because of the wealth of comparison data available. To initialize the turbulent flow, disturbances with large amplitudes are used to initiate rapid transition. In the transitional regime, the turbulence model is turned on using

---

[1] In this notation, the first index refers to periodicity in time (here "0" means steady), the second index refers to the periodicity in spanwise directino (here "1" means first spanwise mode).

a spectral ramping function. This approach is based on the energy transfer to the higher spanwise Fourier modes during transition, which corresponds to the increasingly three-dimensional structure of the boundary layer in the transition region. This model has the great advantage of being independent of the actual flow geometry and turbulence production mechanisms (wall versus shear layer for the wall jet application). We are confident that this model can be used with only minor modifications for the investigations of the turbulent wall jet.

The compressible LES code is currently being tested for subsonic and supersonic transitional flat plate boundary layers. In this code, the subgrid-scale model is turned on in the transitional region using a criterion based on the momentum thickness of the boundary layer. We will, however, implement the spectral ramping function after the code has been validated successfully.

4. ADDITIONAL RESEARCH CARRIED OUT THAT IS RELEVANT TO PROJECT

4.1 Experimental

Detailed experiments were completed on the forced laminar wall jet as pointed out in the appendix, (Quintana et al, 1996). Of particular interest is the unsteady heat flux, $<v't'>$, and the "turbulent" Prandtl number for all the forced cases considered.

In the laminar wall jet, attention was focused primarily on the effects of temperature gradient and of forcing on the heat transfer from the wall. In the film-cooling problem however, the control of heat transfer is related not only to the wall temperature and gradient but also to the temperature of the wall-jet in relation to the temperature of the freestream. The mixing or dilution of the jet by entrainment of the freestream fluid has been traditionally characterized by the film cooling effectiveness. In future work we would like to propose a study of the three temperature problem in the strong laminar wall jet. We plant to heat or cool the jet fluid above or below the ambient fluid, and will also replace the isothermal wall with an adiabatic wall instrumented for surface temperature. By heating or cooling the entire jet, the temperature gradient spans the entire shear-flow rather than the thin region near wall and therefore, the effects of temperature on the stability of the jet will not be confined to the wall region only. By heating or cooling the jet, the mean and fluctuating temperatures and velocities, will provide evidence of

the entrainment and mixing of outer freestream fluid with the wall jet fluid. By appropriate forcing of the laminar jet at either inner or outer modes, we plant to explore the interaction of the outer shear layer with the wall region and its manifestation in the distribution of the wall temperature.

In another investigation aimed at the understanding of separation and its control, we have simulated the flow downstream of a slotted flap by considering a "weak" wall jet embedded in an external stream. Velocity ratios (U_{jet} / U_{main} from 1.1 to 1.7 were considered. A wall jet is considered "weak" when there is a velocity minimum in the mean velocity profile in the upstream region (figs. 21,22). It may occur when the jet momentum is low or when the momentum deficit in the upstream boundary layer is large. In the first case, the flow developed into a strong wall jet type profile after the velocity minimum disappeared (fig. 21) while in the second case the flow directly developed into a boundary layer type profile after the velocity minimum disappeared (fig. 22). From our experience, whenever the ratio of the momentum deficit in the upstream boundary layer to the momentum injected by the wall jet is less than 0.035 (i.e. $U_{\infty}^2 \theta / J < 0.035$), one may collapse all the velocity profiles onto a single curve provided one uses two velocity scales and two length scales (figure 23a). This was shown previously for the strong wall jet in an external stream (Zhou and Wygnanski, 1993). Three length and velocity scales are needed to collapse the data containing a velocity minimum in the flow (figure 23b). Thus it appears that one may scale the wall jet properly provided the number of length and velocity scales used is identical to the number of vortical layers in the velocity profile. The coupling of the vortical layers with temperature gradients is an important ingredient in film cooling configurations where the cold jet intended to protect a surface is injected tangentially to it and is embedded in a thick external boundary layer. Needless to say, such a flow is indeed very complex but the similarity approximation exposed in figure 23 may make it more tractable for theoretical analysis and numerical computation. This combined experimental, theoretical, and computational approach has already enabled us to make substantial inroads in understanding the laminar wall jet and the complex process of separation.

External excitation may affect different layers in the weak wall jet differently (figure 24). Our previous work suggested that there are three instability modes and two of them are closely coupled. Their length scales, velocity scales and consequently the instability frequencies are very

close to each other. For example, forcing the jet at 104 Hz excites mostly the innermost wall layer, while switching to 75Hz, the middle and the outer instability modes are excited. One may observe the differences from the phase locked, amplitude distributions across the jet (fig. 24). Skin friction reductions of up to 30% were observed due to forcing at 104Hz up to 30 slot widths downstream of the slot (fig. 25). The present work aims to expand this work to investigate the effects of temperature and the possibility of controlling heat transfer and adiabatic effectiveness for this basic flow.

4.2 Computational

Numerical investigations are currently focusing on the effects of heating and cooling on the nonlinear, two- and three-dimensional stages of the transition process for transitional strong wall jets. Selected phenomena, found to be relevant in the incompressible calculations, are under investigation. These include, for example, the distortion of the u-velocity profile for large amplitude forcing due to the nonlinear interaction of the disturbance waves. These calculations will also clarify the importance of the unheated starting length on the later stages of transition. In close cooperation with the experimental work, the reasons for the changes in wall shear stress and wall heat flux, observed when the flow is disturbed using large amplitude waves are under investigation. The effect of the unheated starting length was included in the simulations by using an artificial Prandtl number. This strategy does not take the effect of the sudden change of the wall temperature into account. Therefore, we are also performing calculations where the wall temperature is changed within the integration domain (simulating the start of the cooling surface as in the laboratory set-up). Possible receptivity mechanisms can be found which may help to understand phenomena in the experimental results that are not yet understood. Another phenomenon already investigated in detail for the isothermal case is the ejection of mushroom shaped vortices. This rapid momentum and energy transfer away from the wall, and particularly the feasibility of exploiting this phenomenon for wall cooling by directly triggering such vortices will be investigated.

The implementation of the energy equation in the incompressible code is being completed. This will enable us to clearly separate the effects of compressibility on the stability of the wall jet. Concurrently, the stability investigation of the turbulent wall jet will be initiated. Towards this end, both the incompressible and the compressible LES codes were adapted to the

19

wall jet geometry and Large Eddy Simulations are being performed for the isothermal and cooled cases (without free-stream). Calculations will be carried out for both linear as well as nonlinear disturbance amplitude levels. Building on the understanding gained from our isothermal, incompressible calculations (both linear stability theory and Navier-Stokes simulations), investigations of the two frequency resonance mechanisms were be initiated. This will provide insight that is currently not obtainable from either the theoretical or the experimental work, especially with regard to the possible improvement of the heat transfer from the wall to the fluid. Since wall heating or cooling significantly changes the phase velocity of the disturbances, it is possible that a considerable influence on the resonance condition exists.

5. REFERENCES

Arpaci, V. S., Dec, J. E., and Keller, J. O., 1992, "Heat Transfer in Pulse Combustor Tailpipes," Combustion Science and Technology, Special Issue on Pulsating Combustion (in press).

Chun, D.H. and Schwarz, W.H., 1967, "Stability of the Plane Incompressible Viscous Wall Jet Subjected to Small Disturbances," Phys. Fluids, 10, 5, 911-915.

Cohen, J. and Wygnanski, I., 1987, "The Evolution of Instabilities in the Axisymmetric Jet" parts I & II, J. Fluid Mech., Vol. 172, pp. 191-235.

Craik, A. D. D., 1985, Wave Interactions and Fluid Flows, Cambridge University Press, New York.

Dec, J. E. and Keller, J. O., 1990, "Time Resolved Gas Temperatures in the Oscillating Turbulent Flow of a Pulse Combustor Tail Pipe," Combustion and Flame, Vol. 80, pp. 358-370.

Eckert, E. R. G. and Drake, R. M., 1972, Analysis of Heat and Mass Transfer, McGraw-Hill, New York.

Falco, R.E., 1977, "Coherent Motions in the Outer Region of Turbulent Boundary Layers" Phys. of Fluids Suppl. 20,124

Fasel, H., 1990, "Numerical Simulation of Instability and Transition in Shear Flows," Invited Paper, *Procceedings of 3rd IUTAM Symposium on "Laminar-Turbulent Transition,"* Toulouse, France, Springer-Verlag.

Fiedler, H.E., Dziomba, B., Mensing, P. and Rosgen, T., 1981, "Initiation, Evolution and Global Consequences of Coherent Structures in Turbulent Shear Flows" Lecture Notes in Physics vol. 136, pp. 219-251. Springer Verlag, Berlin.

Gaster, M., Kit, E. and Wygnanski, I., 1985, "Large Scale Structures in Forced Turbulent Mixing Layer" J. Fluid Mech., Vol. 150, pp. 23-39.

Germano et al, 1990, "Studying Turbulence Using Numerical Simulation Databases," Center for Turbulence Research, Proceedings of the Summer Program 1990.

Goldstein, R. J., 1972, "Film Cooling," pages 321-379 in Advances in Heat Transfer, Vol. 7 (J. P. Hartnett and T. F. Irvine, Jr., eds.), Academic Press, New York.

Hager, J.M., Simmons, S., Smith, D., Onishi, S., Langley, L.W., and Diller, T.E., 1991, "Experimental Performance of a Heat Flux Microsensor," ASME Jnl Eng for Gas Turbines and Power, 112, 246-250.

Hanby, V. I., 1969, "Convective Heat Transfer in a Gas-Fired Pulsating Combustor," ASME J. Engr. for Power, Vol. 91, pp.48-52.

Harris, P. J. and Fasel, H., 1996, "Numerical Investigation of Unsteady Plane Wakes at Supersonic Speed," AIAA Paper 96-0686.

Holmberg, D.G. and Pestian, D.J., 1996, Wall-jet Turbulent Boundary Layer Heat Flux, Velocity, and Temperature Spectra and Time Scales, 1996 Intl Gas Turbine Conference.

Hussain, A.K.M.F., 1983, " Coherent Structures-Reality and Myth" Physics of Fluids, 26 2816-2850.

Hussain, A.K.M.F. and Reynolds, W.C., 1970, "The Mechanics of Organized Wave in Turbulent Shear Flow" J. Fluid Mech., 41, 241.

Hussain, A.K.M.F. and Reynolds, W.C., 1972, "The Mechanics of Organized Wave in Turbulent Shear Flow" J. Fluid Mech., 54, 241-261.

Ireland, P. T. and Jones, T. V., 1985, "The Measurement of Local Heat Transfer Coefficients in Blade Cooling Geometries," Paper 28, AGARD Conf. on Heat Transfer and Cooling in Gas Turbines, CP 390, Bergen, Norway.

Ireland, P. T. and Jones, T. V., 1987, "The Response Time of a Surface Thermometer Employing Encapsulated Thermochromic Liquid Crystals," J. Physics Eng., Sci. Instrum. 20, I.O.P. Publishing Ltd., England.

Irwin, H. P. A. H., 1973, "Measurements in a Self-Preserving Plane Wall Jet in Positive Pressure Gradient," J. Fluid Mech., Vol. 61, p. 33.

Jumper, G. W., Elrod, W. C., and Rivir, R., 1991, "Film Cooling Effectiveness in High Turbulence Flow," J. Turbomachinery, Vol. 113, pp. 479-483.

Katz, Y., Horev, E., and Wygnanski, I., 1991, "The Effects of External Excitation on the Reynolds Averaged Quantities in a Turbulent Wall Jet," Global Geometry of Turbulence (J. Jimenez, ed.), NATO ASI Series B, Vol. 268, pp. 67-87, Plenum Press, New York.

Katz, Y., Nishri, B., and Wygnanski, I., 1989, "The Delay of Turbulent Boundary Layer Separation by Active Control" AIAA Paper 89-1027.

Kays, W. M. and Crawford, M. E., 1980, Convective Heat and Mass Transfer, McGraw-Hill, New York.

Kim, J., Simon, T.W., and Russ, S.G., 1992, "Free Stream Turbulence and Concave Curvature Effects on Heated Transitional boundary Layers," ASME Jnl Heat Transfer, Vol. 114, 339.

Kline, S. J., Reynolds, W. C., Schraub, F. A., and Runstadler, P. W., 1967, "The Structure of Turbulent Boundary Layer" J. Fluid Mech., vol. 50, pp. 133.

Landhal, M.T., 1990, "On sublayer Streaks" J. Fluid Mech., 212, 593-614.

Ligrani, P. M., Subramanian, C. S., Craig, D. W., and Kaisuwan, P., 1991, "Effects of Vortices with Different Circulations on Heat Transfer and Injectant Downstream of a Row of Film-Cooling Holes in a Turbulent Boundary Layer," ASME J. Heat Transfer, Vol. 113, pp. 79-90.

Liu, C., Tai, Y.-C., Huang, J.-B., and Ho, C.-M., 1994, "Surface Micromachined Thermal Shear Stress Sensor," ASME FED-Vol. 197, Application of Microfabrication to Fluid Mechanics, 9-15.

Liu, J.T.C., 1971, " Non Linear Development of an Instability Wave in a Turbulent Wake" Phys. Fluids, vol. 14, pp.2251-2257.

MacArthur, C. D., 1986, "Fluid Dynamics and Heat Transfer of the Circular Tangential Wall Jet," Ph.D. thesis, University of Dayton, Dayton, Ohio.

MacMullin, R., Elrod, W., and Rivir, R., 1989, "Free-Stream Turbulence from a Circular Wall Jet on a Flat Plate Heat Transfer and Boundary Layer Flow," J. Turbomachinery, Vol. 111, pp. 78-86.

Marasli, B. Champagne, F.H. and Wygnanski, I.J., 1989, " Modal Decomposition of Velocity Signals in a Plane Turbulent Wake" J. Fluid Mech., 198, p.255-273

Meitz, H., 1996, "Numerical Investigation of Suction in a Transitional Flat-Plate Boundary Layer," Dissertation, Department of Aerospace and Mechanical Engineering, The University of Arizona.

Mele, P., Morganti, M., Scibillia, M.F., and Lasek, A., 1986, "Behavior of Wall Jet in Laminar-to-Turbulent Transition," AIAA Jnl, 24, 938-939.

Metzger, D. E. and Cordaro, J. V., 1979, "Heat Transfer in Short Tubes Supplied from a Cross Flowing Stream," ASME Paper 79-WA/H-16.

Mitachi, K. and Ishiguro, R., 1974, "Heat Transfer of Wall Jets," Heat Transfer: Japanese Research, 27-40.
Myers, G. E., Schauer, J. J., and Eustis, R. H., 1963, ASME J. Heat Transfer, Vol. 85.

Nagano, Y. and Tagawa, M., 1987, "Statistical Characteristics of Transfer Processes in a Wall Turbulent Shear Flow," 2nd Int. Symp. on Transport Phenomena in Turbulent Flows, Tokyo, Japan.

Nygaard, K. J. and Glezer, A., 1991, "Evolution of Streamwise Vortices and Generation of Small-Scale Motion in a Plane Mixing Layer," J. Fluid Mech., Vol. 231, pp. 257-301.

Oster, D., Wygnanski, I., Fiedler, H.E., and Dziomba,B., 1978, " The Effects of Initial Conditions on the Two Dimensional Mixing Layer" Lecture Notes in Physics Vol. 75, pp. 48-65.

Oster, D. and Wygnanski, I., 1982, "The Forced Mixing Layer Between Parallel Streams" J. Fluid Mech., vol. 123, pp. 91-130.

Padmanabhan, A., Goldberg, H.D., Breuer, K.S., and Schmidt, M.A., 1995, "A Silicon Micromachined Floating-Element Shear Stress Sensor with Optical Position Sensing by Photodiodes," Technical Digest, 8th Intl Conf on Solid-State Sensors and Actuators, Eurosensors IX, Stockholm, Sweden, 436-439.

Schubauer, G. B. and Skramstadt, H. K., 1947, "Laminar Boundary Layer Oscillations and Transition on a Falt Plate" NACA Rep. No: 909.

Seifert, A., Bachar,T. , Koss, D. , Shepshelovich, M., Wygnanski, I., 1993, "Oscillatory blowing: A tool to delay boundary-layer separation," AIAA Journal, vol 31, No.11, pp.2052-2060.

Seifert, A., Darabi, A., Wygnanski, I., 1996, "On the delay of airfoil stall by periodic excitation," J. Aircraft, Aug. 1996.

Speziale, C. G., 1996, "Computing Non-Equilibrium Turbulent Flows with Time-Dependent RANS and VLES," 15th International Conference on Numerical Methods in Fluid Dynamics, Monterey.

Squires, Kyle D., 1991, "Dynamic subgrid-scale modeling of compressible turbulence," Center for Turbulence Research, Annual Research Briefs, 1991.

Tam, C.K.W. and Chen, K.C., 1979, " A Statistical Model of Turbulence in Two Dimensional Mixing Layer" J. Fluid Mech., 92, p.303.

Tourbier, D. and Fasel, H., 1994, "Numerical Investigation of Transitional Axisymmetric Wakes at Supersonic Speeds," AIAA Paper 94-2286.

Tourbier, D. and Fasel, H., 1995, "Stability of the Supersonic Axisymmetric Wake for Free Stream Mach Number of M=1.2," Proceedings of 6th International Symposium on Computational fluid Dynamics, Lake Tahoe.

Tsuji, Y., Morikawa, Y., Nagatani, T., and Sakou, M., 1977, "The Stability of a Two-Dimensional Wall Jet," Aeronautical Quarterly, V XXVIII, pp. 235-246.

VandenBerghe, T. and Diller, T.E., 1989, "Analysis and Design of Experimental Systems for Heat Transfer Measurement from Constant-Temperature Surfaces," Experimental Thermal and Fluid Science, 2, 236-246.

Wieghardt, K., 1946, AAF Translation No. F-TS-919-RE; cited by R. J. Goldstein, "Film Cooling," Advances in Heat Transfer, Vol. 7, Academic Press, New York, pp. 321-379 (1972).

Wernz, S. and Fasel, H., 1996, "Numerical Investigation of Unsteady Phenomena in Wall Jets," 34th Aerospace Sciences Meeting & Exhibit, Reno.

Wygnanski, I., Katz, Y., and Horev, E., 1992, "On the Applicability of Various Scaling Laws to the Turbulent Wall Jet," J. Fluid Mech., Vol. 234,pp. 669-690.

Yang, K.-S. and Ferziger, J.H., 1993, "Large-Eddy Simulation of Turbulent Obstacle Flow Using a Dynamic Subgrid-Scale Model," AIAA Journal, Vol. 31, pp. 1406-1413.

Zhou, M.D., Rothstein,J. and Wygnanski,I. 1992, " On the hydrodynamic stability of the wall jet", Proc. 11th Australian Fluid Mechanics Conference, Hobart.

Zhou, M. D. and Wygnanski, I., 1993, " The forced wall jet in an external stream," AIAA 93-3250, Orlando.

Zhou, M.D., Heine,C., and Wygnanski, I., 1996 "The effects of excitation on the coherent and random motion" J Fluid Mech. vol.310, pp.1-37.

6. LIST OF FIGURES
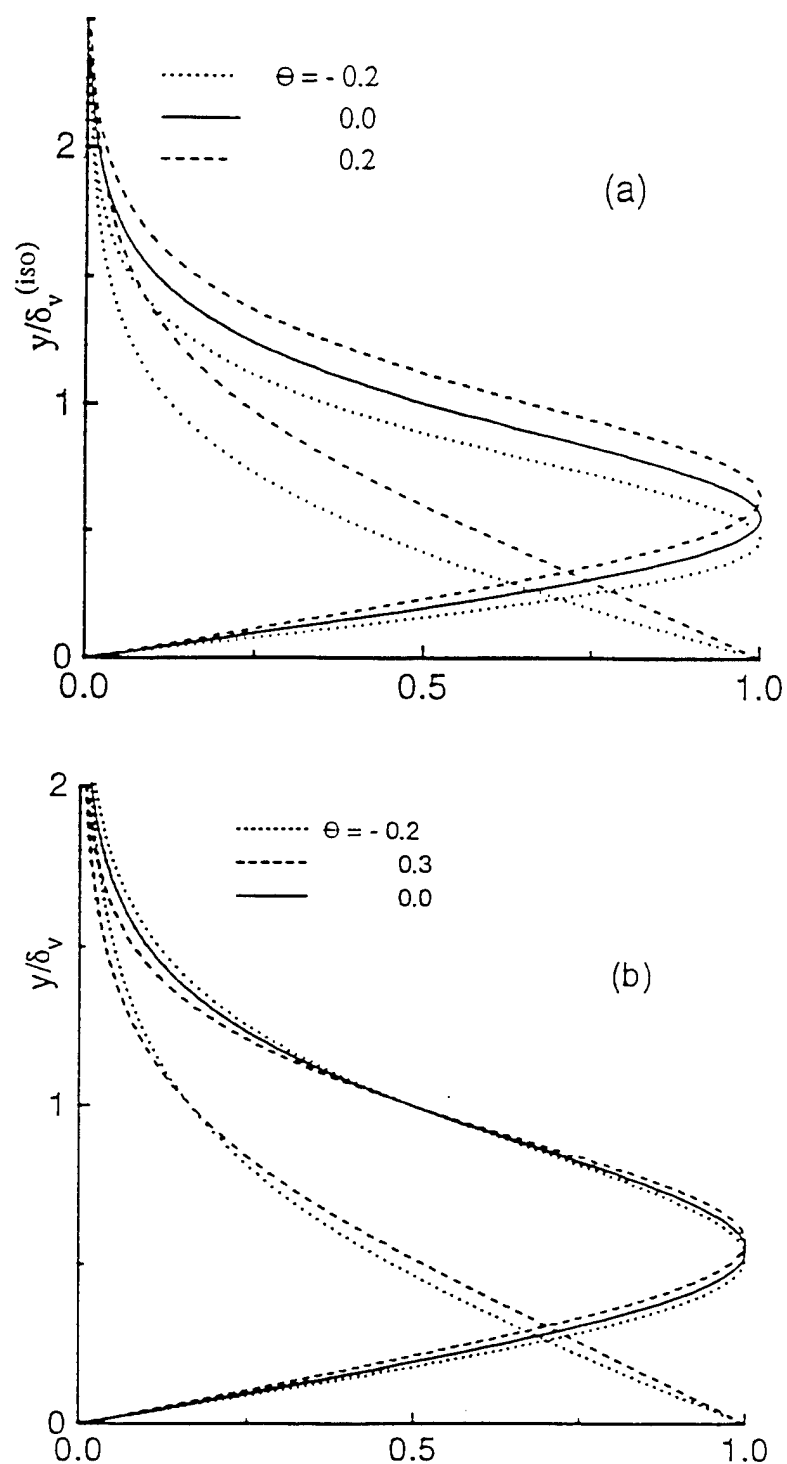
Figure 1. Non-dimensional mean velocity and temperature profiles for different values of the wall temperature deficit $\Theta = \left(T_w - T_0\right)/T_0$ (a) scaled with the isothermal half-width $\delta_v^{(iso)}$ and (b) by own scales $\delta_v(\Theta)$.
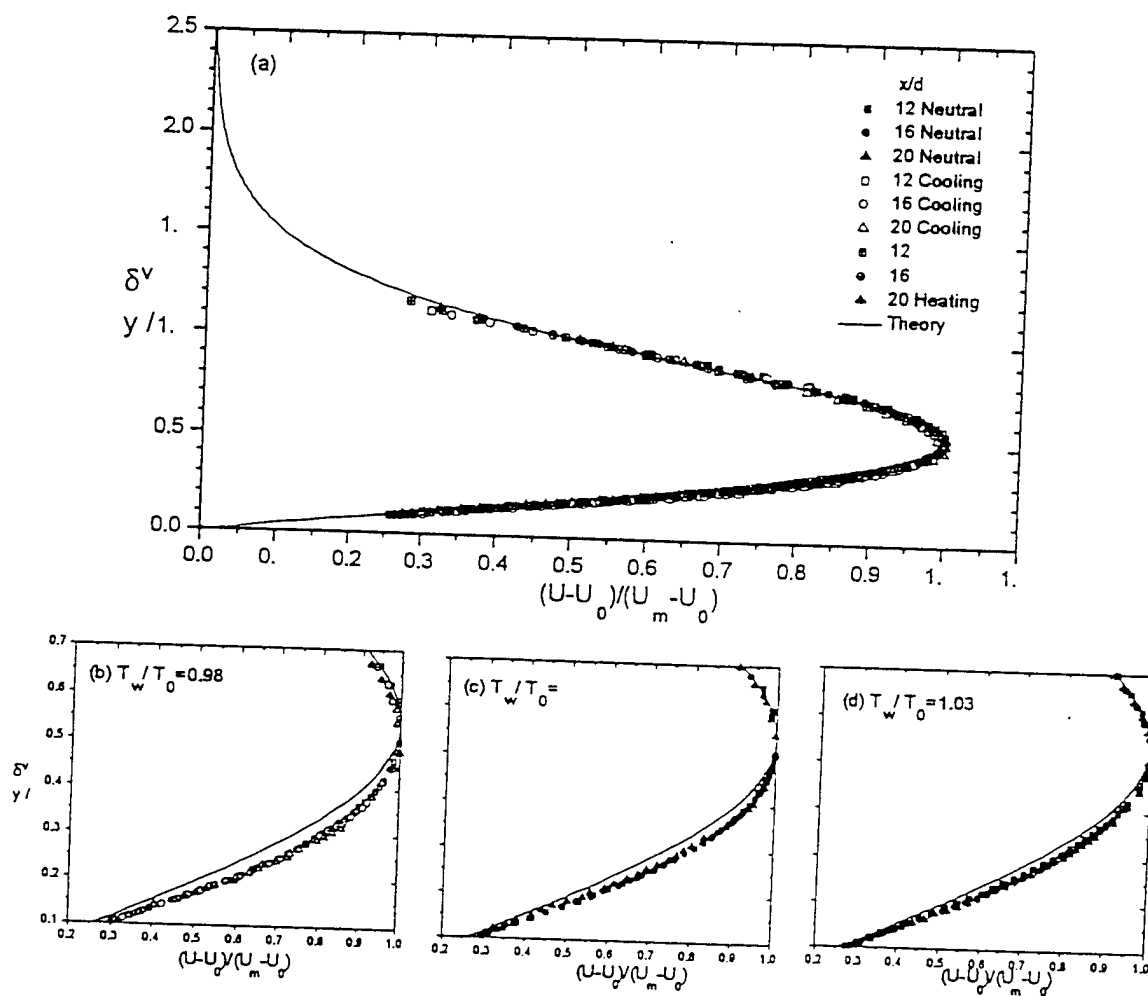
Figure 2. Comparison of normalized velocity profiles at three x/d locations and for T_w/T_o = 0.98, 0 and 1.03 (a) full profile, (b), (c) and (d) near-wall region.
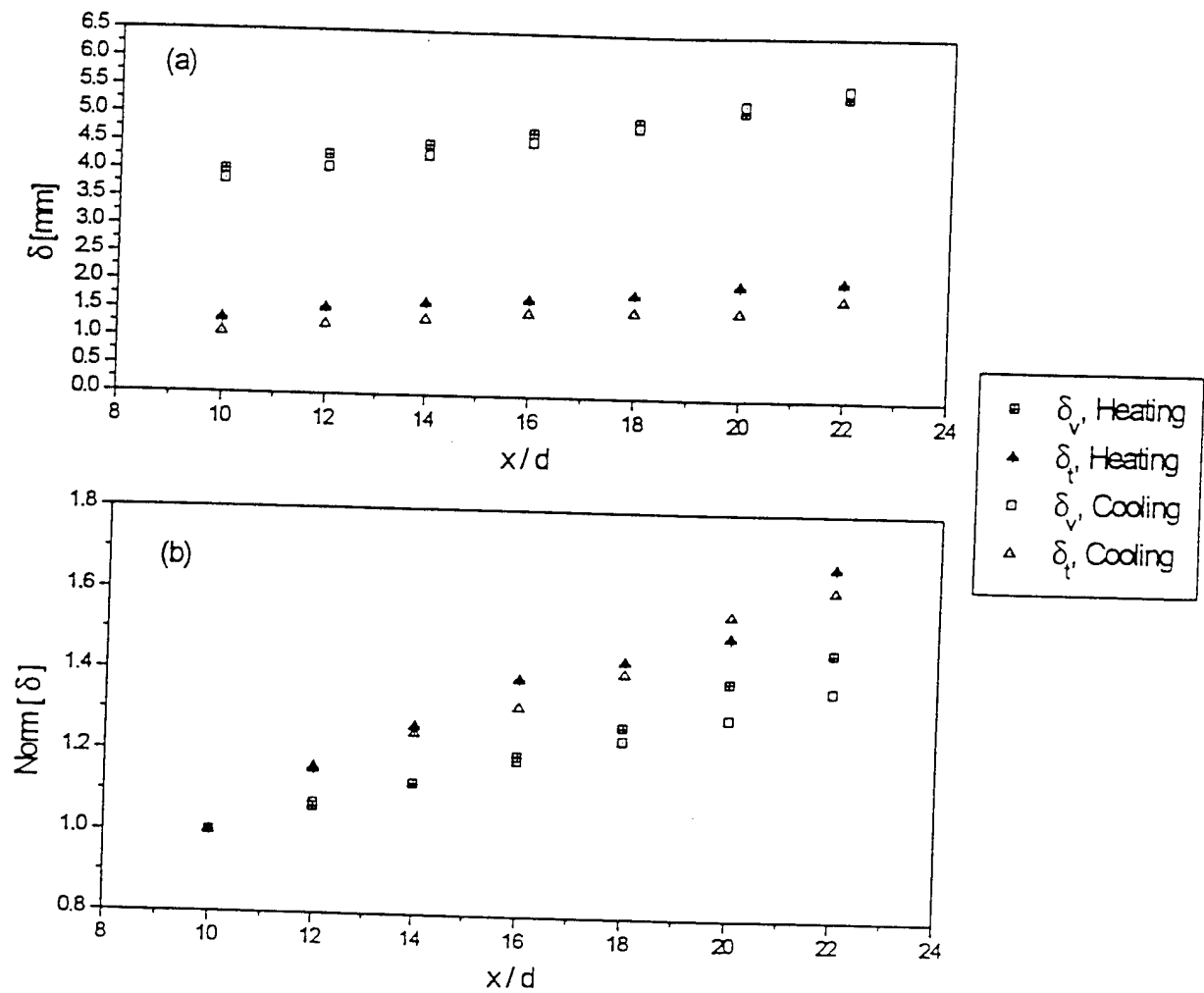
Figure 3. The downstream development of hydrodynamic and thermal boundary layer thicknesses, (a) dimensional and (b) normalized.
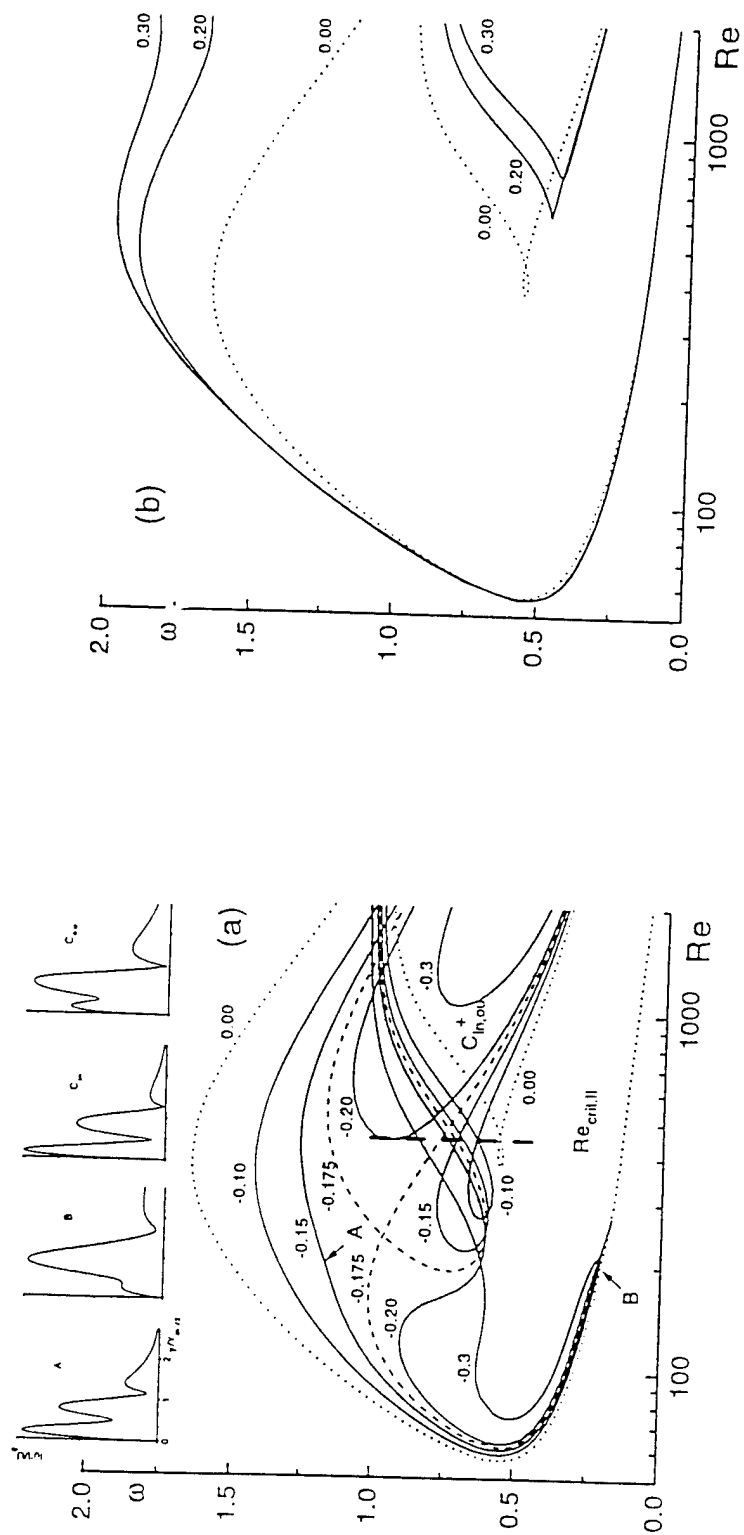
(a)

(b)

Figure 4.   Neutral stability diagram for a wall-jet flowing over a constant temperature surface for (a) the cold $\Theta<0$ and (b) the hot $\Theta>0$ surface.
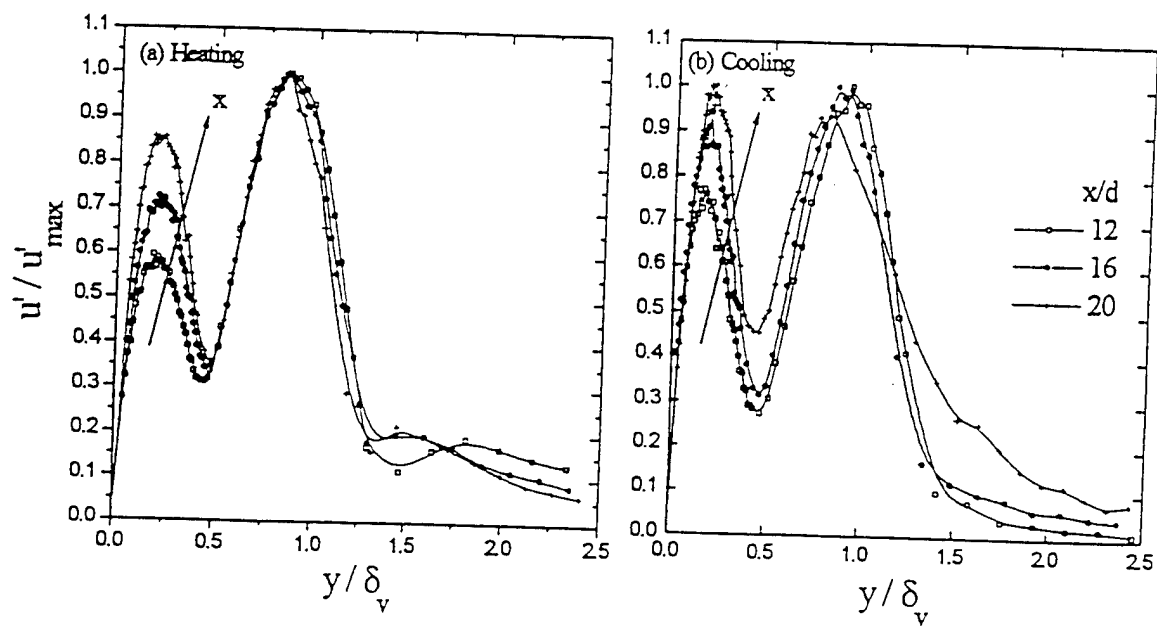
Figure 5. Normalized fluctuating streamwise velocity comparison at three x/d locations and for outer mode forcing at excitation level of 0.6%, (a) wall heating and (b) wall cooling.
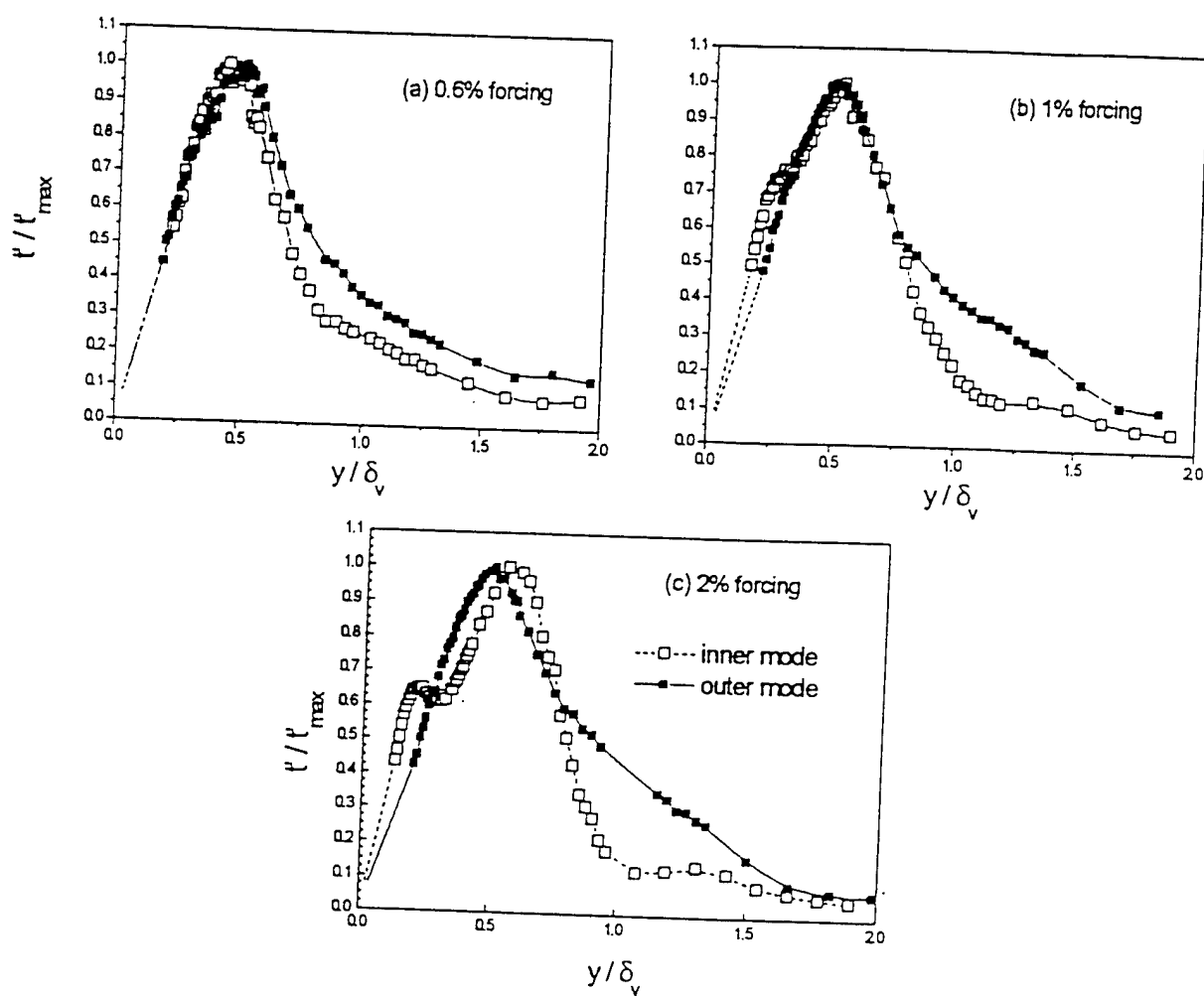
Figure 6. Normalized fluctuating temperature distribution for inner and outer mode forcing for (a) 0.6%, (b) 1% and (c) 2% excitation levels ($x/d = 16$ and $T_w/T_o = 1.03$).
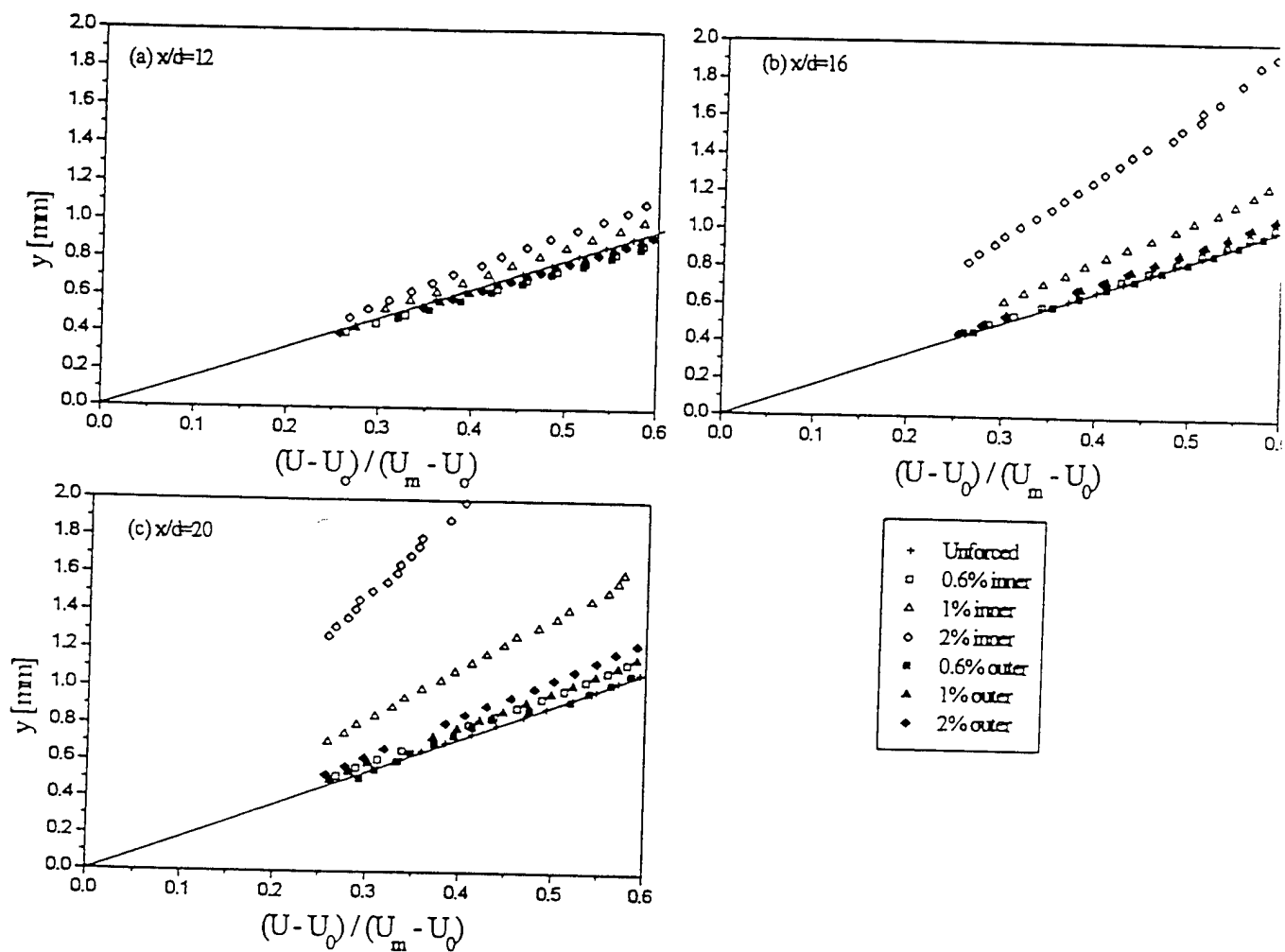
Figure 7. Near-wall velocity gradient comparison for different excitation levels and frequencies at x/d of (a) 12, (b) 16 and (c) 20 and for $T_w/T_o = 1.03$.
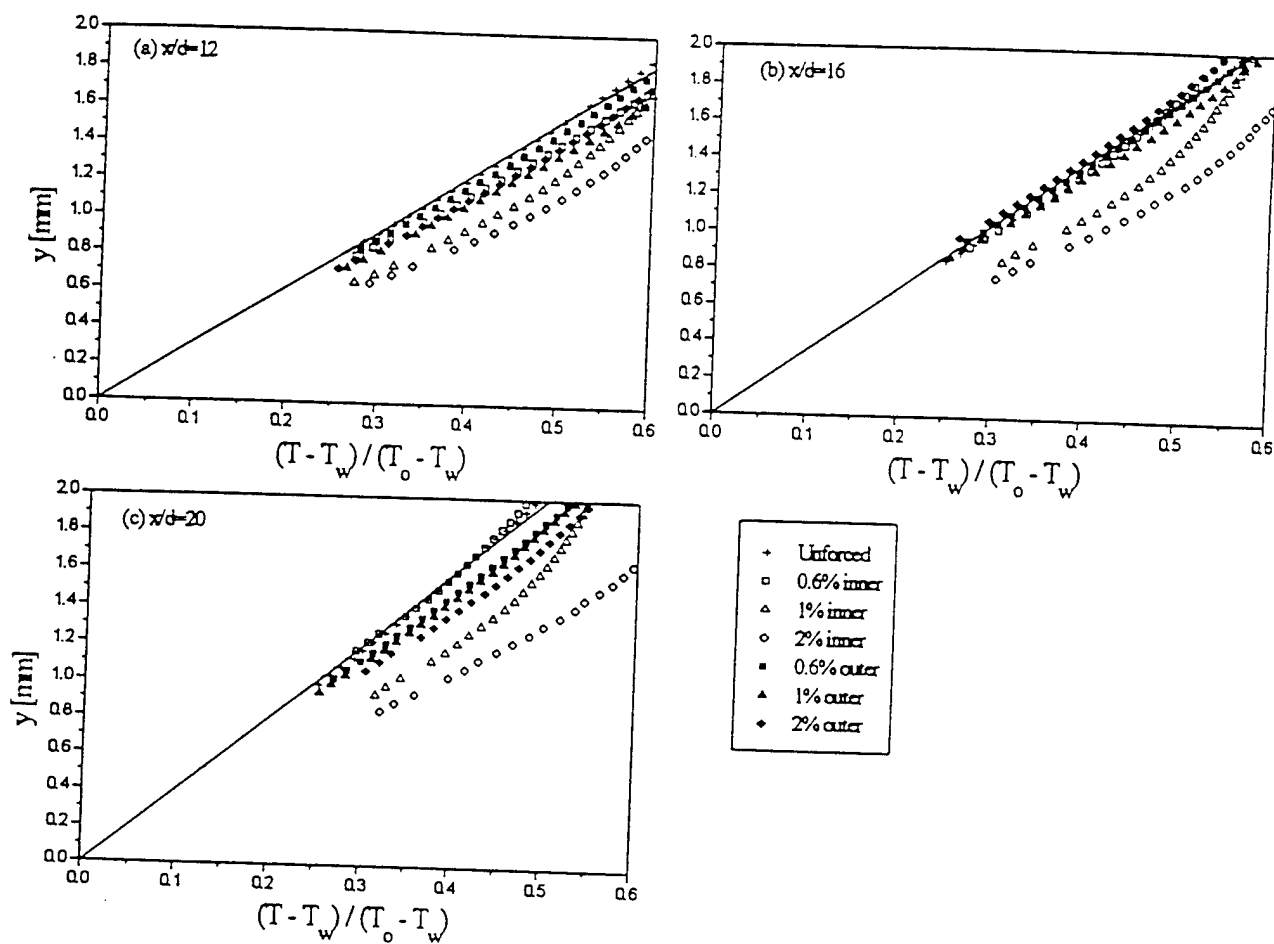
Figure 8. Near-wall temperature gradient comparison for different excitation levels and frequencies at x/d of (a) 12, (b) 16 and (c) 20 and for $T_w/T_o = 1.03$.
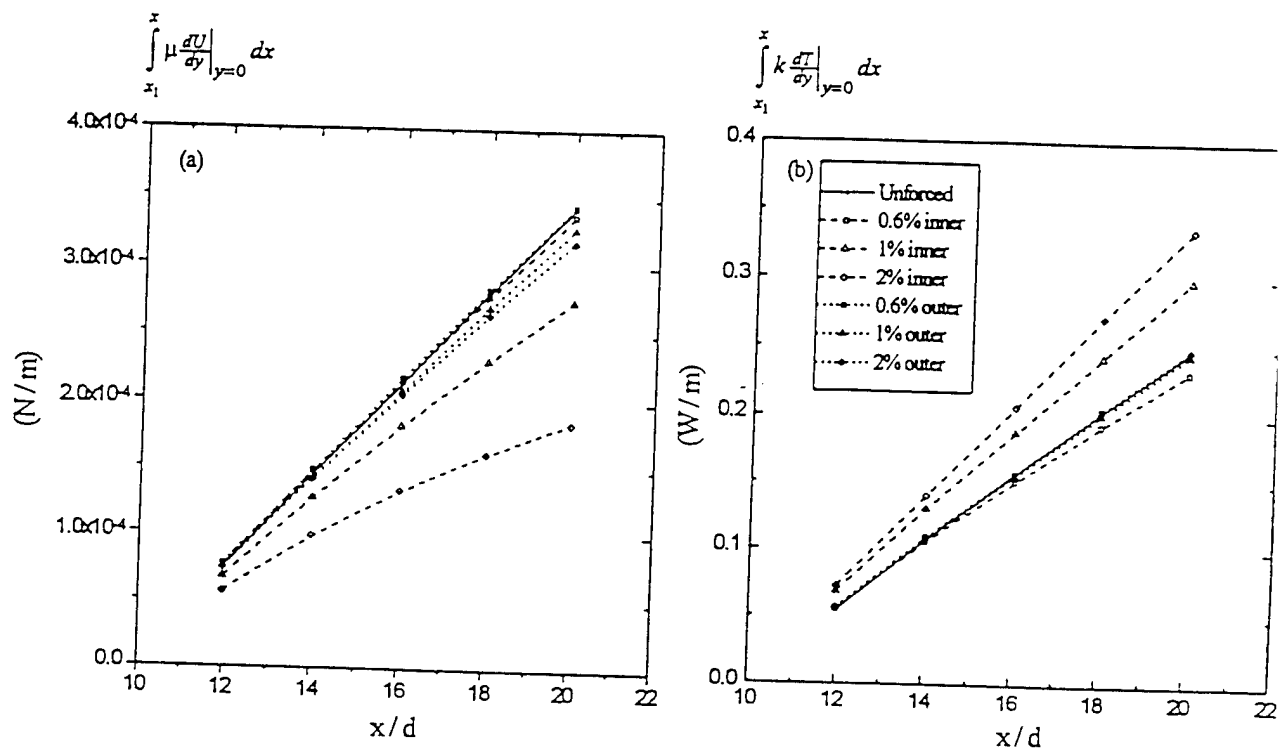
Figure 9. Integrated (a) skin friction drag and (b) total heat flux
for various excitation levels and frequencies and for $T_w/T_o = 1.03$.
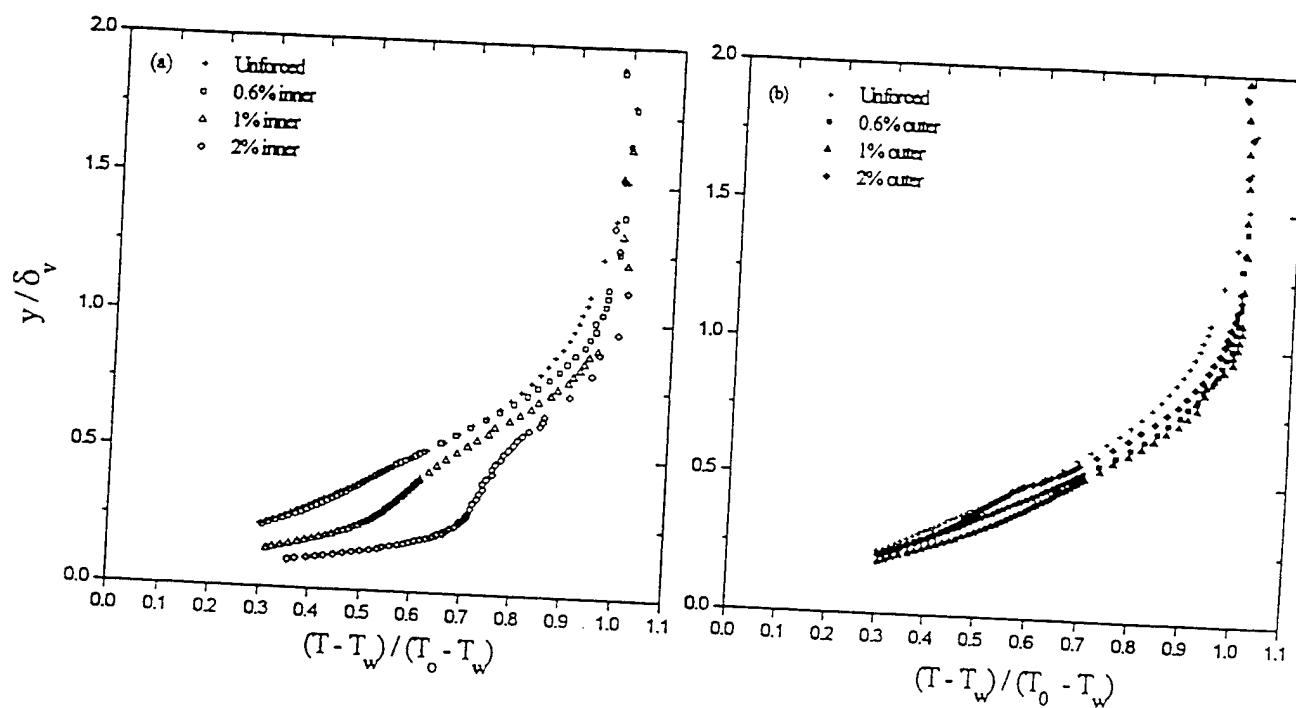
Figure 10. Comparison of normalized temperature profiles measured at $x/d = 20$ at different excitation levels for (a) inner mode forcing and (b) outer mode forcing for $T_w/T_o = 1.03$.
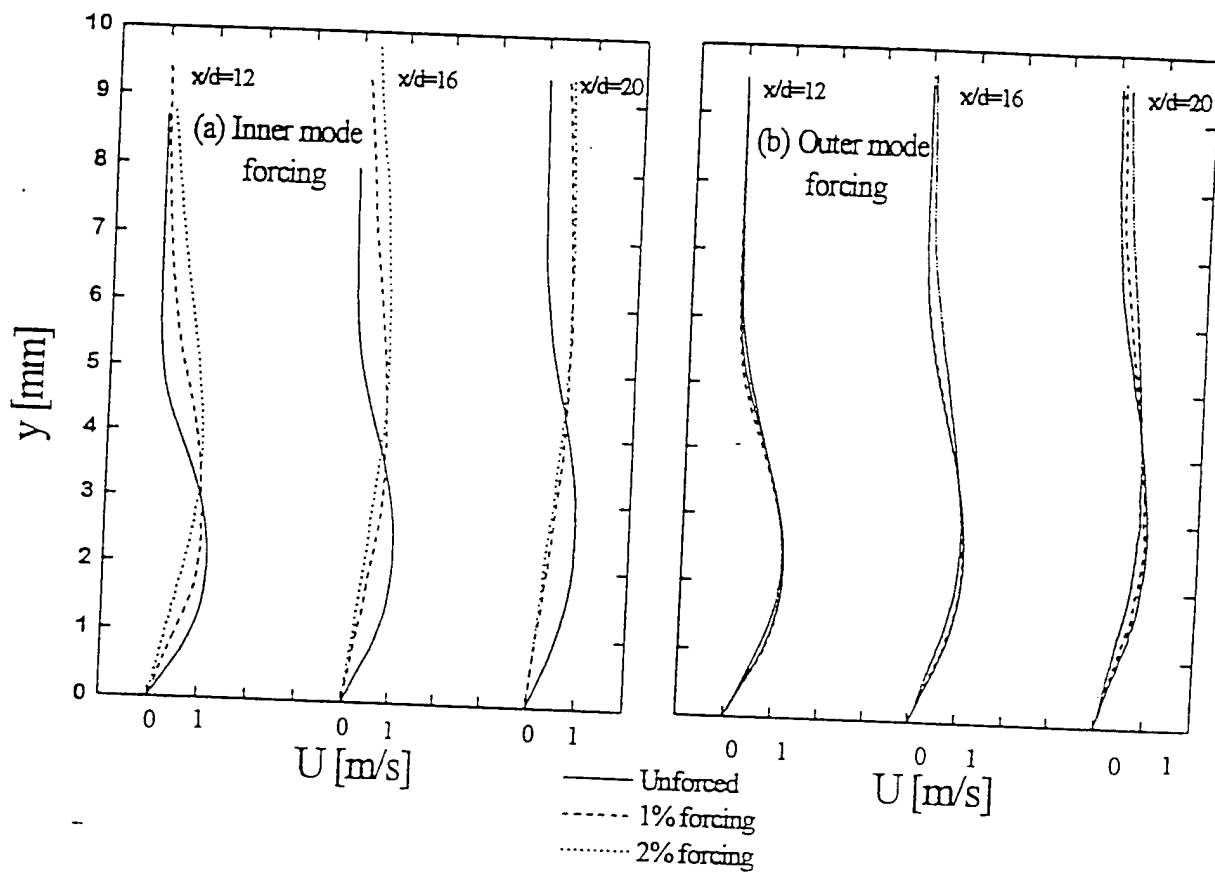
Figure 11. Dimensional mean velocity profiles for various excitation levels and downstream locations (a) inner mode forcing and (b) outer mode forcing for $T_w/T_o = 1.03$.
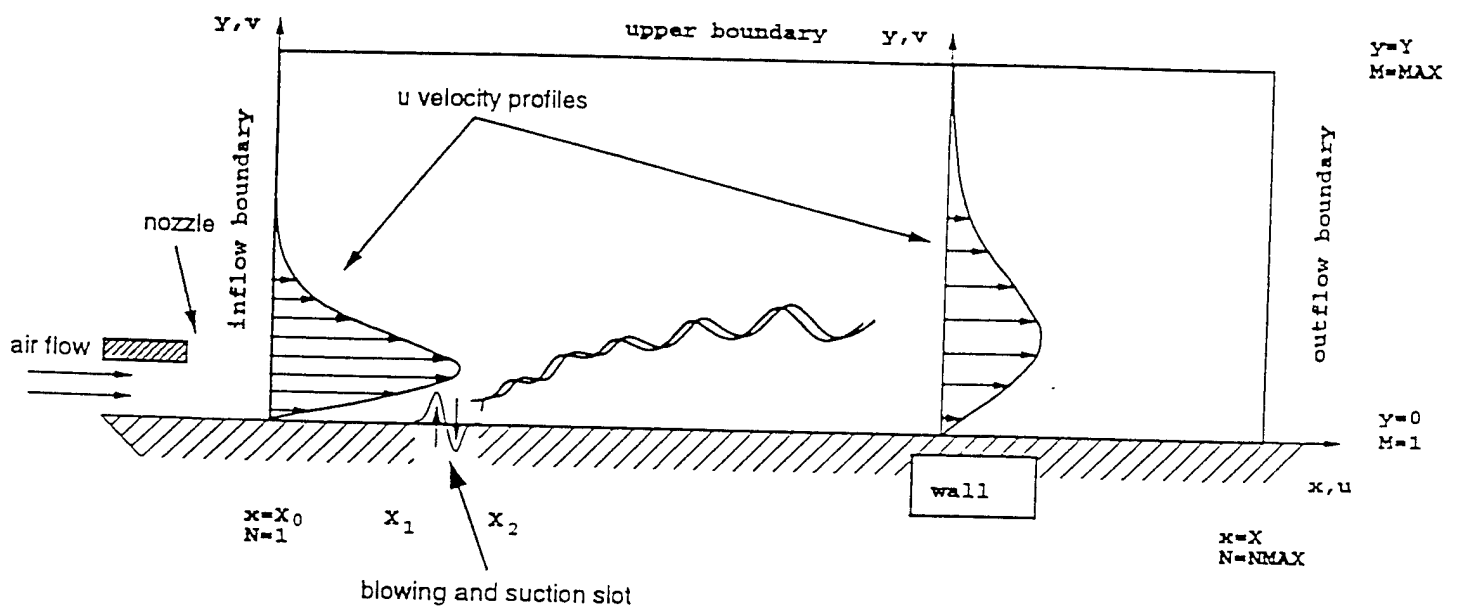
Figure 12. Integration domain for computation of forced laminar wall jet.
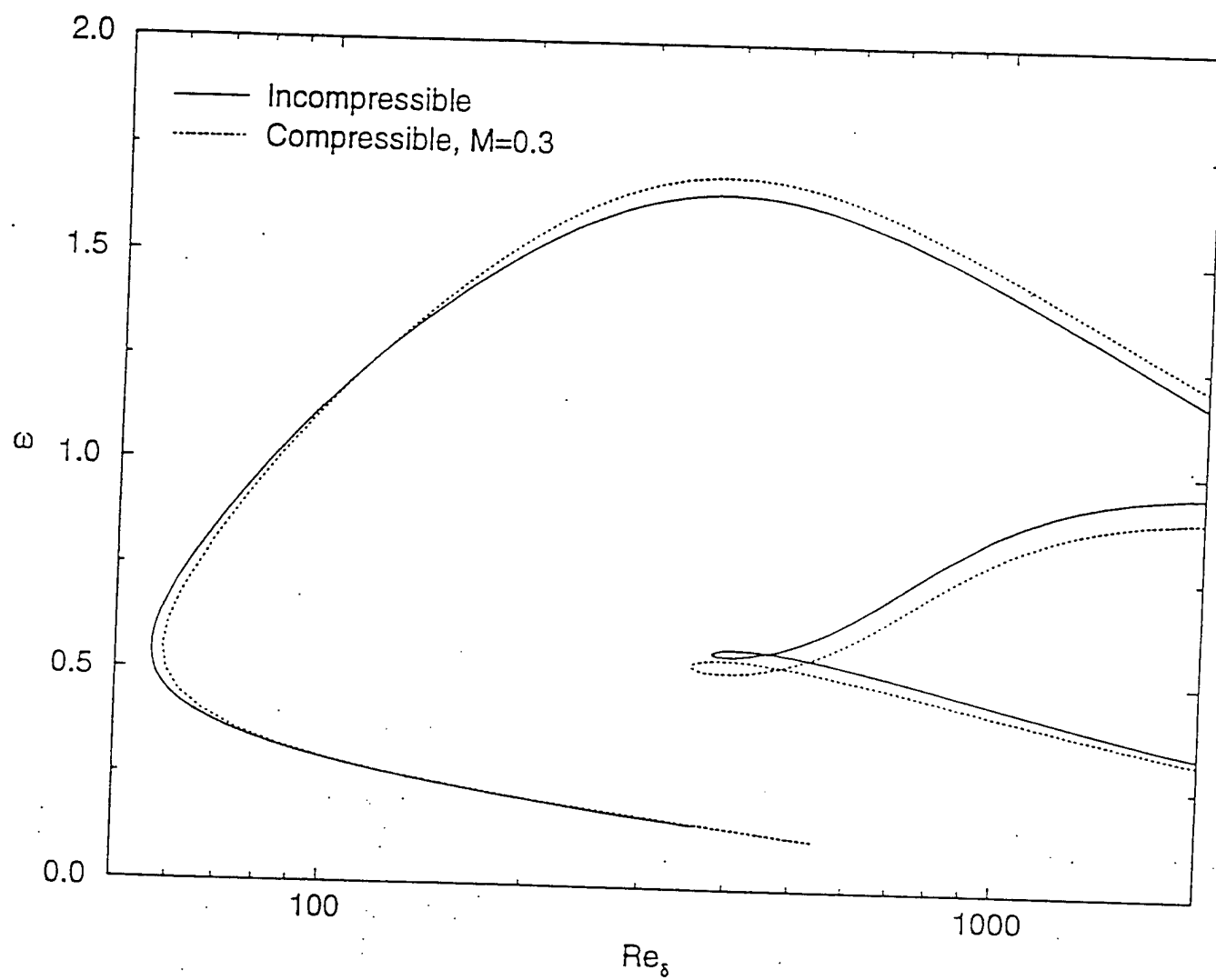
Figure 13. Comparison of the neutral curves from incompressible and compressible (M=0.3) Linear Stability Theory.
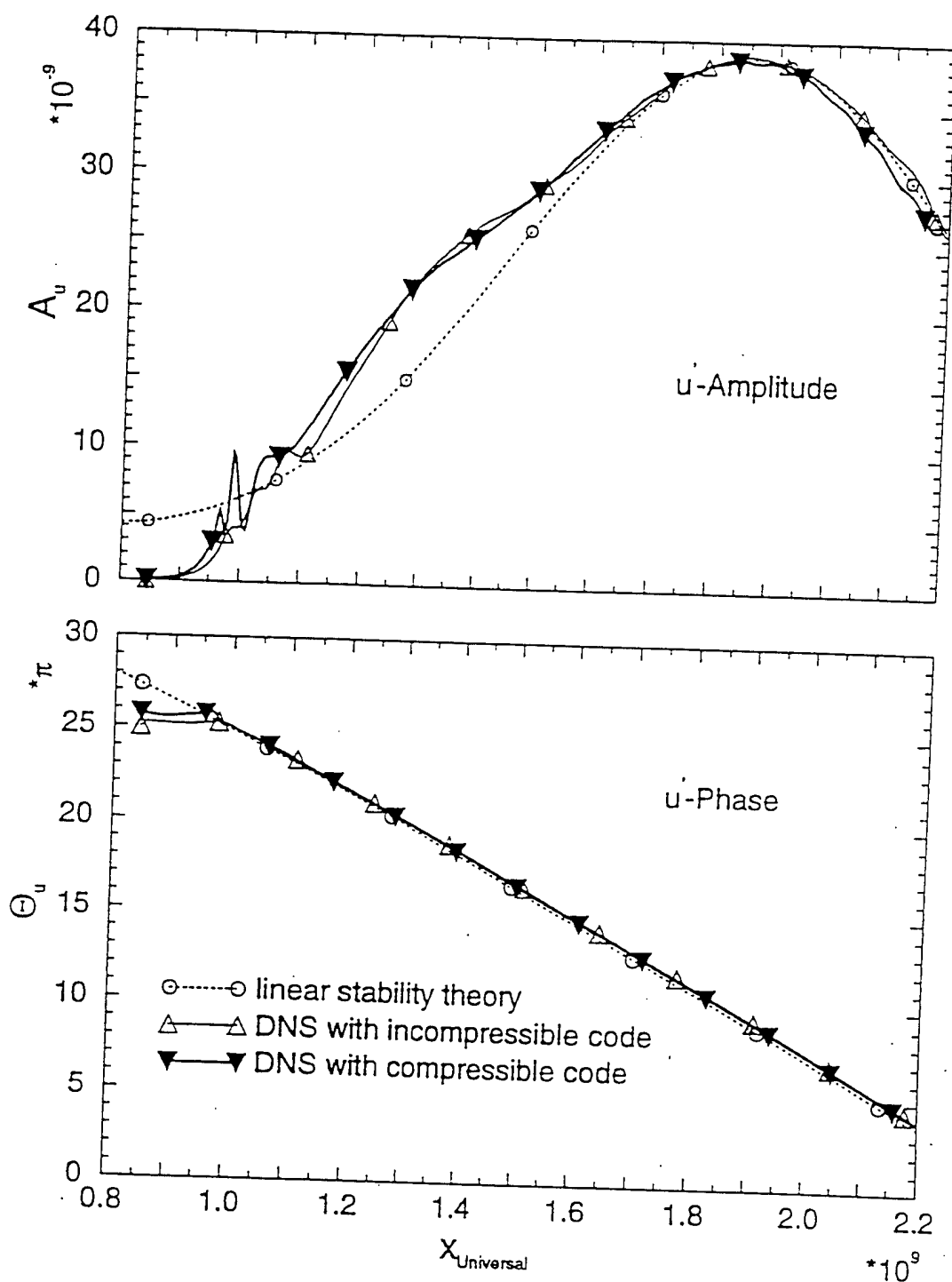
Figure 14. Amplitudes and phases for the maximum of the u-disturbances versus downstream location x.
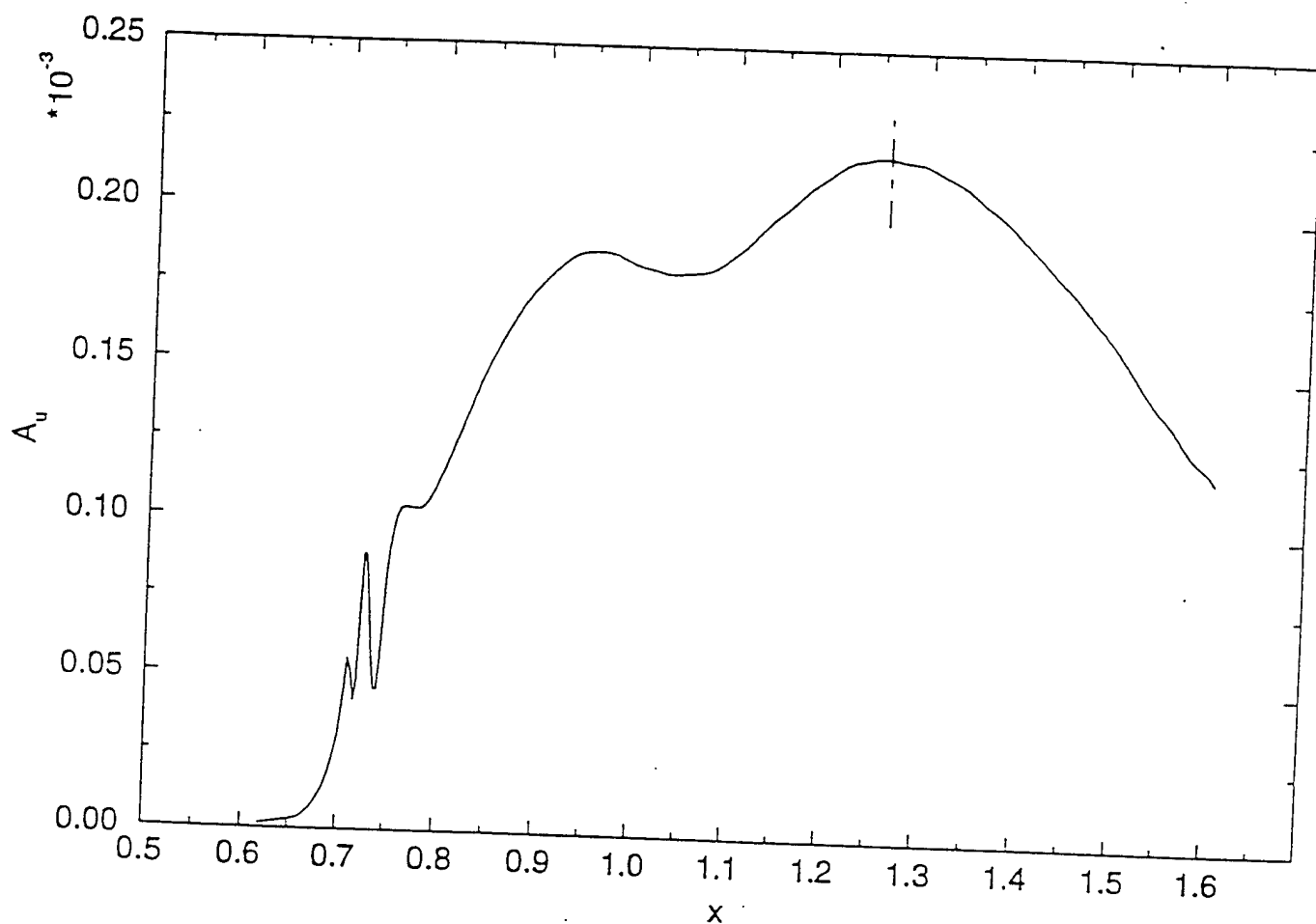
Figure 15. Fourier amplitudes for the maximum of the u-disturbances versus downstream location x (Q=-0.1). The dashed line indicates the location of the neutral point.
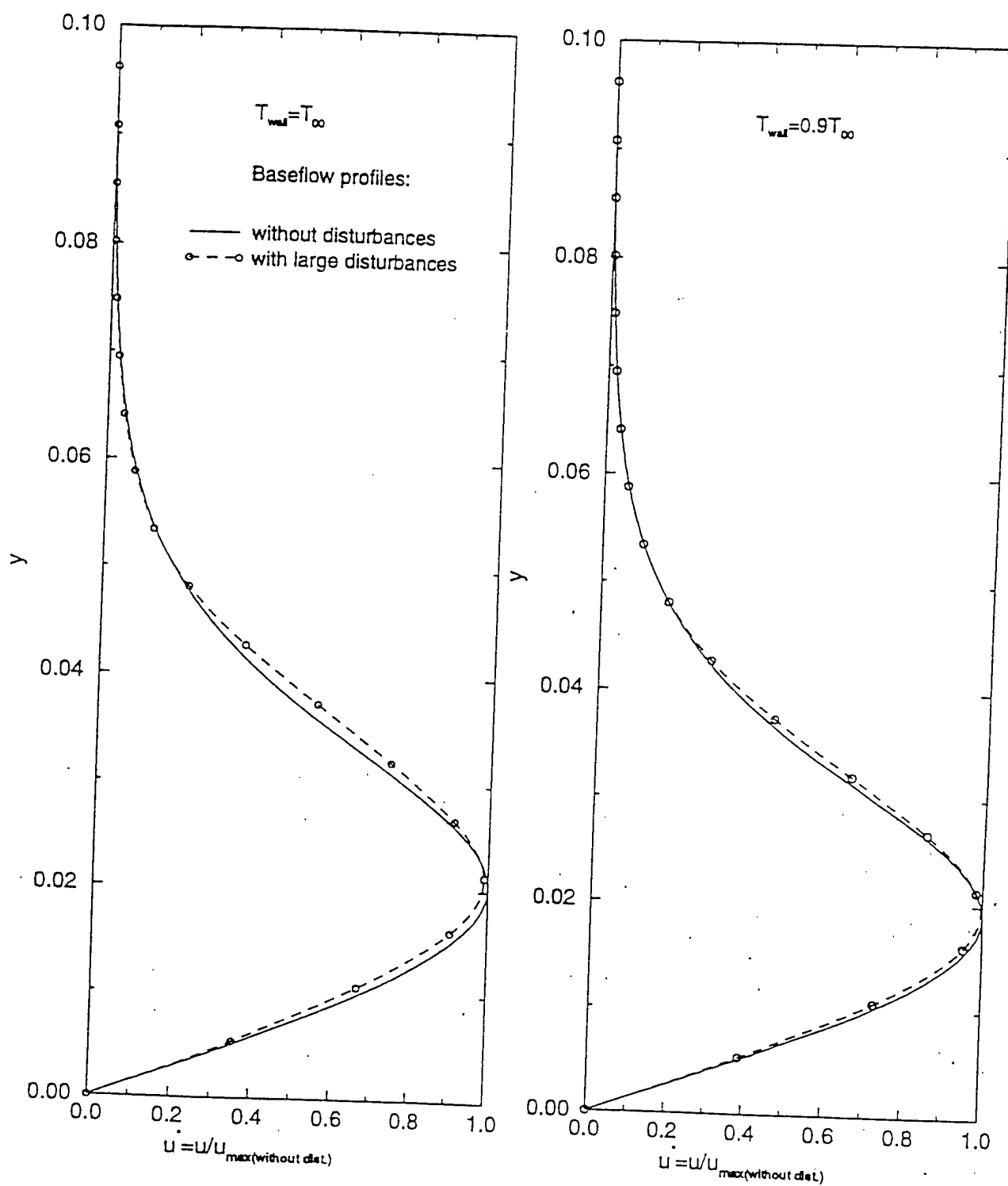
Figure 16.   Baseflow u-velocity profiles for different wall temperatures for the case without disturbances and the case with large disturbances.
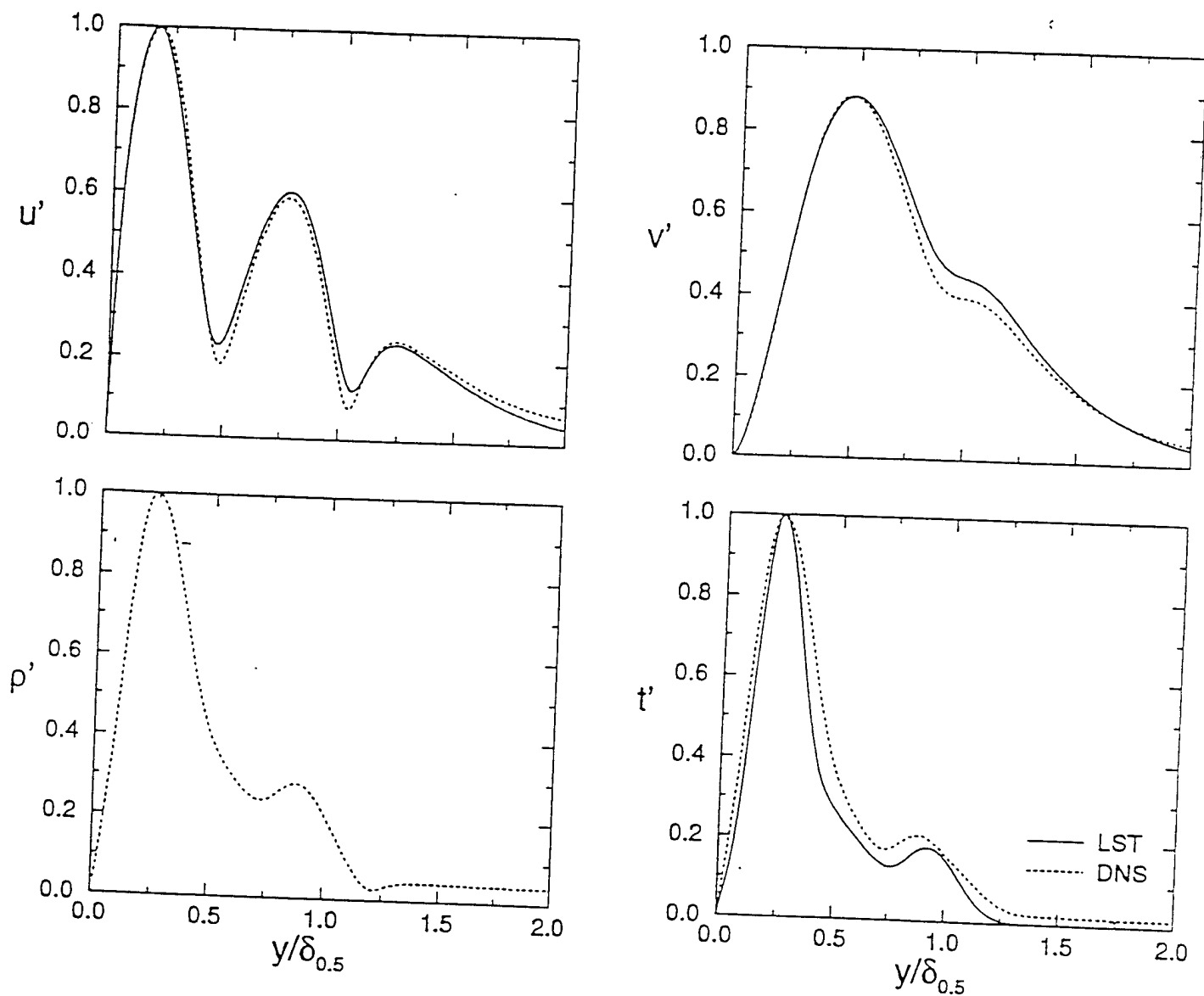
Figure 17. Comparison of eigenfunctions, obtained from Linear Stability Theory (LST) and Direct Numerical Simulations (DNS) for the case including the unheated starting length.

Figure 18. Influence of the disturbance level on the meanflow. The graphs from top to bottom show the decrease of the local u-velocity maximum, the increase of the half width of the wall jet and the decrease of the wall shear as functions of the local u-amplitude maximum of the fundamental disturbance wave.
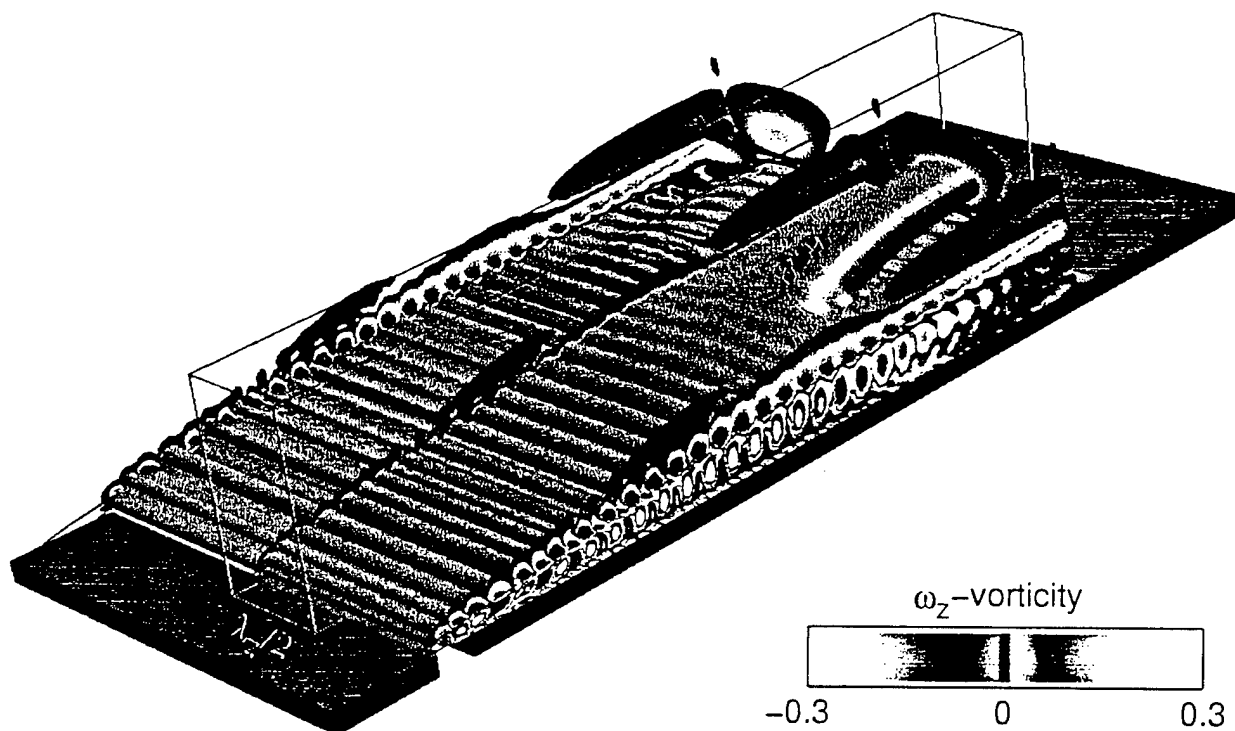
Figure 19.   Iso-surfaces of the spanwise vorticity for a wall jet that is forced with two-
dimensional blowing and suction at a large amplitude (f=56Hz, A=4e-3) and that
is simultaneously forced with three-dimensional blowing and suction of the same
frequency at a much smaller   amplitude (f=56Hz, A=1e-5,): fundamental
resonance.
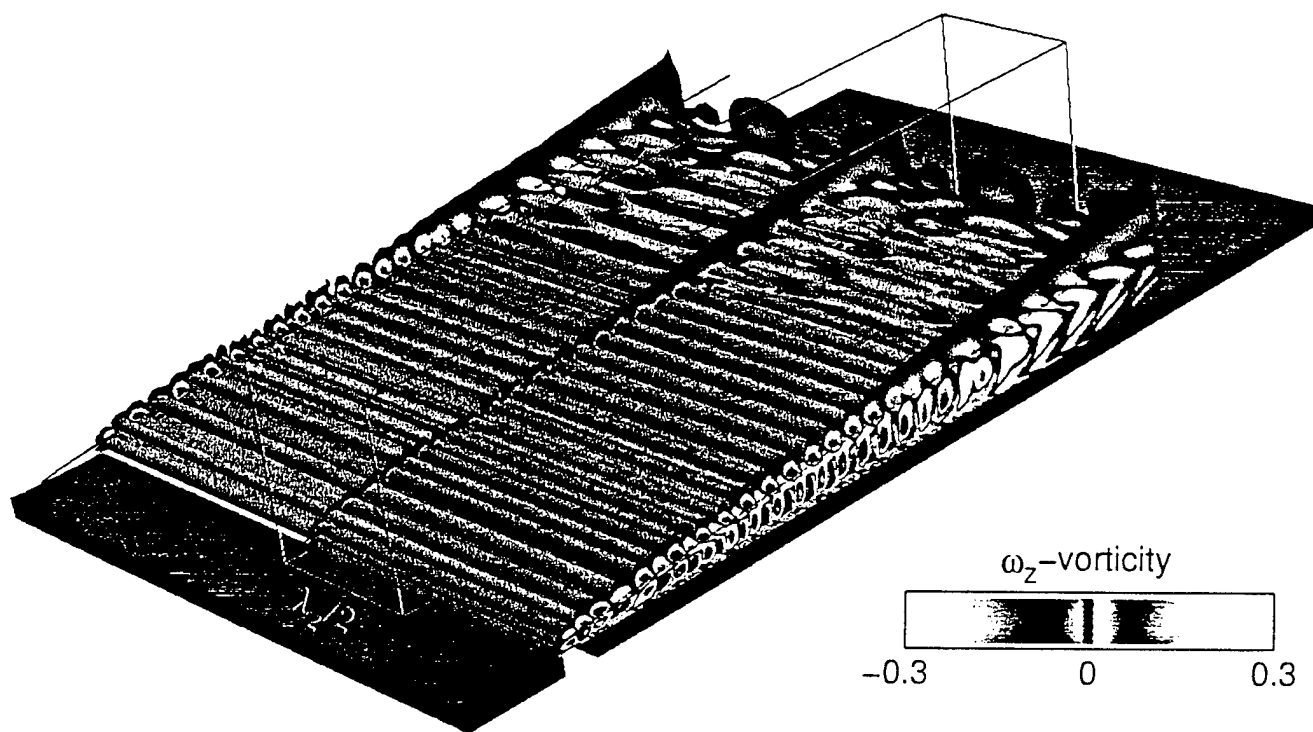
Figure 20.　Iso-surfaces of the spanwise vorticity for a wall jet that is forced with two-dimensional blowing and suction at a large amplitude (f=56Hz, A=4e-3) and that is simultaneously forced with three-dimensional blowing and suction of half that frequency at a much smaller amplitude (f=28Hz, A=1e-5): subharmonic resonance.
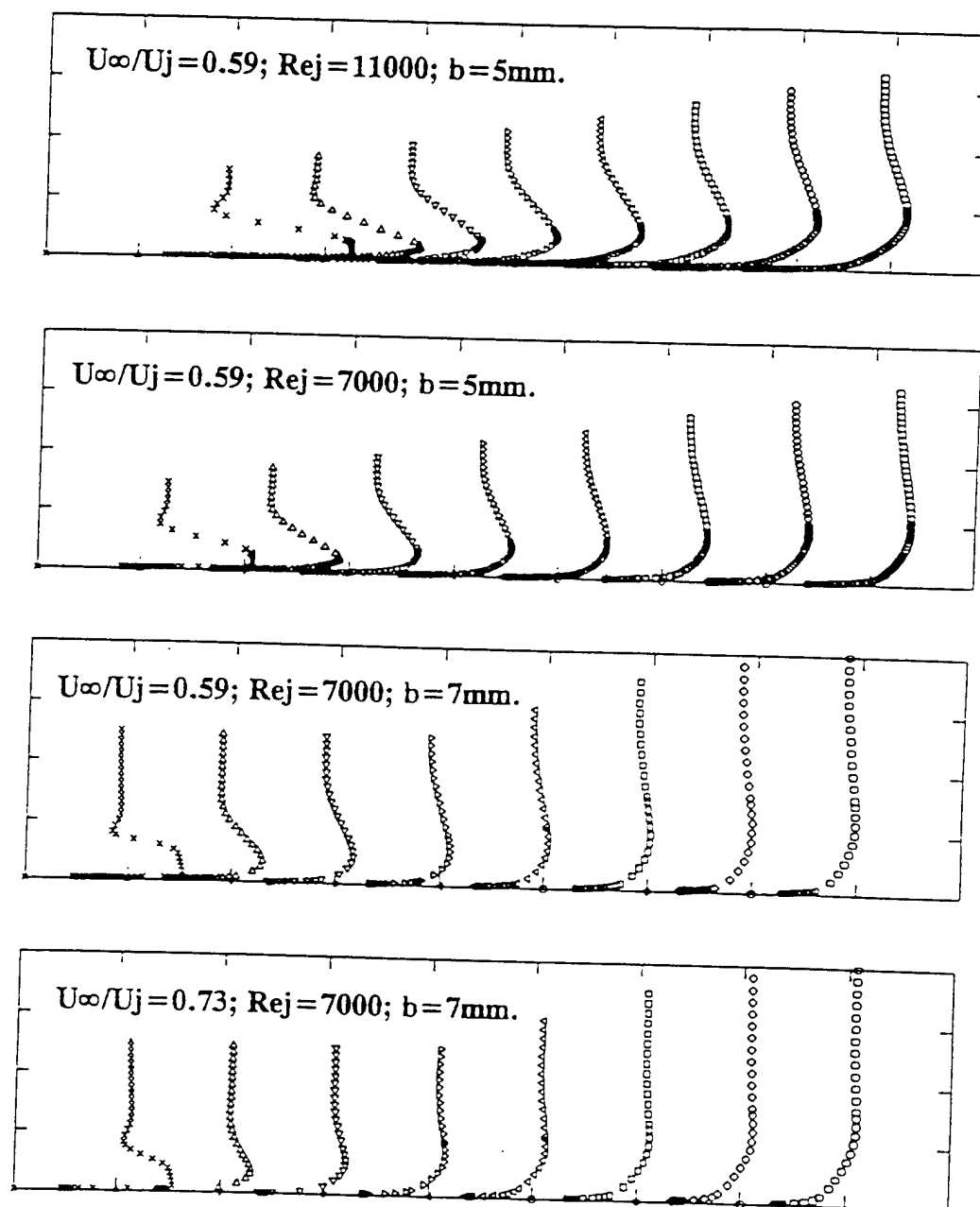
Figure 21. Mean velocity distributions of the weak wall jets with $U_\infty{}^2\theta/U_j{}^2 b < 0.035$.
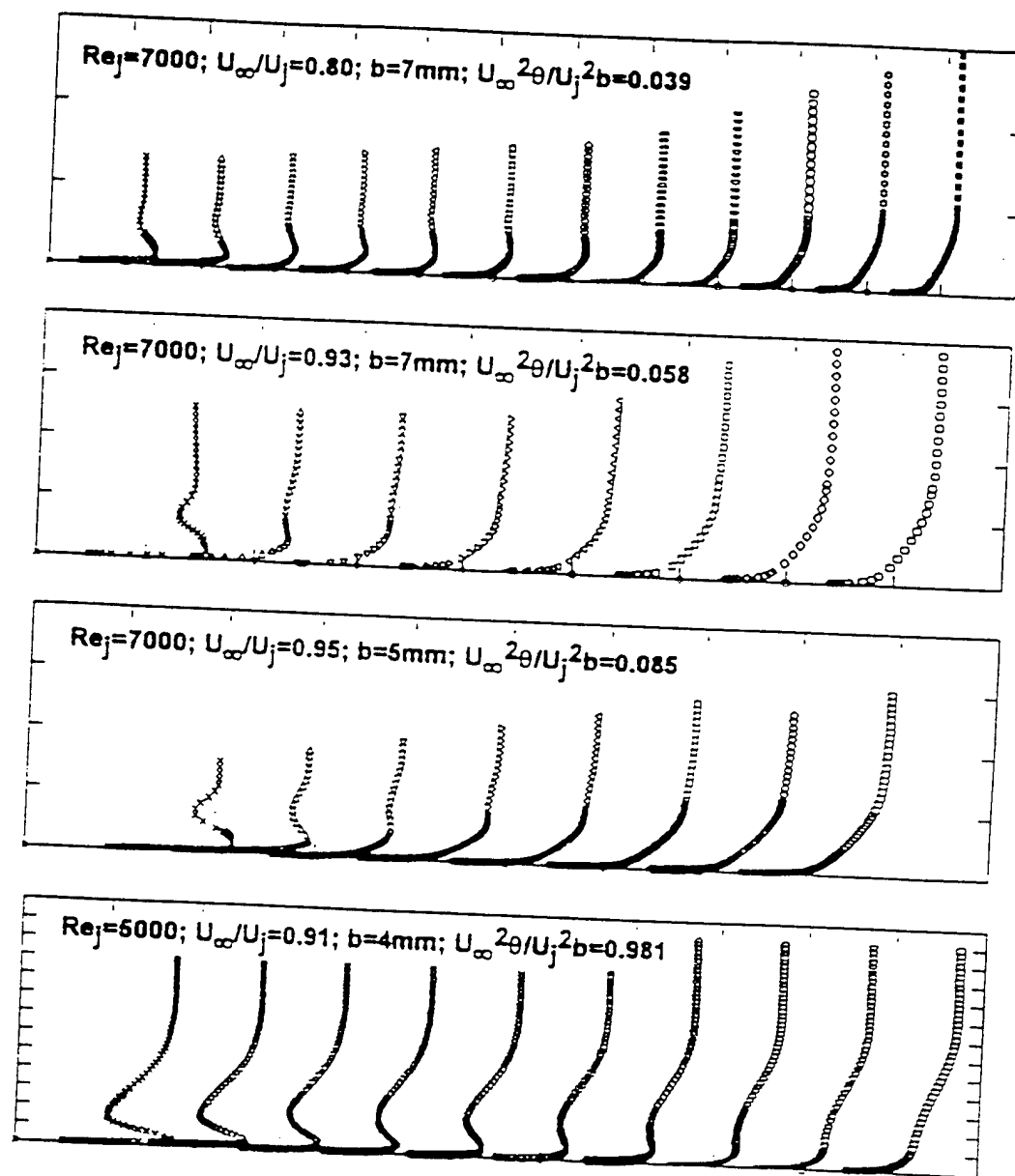
Figure 22. **Mean velocity distributions of the weak wall jets with** $U_\infty^2\theta/U_j^2b > 0.035$.

(b)

(a)
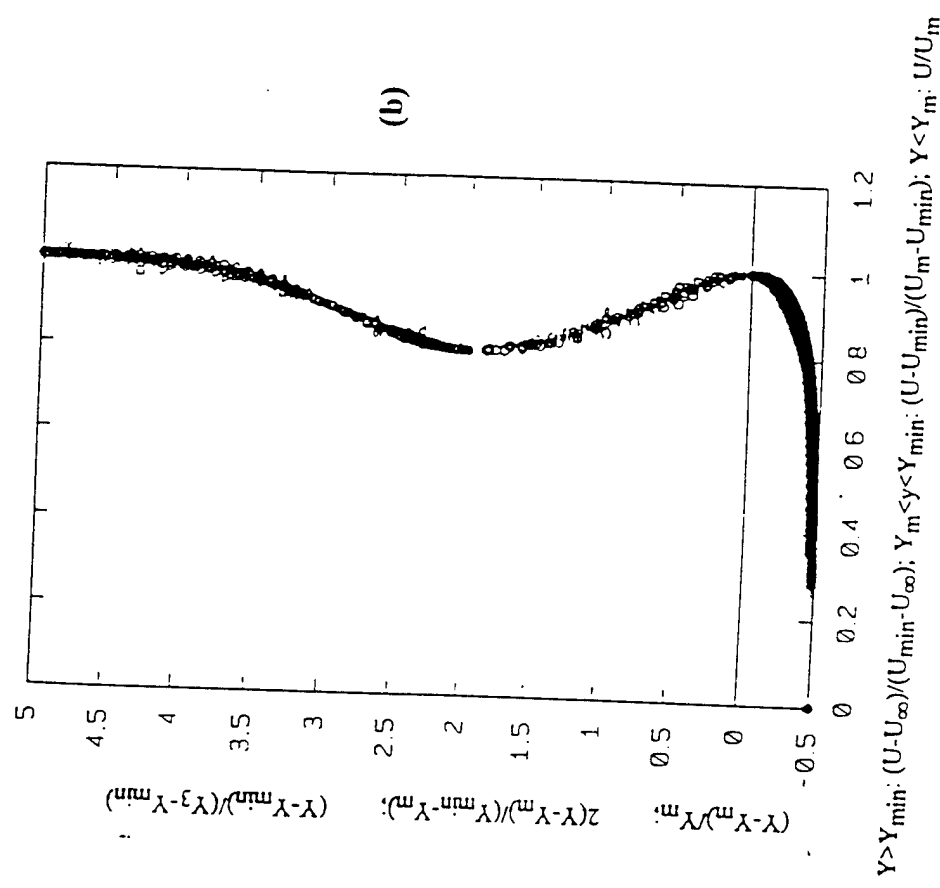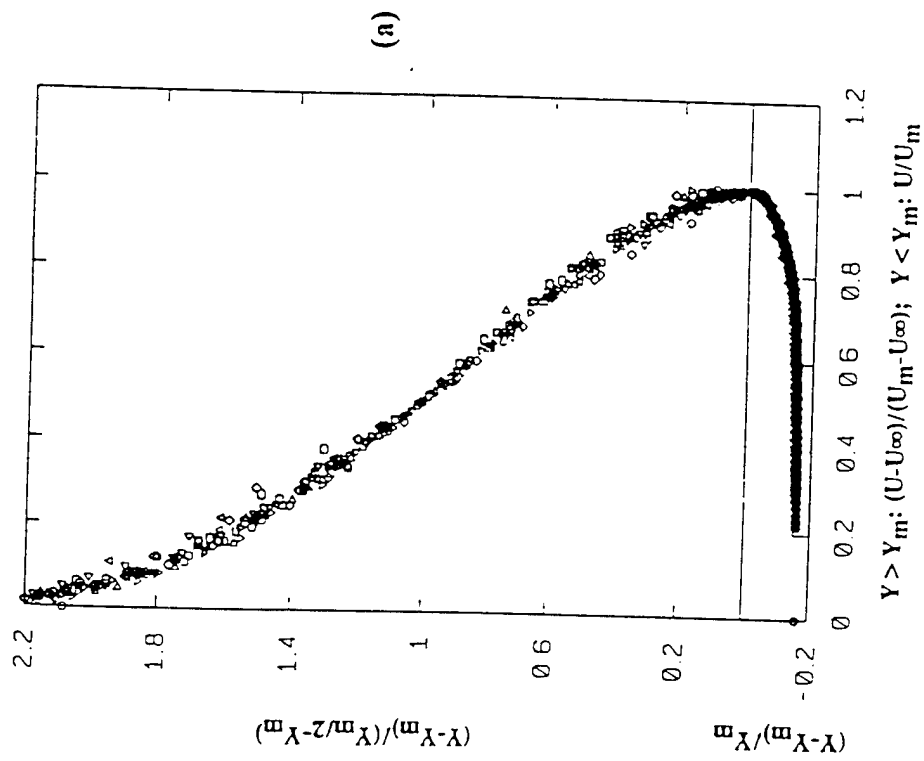
Figure 23. Normalized mean velocity profiles of the weak wall jets.
(a) normalized with two length scales and two velocity scales.
(b) normalized with three length scales and three velocity scales.
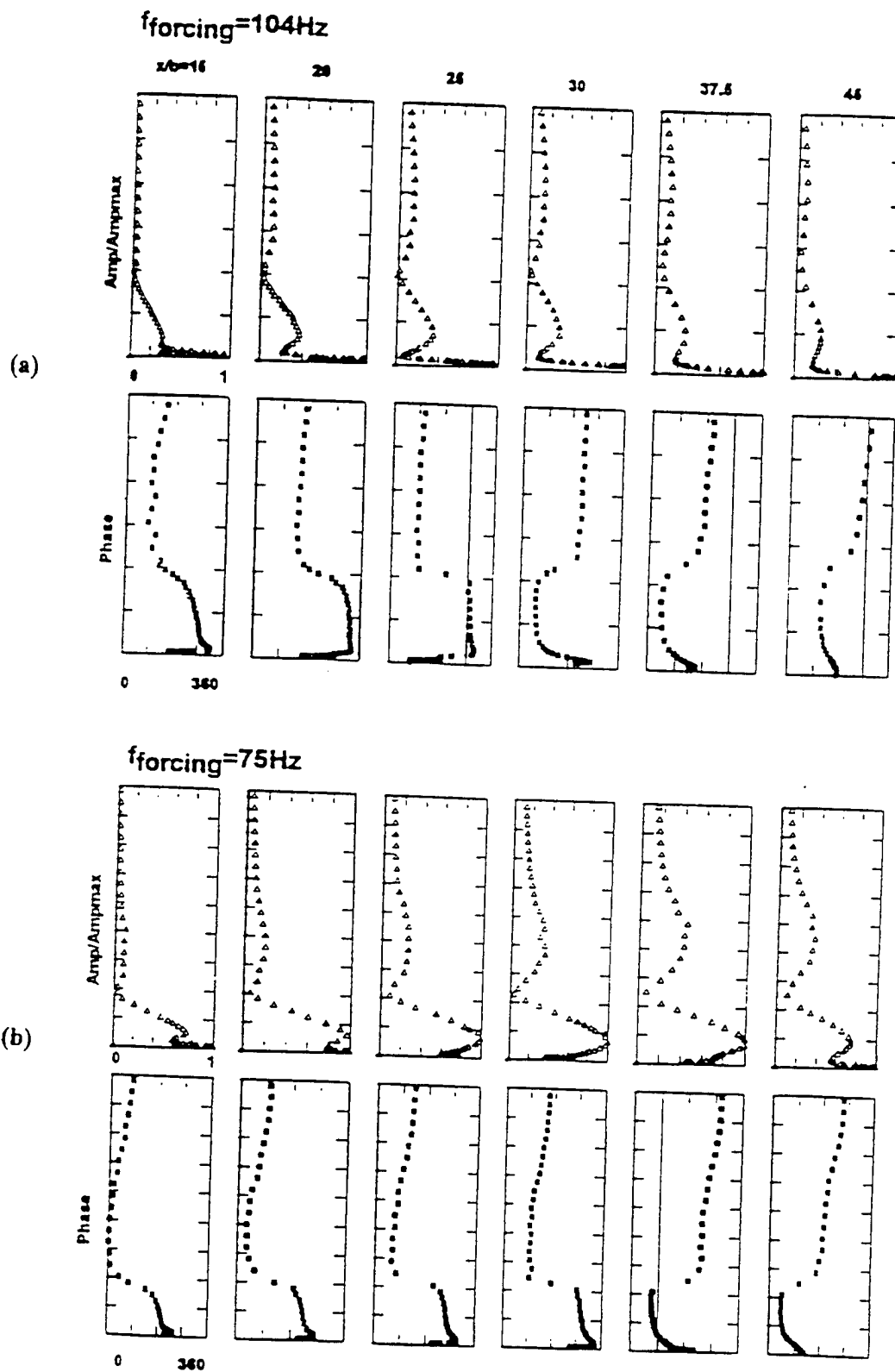
Figure 24   Normalized amplitude and phase distribution of the disturbances in a weak wall jet.
Rej=5000; U_∞/U_j=0.91; b=4mm;
(a) forced at 104 Hz.
(b) forced at 75 Hz.
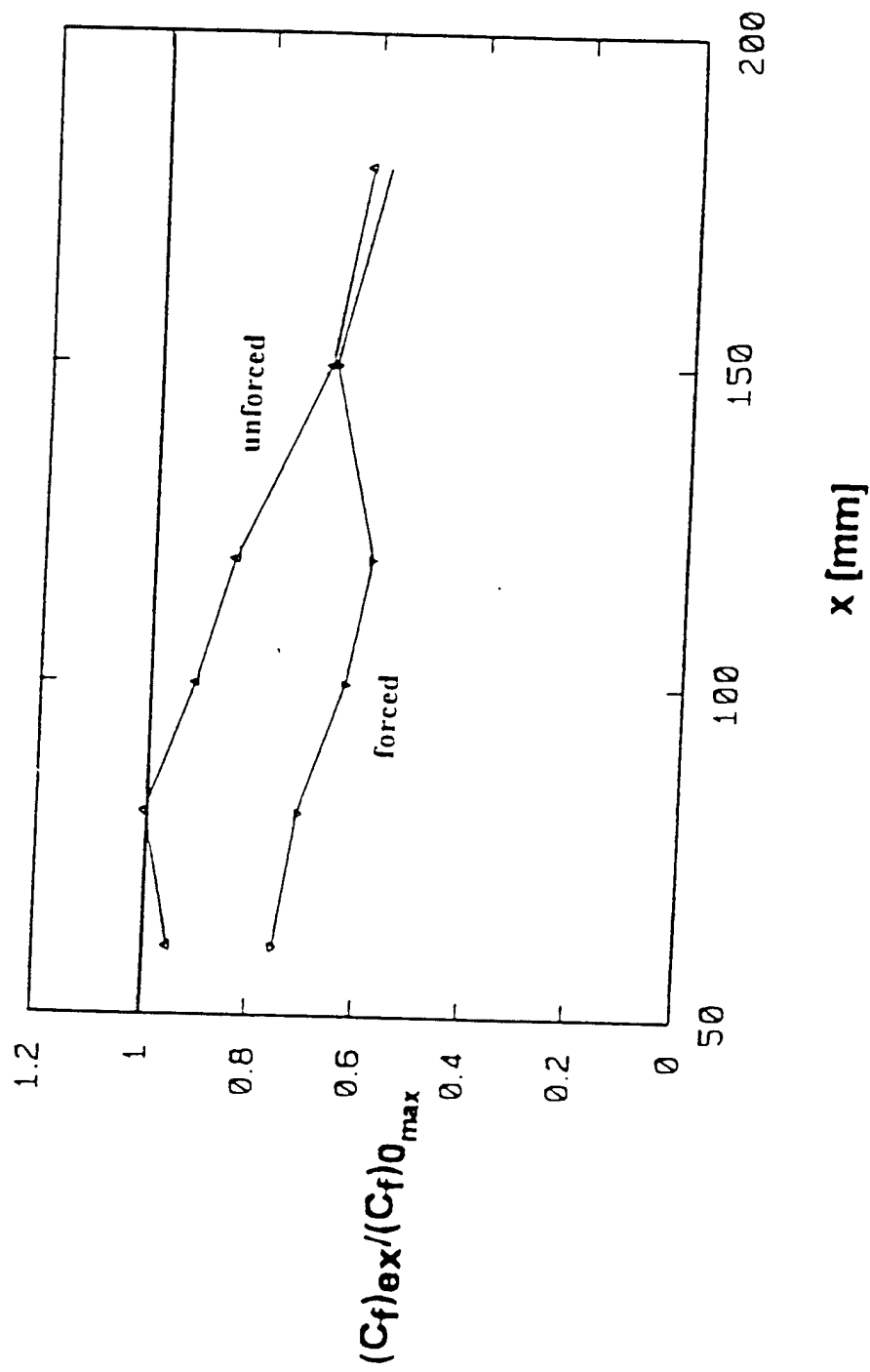
Figure 25. The skin friction reduction in a weak wall jet. Rej=5000; U_∞/Uj=0.91; b=4mm; f=104 Hz; Λ=7.5%.
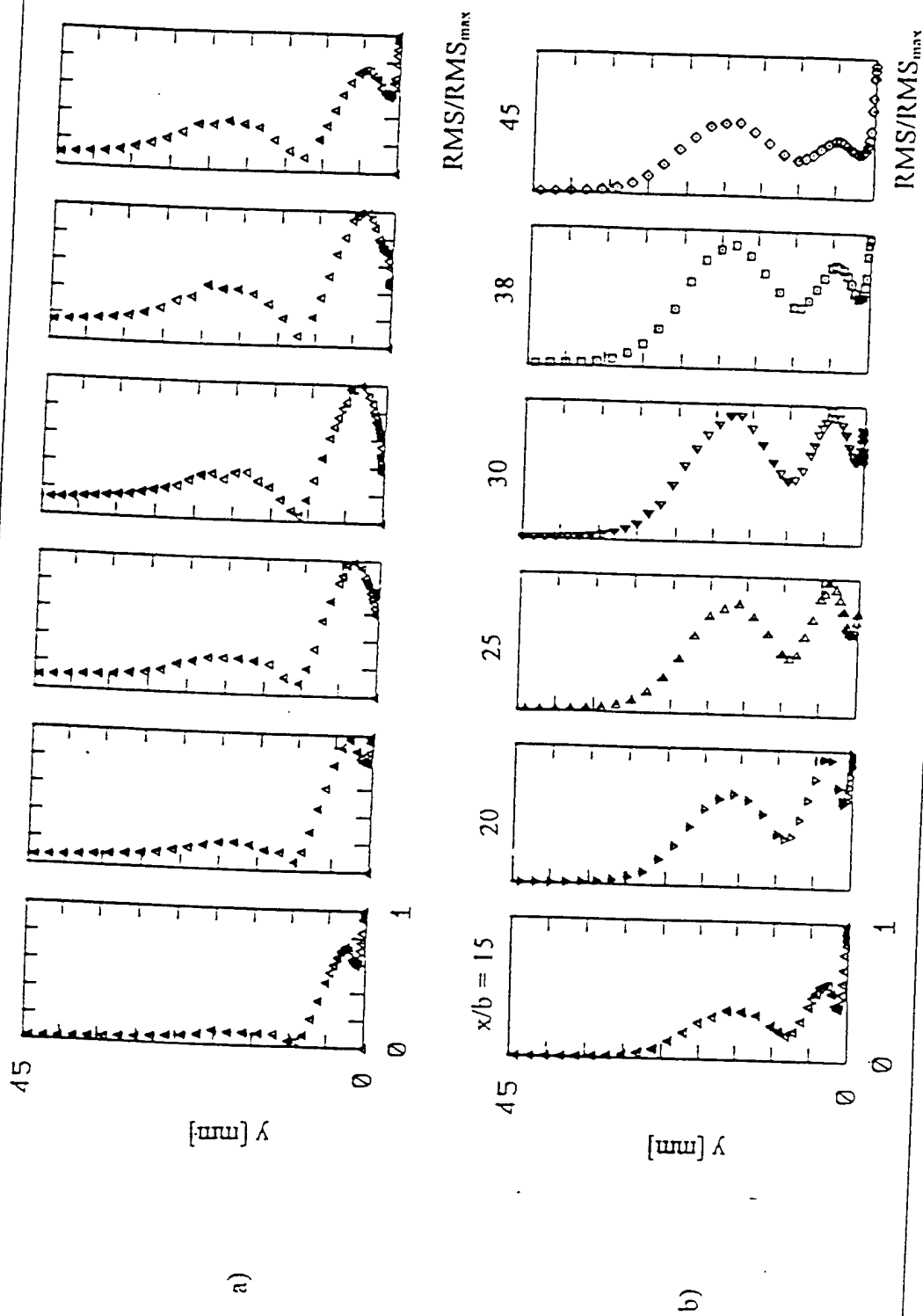
Figure 26. The normalized amplitude distribution in a weak wall jet, $Rej=5000$, $U\infty/Uj=0.91$, $b=4mm$, forced at $f=75Hz$, calculated by:
(a) the conventional phase-locked ensemble averaging procedure.
(b) the new triple decomposition technique - temporal pattern recongnition.

7. APPENDIX A
Papers in Publication

ON THE STABILITY OF A LAMINAR WALL-JET WITH HEAT TRANSFER

By: O. Likhachev, M.D. Zhou, A. Tumin, and I. Wygnanski

Aerospace and Mechanical Engineering Department
University of Arizona
Tucson, Arizona 85721, USA
&
Fluid Mechanics and Heat Transfer Department,
Faculty of Engineering, Tel-Aviv University
Ramat-Aviv. P.O.B. 39040, Tel-Aviv 69978, Israel
December 20, 1994

ABSTRACT

The flow of a plane, laminar, low speed and perfect gas wall jet, was investigated for two categories of heat transfer through the wall. In the first category the entire surface was maintained at a constant temperature which differed from the temperature of the ambient fluid, while in the second, a constant heat flux from or to the surface was maintained. The velocity and temperature distribution across the flow were calculated for both categories for a variety of temperature differences between the ambient fluid and the surface. The boundary layer equations representing these flows were solved by using the Illingworth-Stewartson transformation thus extending the classical Glauert's solution to a thermally non-uniform flow. The effects of heat transfer on the linear stability characteristics of the wall jet were assessed by making the "quasi-parallel flow" approximation. It was established that the inner, boundary layer type, mode of instability was sensitive to the temperature difference between the surface and the ambient fluid while the outer mode was not. Thus the balance existing between those modes in isothermal flow was altered by either heating or cooling. The possibility of various resonant interactions among plane modes was considered theoretically, in addition to some possible interactions among different planar and oblique modes. One, nonlinear interaction was investigated experimentally for the isothermal flow case and was proven to be valid. It is thus believed that additional scales, coexisting in a naturally perturbed wall jet, stem from such interactions.

1. INTRODUCTION

Wall jets are used extensively for boundary layer control and film-cooling. In the latter application jets absorb heat from the surrounding fluid and convect it downstream while concomitantly protecting the surface above which they flow. Consequently the temperature of the medium varies across the jet. Although the flow in these applications is mostly turbulent, laminar wall-jets are often investigated for reasons of clarity and relative ease of analysis. The present theoretical and experimental investigation represents such a case.

Two, linearly unstable modes coexist in the disturbed laminar wall-jet: one is associated with a boundary layer instability occurring in the vicinity of the wall, and the other with the inviscid, inflectional instability prevailing in the outer part of the flow (Chun and Schwartz, 1967; Tsuji et al, 1977; Mele et al, 1986; Cohen et al, 1992; Zhou et al, 1992). There is a disparity of scales between the two modes whereupon small scale disturbances prevail near the surface while the larger ones are dominant in the outer region. It is anticipated that the second order, non linear interaction among the various modes might explain observations made on coherent structures in the corresponding turbulent flow (Zhou et al; 1992) .

The self similar solution for the incompressible and isothermal wall jet (Glauert 1956) was used in the formulation of the steady flow problem, while the Orr-Sommerfeld equation provided the basis for the linear stability analysis. Compressible wall-jets were not analyzed in detail previously and their stability characteristics were never considered. One of the goals of the present investigation was to obtain a self-similar solution for a compressible wall jet which transports heat between the ambient fluid and the surface and to calculate the effects of the temperature gradient on the stability of the mean flow. Whenever possible, the analysis was validated by an experiment or the experimental observation was analized theoretically.

The experiments were carried out in the low turbulence wind tunnel at the University of Arizona. A detailed description of the facility and the experimental procedures used appears in the article of Zhou & Wygnanski 1993 and will not be repeated presently. Special precautions were taken in order to mainatain laminar flow. A muffler separating the blower from the jet facility was installed into the air-supply system and a sensitive heat exchanger provided the necessary temperature control in

the isothermal flow case. Thus the jet emerged from the nozzle with a "top-hat" velocity profile and the turbulence level at its core was less than 0.2%. The uniformity of the flow across the span was better than 2% and it was checked at numerous streamwise locations. Finally the temperature of the jet, the surface and the temperature of the ambient fluid were controlled separately and maintained within 0.1°C of one another. The placement of the wall jet in a close-loop wind tunnel eliminated the effects of room drafts but induced a free stream velocity whose magnitude did not exceed 5% of the local maximum velocity of the jet in the region of interest. The induced "free stream" velocity was subtracted from the data in the outer flow as suggested by Zhou and Wygnanski (1993) for the turbulent case. The slot width b, in the experiments presented was 3.2mm and the jet Reynolds number at the nozzle was $Re_j = 320$.

2. ANALYSIS OF THE SELF-SIMILAR, COMPRESSIBLE MEAN FLOW

Consider a laminar, plane jet of a perfect gas emerging horizontally from a thin slit in the surface and mixing with a quiescent, identical ambient gas which is maintained at a constant temperature T_0. The use of the boundary-layer approximation reduces the governing equations to the following form:

$$\frac{\partial \rho u}{\partial x} + \frac{\partial \rho v}{\partial y} = 0, \tag{2.1a}$$

$$\rho u \frac{\partial u}{\partial x} + \rho v \frac{\partial u}{\partial y} = \frac{\partial}{\partial y}\left(\mu \frac{\partial u}{\partial y}\right), \tag{2.1b}$$

$$\frac{\partial p}{\partial y} = 0, \tag{2.1c}$$

$$\rho u \frac{\partial H}{\partial x} + \rho v \frac{\partial H}{\partial y} = \frac{\partial}{\partial y}\left(\frac{\mu}{Pr}\frac{\partial H}{\partial y}\right) + \frac{\partial}{\partial y}\left(\left(1 - \frac{1}{Pr}\right)\mu \frac{\partial}{\partial y}\frac{u^2}{2}\right), \tag{2.1d}$$

where the origin of the jet and the coordinate system were made to coincide, the surface is located at $y = 0$, u and v denote the corresponding velocity components in the x and y directions respectively, p is the pressure, H is the total energy per unit mass of gas, ρ and μ denote the density and the dynamic viscosity of the fluid. The Prandtl number is: $Pr = \mu/\kappa c_p$, where κ is the thermal conductivity and c_p is specific heat at constant pressure. For the perfect gas under consideration the equation of state is given by:

$$p = (c_p - c_v)\rho T. \tag{2.2}$$

Since under most circumstances the specific heats c_p and c_v are approximately constant; the dimensionless total energy is:

$$\overline{H} = \overline{T} + \frac{(\gamma-1)}{2} M_0^2 \overline{u}^2, \tag{2.3}$$

where $\gamma = c_p/c_v$ and the enthalpy of the surrounding gas $I_0 = c_p T_0$ was chosen as the appropriate energy scale. The Mach number $M_0 = U/a_0$ is defined by the ratio between the characteristic velocity U (defined in Eq. (2.12)), and the speed of sound in the surrounding gas a_0 whose undisturbed density and viscosity are denoted by ρ_0 and μ_0 respectively. Equations (2.1) and (2.2) provide another important relationship in the absence of an external pressure gradient:

$$\rho T = \rho_0 T_0 = const. \tag{2.4}$$

By limiting the proposed solutions to small Mach numbers, one may drop the last terms on the right-hand side of Eq.(2.1d) and Eq. (2.3) which are both proportional to M_0^2. Moreover, the Prandtl number is approximately constant across the jet provided the temperature variations are not too large. The boundary conditions stemming from the geometry are:

$$y = 0: \quad u = v = 0;$$
$$y \to \infty: \quad u \to 0, \quad T \to T_0. \tag{2.5}$$

Additional boundary conditions for the energy equation are specified by the temperature of the surface or by the nature of the heat transfer through the wall.

The continuity equation (2.1a) enables one to introduce a stream function Ψ such that:

$$\frac{\partial \Psi}{\partial y} = \rho u,$$
$$\frac{\partial \Psi}{\partial x} = -\rho v. \tag{2.6}$$

In an attempt to broaden the self similar solution of *Glauert* (1956) to compressible and non-isothermal cases, we considered the possibility of the velocity $(u,v) \propto x^a$, the jet thickness $L \propto x^b$, and the temperature deficit $(T-T_0) \propto x^c$. New dimensionless variables were introduced

$$(u,v) = U(\overline{u}, \overline{v}),$$
$$\Psi = \mu_0 \overline{\Psi}, \tag{2.7}$$
$$\Delta T = (T-T_0) = T_0 \overline{t},$$

and a coordinate transformation

$$x = \frac{\mu_0 \overline{x}}{\rho_0 U},$$
$$\eta = \frac{(1-b)U}{\mu_0 \overline{x}^b} \int_0^y \rho \, dy. \tag{2.8}$$

was used. It will be shown that this transformation, which is similar to Illingworth-Stewartson transformation for the boundary layer, allows one to decouple the velocity and temperature fields reducing the transformed equations to the isothermal form provided the viscosity coefficient is proportional to temperature.

The dimensionless stream function $\overline{\Psi}$ chosen had the same form as Glauert's:

$$\overline{\Psi} = \overline{x}^{(1-b)} f(\eta),\qquad\qquad (2.9)$$

thus, by substituting Eqs. (2.8) and (2.9) into the x-momentum equation (2.1b) one gets:

$$(Cf'')' + ff'' + \alpha(f')^2 = 0,\qquad\qquad (2.10)$$

where derivatives with respect to η are denoted by a primes, while:

$C = \dfrac{\rho\mu}{\rho_0\mu_0}$ - is commonly referred to as the Chapman - Rubesin factor and,

$$\alpha = \frac{2b-1}{1-b}.\qquad\qquad (2.10a)$$

The boundary conditions become:
$$\eta = 0: \quad f = f' = 0,$$
$$\eta \to \infty \quad f' \to 0.\qquad\qquad (2.11)$$

Equation (2.4) yields $C = 1$ whenever $\mu \propto T$ reducing Eq. (2.10) to the isothermal case considered by *Glauert* (1956). This equation has a non trivial solution satisfying the boundary conditions (2.11) when $\alpha = 2$; from which it follows that $a = -1/2$, $b = 3/4$. Glauert's integral constraint, F, by being an invariant of the flow, enables one to define a characteristic velocity for this special case:

$$F = \int_0^\infty \rho u \left(\int_y^\infty \rho u^2 dy \right) dy = \left(\frac{\mu_0}{\rho_0} \right)^2 \frac{U}{40} = const.\qquad\qquad (2.12)$$

Another constraint is derived from the energy conservation equation whose integral form can be written as follows:

$$\int_s \rho H u_j n_j dS = \int_s \kappa \frac{\partial T}{\partial x_j} n_j dS + \int_s u_i \sigma_{ij} n_j dS,\qquad\qquad (2.13)$$

where subscripts i, j denote the components of the outward normal unit vector **n** in the x and the y directions respectively which are also parallel and perpendicular to the surface. The last term on the right-hand side of Eq. (2.13) represents the rate of dissipation of mechanical energy in the material volume of fluid bounded by S and it is negligible when compared to the first term for $M_0 \ll 1$ (σ_{ij} in this integral represents the stress tensor). The form of the self-similar solution of the energy equation thus depends on boundary conditions. We shall now consider three of the most important cases of a heat transfer through the wall.

(a) The Adiabatic Wall Problem

For the thermally insulated wall, the energy carried by the flow across the half plane bounded by $x>0$ is constant and equal to the energy released from the slit. Hence, Eq. (2.13) is reduced to the following form:

$$\int_0^\infty t f' d\eta = Q, \qquad (2.14)$$

where $Q = (1-b) h \rho_l u_l (T_l - T_0)/(\mu_0 T_0)$; the subscript l denotes initial values of the jet and t is the dimensionless, self-similar temperature deficit:

$$t(\eta) = \frac{(T - T_0)}{T_0} \cdot \bar{x}^{1/4}.$$

Eq. (2.1d) becomes:

$$\mathrm{Pr}^{-1} t' = -ft \qquad (2.15)$$

which can be solved subject to the condition that $t \to 0$ as $\eta \to \infty$ and thus:

$$t(\eta) = A \cdot Q \cdot \exp\left(-\mathrm{Pr} \int_0^\eta f d\eta\right), \qquad (2.16)$$

where

$$A = \left\{ \int_0^\infty f' \exp\left(-\mathrm{Pr} \int_0^\eta f d\eta\right) d\eta \right\}^{-1}.$$

(b) The Constant Wall Temperature Problem

Another self-similar solution is obtained when the surface temperature is kept at a constant level T_w. In this case the temperature deficit can be expressed by the following:

$$t(\eta) = \frac{(T - T_0)}{(T_w - T_0)}. \qquad (2.17)$$

Substituting (2.17) into the energy equation (2.1d) making use of the transformation given in (2.8) and the the definition of a stream function (2.9) gives a total differential equation for t :

$$\mathrm{Pr}^{-1} t'' = -ft', \qquad (2.18)$$

which is subject to the boundary conditions

$$\eta = 0: \quad t = 1,$$
$$\eta \to \infty: \quad t \to 0. \qquad (2.19)$$

The Eq. (2.18) is integrated directly by making use of Glauert's (1955) analytical solution to the Eq. (2.10) for $C = 1$ and by using the coordinate transformation:

$$z = \mathrm{Pr} \cdot \eta.$$

The solution has the form

$$t = 1 - g(z), \tag{2.20}$$

where g is a function of z defined in an implicit form:

$$z = \log \frac{\sqrt{(1 + g + g^2)}}{1 - g} + \sqrt{3} \tan^{-1} \frac{\sqrt{3}g}{2 + g}.$$

(c) The Problem of Constant Heat-Flux Through the Wall

Consider now the solution of the energy equation (2.1d) subject to constant heat flux through the wall q_w. Since the coordinate transformation (2.8) yields a solution for the hydrodynamic problem, the form of the temperature deficit is determined from the constraint given in Eq. (2.13), i.e.:

$$t(\eta) = \frac{(T - T_0)}{T_0 Q} \cdot \bar{x}^{-3/4}, \tag{2.21}$$

where $Q = q_w / (c_p \rho_0 U T_0)$ and $q_w = -\kappa(\partial T / \partial y)$ at $y=0$. Substituting (2.21) into (2.1d) while making use of (2.6)-(2.9) yields

$$\mathrm{Pr}^{-1} t'' = 3 f' t - f t'. \tag{2.22}$$

This equation must be solved subject to the boundary conditions:

$$t = \tau, \quad t' = -\mathrm{Pr} \quad (\eta = 0) \tag{2.23}$$

for numerous values of τ which yield:

$$\int_0^\infty t f' d\eta = 1.$$

3. THE CALCULATED VELOCITY AND TEMPERATURE DISTRIBUTIONS

Since the self-similar solutions of Eqs. (2.1) are based on a transformation of variables which extended Glauert's solution to non-isothermal wall-jets, an inverse coordinate transformation is required in order to get the velocity and temperature distributions in a physical space:

$$y = \frac{4\mu_0}{\rho_0 U} \cdot \bar{x}^{3/4} \int_0^\eta \left(1 + \Theta \bar{x}^\lambda \cdot t\right) d\eta, \tag{3.1}$$

where Θ, λ and $t(\eta)$ depend on the kind of the heat transfer process taking place at the wall. In the following discussion we shall be concerned with the flow over an isothermal plate held at a constant temperature T_w while the ambient fluid is at another temperature T_0. We shall also explore the influence of heat transfer and temperature

gradients on the linear stability of such wall-jets. Thus the parameters appearing in Eq. 3.1 become: $\lambda = 0$ and $\Theta = (T_w - T_0)/T_0$.

For the self similar wall jets discussed, the normalized forms of the velocity and temperature profiles are identical at all x-locations. The velocity and length scales chosen by Glauert (1956) were based on the conservation of the outer momentum flux F, defined in Eq. (2.12) leading to: $U = 40F\rho_0^2/\mu_0^2$ and $L = \mu_0/(\rho_0 U)$. The traditional velocity and length scales used in the linear stability analysis are simpler ones because the analysis assumes that the steady flow is, a priori determined. Thus conforming with the convention, we also chose the maximum velocity in the wall-jet, u_m, the outer transverse coordinate at which this velocity was reduced to 1/2 of its maximumvalue, $Y_{m/2}$, and the maximum temperature deficit, Θ, as being the appropriate scales of the problem. The calculated velocity and temperature-deficit distributions for different values of Θ and Prandtl number $Pr = 0.72$ are plotted in Fig. 1. The scales chosen to normalize these distributions correspond to the scales <u>calculated for isothermal flow</u> in order to emphasize their dependence on Θ. A quantitative assessment of the effect of Θ on the two relevant length scales in the jet, Y_m and $Y_{m/2}$ is made in Fig. 1a. The results indicate that a hot surface enhances the lateral rate of spread of the wall jet. It implies therefore, that a given loss of momentum causes a larger deceleration of the lower density fluid. Dimensionless profiles normalized by their own scales are plotted in Fig.2 in order to indicate the degree of distorsion generated by Θ. Even for these normalized profiles, cooling of the wall results in an increase of the velocity gradient close to surface. Furthermore, the distortion in the shape of the velocity profile is expected to have a mojor effect on the stability of the flow.

4. STABILITY ANALYSIS

(a) Method of solution

Linear stability analysis was carried out by assuming that the flow is locally parallel and the amplitude of the perturbation is small. These assumptions allowed us to describe the disturbances in terms of the usual linearized Navier-Stokes equations provided the rate of spread of the jet is slight.

When the disturbances are two-dimensional they have only two unknown velocity components, $\bar{u}(x,y,t)$, $\bar{v}(x,y,t)$, a pressure disturbance $\bar{p}(x,y,t)$ and temperature disturbance $\bar{\theta}(x,y,t)$. The particular solution of linearized Navier-Stokes equations is assumed to be of the form:

$$\bar{q}(x,y,t) = \hat{q}(y) \cdot e^{i(\alpha x - \alpha t)}, \qquad (4.1)$$

where $\hat{q}(y)$ belongs to the eigenvector representing the solutions of the linearized Navier-Stokes equations under the assumption of the locally parallel flow; α is complex while ω is real and represents a dimensionless frequency.

Making use of the linearized equations (2.1) and the particular form of the solution described in Eq. (4.1) as well as the local parallel-flow assumption (4.2), one gets the following set of six ordinary, first order differential equations:

$$\frac{dZ}{dy} = H_j Z, \qquad\qquad (4.3)$$

where H_j is a 6×6 matrix (its non-zero elements are presented in the Appendix) and Z is a six component column vector: $Z_1 = \hat{u}$, $Z_2 = \partial\hat{u}/\partial y$, $Z_3 = \hat{v}$, $Z_4 = \hat{p}$, $Z_5 = \hat{\theta}$, $Z_6 = \partial\hat{\theta}/\partial y$.

The set of equations (4.3) is solved subject to the boundary conditions:
$$y = 0: \quad Z_1 = Z_3 = Z_5 = 0;$$

$$y \to \infty: \quad |Z_j| \to 0, \quad (j = 1,...,6). \qquad (4.4)$$

by using a fourth order Runge-Kutta method with a Gram-Schmidt orthonormaliation procedure. Independent particular solutions of Eqs.(4.3) were obtained and the eigenvalues, α, were found by using a "shooting method" satisfying the boundary conditions (4.4).

(b) The stability of a wall-jet flowing over an isothermal surface which is maintained at a constant but different temperature than the fluid.

The curves of neutral stability ($\alpha_i = 0$) are shown in Fig.3a & b, where ω is plotted versus Re for different values of the parameter $\Theta = (T_w - T_0)/T_0$. The results of the computations for the cold surface $\Theta < 0$ are shown in figure 3a while the results for $\Theta > 0$ are plotted in figure 3b. At low Re there is one unstable mode which at high values of ω (i.e. near the upper branch of the neutral stability diagram) possesses a maximum amplitude of the streamwise velocity component, $|\hat{u}|_{max}$, near the surface (curve A) and is thus dominated by the conditions near the wall. The instabilities near the lower branch of the neutral stability curve are dominated by the inflection point in the outer part of the velocity profile and have their maximum amplitude in that region (B). Both amplitude distribution (A & B) are affected by viscosity due to the no-slip conditions at the surface. Cool surface has a strong effect on the upper branch of the neutral stability diagram dampening most of the high frequency perturbations. It has little effect on the critical Re which remains around $Re_{crit} \approx 60$ provided $\Theta \geq -0.2$.

At high Reynolds numbers (e.g. $Re > 430$ for $\Theta = 0$), the wall-jet possesses two, distinctly different unstable modes which are overlapping in the mid-range of the

unstable frequencies. The region of overlap depends mostly on Re but it is also dependent on the temperature of the surface; a cold surface shifts the region of overlap towards higher values of ω. Even in the region of overlap the sensitivity of each mode to viscosity (i.e. mainly to the "no slip" boundary condition at the surface) differs. The two amplitude distributions of the streamwise perturbations across the flow (corresponding to point C in figure 3a) reflect the dependence of the two modes on viscosity. The outer mode, C_{out}, which is mostly inviscid contains a secondary peak in amplitude close to the wall while the inner mode, C_{in}, contains a secondary peak close to the inflection point. There is also a disparity in scales between the two modes because each one propagates at its characteristic phase-velocity. The large-scale disturbances (corresponding to small ω) are the ones dominated by the inflection point in the outer flow. The second unstable mode starts at $Re_{crit.II} \approx 430$ for all $\Theta > -0.2$. Reducing the relative temperature of the plate below $\Theta = -0.2$, makes the inner layer even more stable and increases $Re_{crit.II}$ further. Consequently cooling between $0 > \Theta \geq -0.2$ increases only the frequency corresponding to $Re_{crit.II}$. At $Re < Re_{crit.II}$. there is an inner stable region which is completely contained within the unstable zone provided $\Theta > -0.175$. The size of this region in the Re-ω plane increases with decreasing Θ and for $\Theta < -0.175$ it joins with the stable zone existing above the upper branch of the main neutral curve. The existence of a small, stable, inner-region in the isothermal wall jet was reported previously by several authors (*Chun & Schwarz* 1967; *Tsuji et al.* 1977; *Mele et al.* 1986 and *Zhou et al.* 1992), and it is marked by a shaded zone on Fig. 3.The larger neutral zones caused by cooling are represented by hatched areas in figure 3a. The separation of the two modes at $\Theta < -0.175$ in the vicinity of $\omega = 1$ and Re=230 becomes thus clear.

The neutral stability diagrams for the flow over a heated wall (figure 3.b) are similar to the ones in the isothermal case except that the upper branches of the outer, neutrally stable modes are shifted toward higher frequency while the lower branches are unaffected. The broadening of the unstable region to higher frequencies at moderately low Re implies that heating destablizes the wall layer without affecting the outer flow. In this aspect the wall jet behaves like a heated laminar boundary layer in air. The first critical Reynolds number is not altered by the heating because it is dominated by the inviscid mode, but $Re_{crit.II}$. shifts towards higher values of *Re and lower* ω with increasing Θ.

One may compute contours of constant amplification, $-\alpha_i$, and constant phase velocity, $c = \omega / \alpha_r$ for each mode separately and superpose them in the (Re, ω) plane (Fig. 4a). For Re < 380 and $\Theta = 0$ both sets of α_i = const. coincide because only one

unstable solution exists in this region. At each Re however, there are two amplified waves of different ω (and therefore a different wave length λ) which propagate downstream at the same phase velocity. It is the phase velocity which may enable us to distinguish between the inner and outer unstable mode. Hence, when two waves propagate at identical phase speed, the one having a higher ω belongs to the inner unstable region whose amplitude distribution is similar to the distribution in a typical boundary layer. The ratio of frequencies of two amplified waves propagating together is commensurate with the ratio of widths of the relevant layers. The contours of constant c of either mode are represented by slightly curved inclined lines in the (Re, ω) plane regardless of the amplification rate. For example, the contour corresponding to c = 0.55 at high values of ω, represents decaying modes but it becomes tangential to the neutral stability curve around Re = 300 & ω = 1.62. The neighboring contour corresponding to c=0.53 represents an amplifying boundary layer mode between 160 < Re < 640. The corresponding lowest frequency contours of c = 0.55 & 0.53 represent amplifying modes also, provided the Reynolds number is small. In the vicinity of Re = 380, these two contours cross the inner, neutral stability loop and the modes they represent starts to decay.

There are however, decaying outer modes containing intermediate frequencies and propagating at the same phase speeds as the amplifying outer modes. These modes are within the amplified zone of the inner (boundary layer type) modes and therefore, the information conveyed in Fig. 4a about their rate of amplification is deceiving. The contours of constant c corresponding to the decaying modes in Fig. 4a have a negative slope suggesting that their frequency decreases with increasing Re while all the contours representing the amplifying modes have a positive slope.

Selective graphs showing the dependence of "c" on ω at constant values of Re are plotted in Fig. 4b. At low Re, the phase velocity decreases rapidly with increasing ω and it attains a minimum around $\omega \approx 0.7$ and increases with increasing ω. At high Re a separate viscous mode emerges whose phase velocity is low at low ω and it increases monotonically with increasing ω. One may observe, three values of ω at which the curves representing the propagation of a given mode intersect a horizontal line representing a locus of constant phase velocity. Near the high and the low frequency intersections, an increase in Re results in a corresponding increase in the crossing frequency, the trend is reversed around the mid range crossing locations (see Fig. 4b). The mid frequency crossing corresponds to the decaying outer mode. Since the different modes are tagged differently in Fig. 4a one is able to distinguish between them at higher Reynolds numbers.

It is worth noting that a constant frequency wave, propagating in the direction of streaming in a laminar wall jet crosses this stability diagram as Re^5 (i.e. ω increases rapidly with increasing Re; see Fig. 4a) . This is because Glauert's solution predicts that $Re \propto x^{1/4}$ while $\omega \propto x^{5/4}$. Thus, the width and characteristic velocity of the wall jet at the location at which a constant frequency perturbation is introduced determines the nature of the instability (i.e. whether it is inner or outer) in the range of of streamwise distances of interest. The propagation velocity of the amplifying outer modes decreases initially with increasing streamwise distance, but as the inner modes take over the propagation velocity starts to increase with x.

There are numerous possibilities of inter-modal interactions in two dimensions, as the inner and outer modes may propagate at the same speed and possibly exchange energy. One may specifically consider the phase velocities of the two independent modes near the upper branches of the neutrally stable modes, because these neutral waves have undergone the highest linear amplification possible. Furthermore, a triad resonance is probable when all three participating waves (i.e. two input waves and one resultant wave) possess a frequency ratio represented by simple, comensurate numbers (e.g. $\omega_1 + \omega_2 = \omega_3 \rightarrow 1+2 = 3$). The vertical line-segment drawn in Fig. 4a prescribes the conditions for a possible occurance of intermodal resonance. A likely scenario appears near Re = 380 where two linearly amplified modes propagating at the same phase velocity posses a frequency ratio of 1:3 generating an output wave having a frequency of 2. This possibility was investigated experimentally and will be discussed later.

The amplification rates of the disturbances are shown in Fig.5 for different values of Θ, and for three Reynolds numbers: Re = 300 ,957 & 2000. At the low Reynolds number there is just one unstable region at $\omega > 0.25$ provided $\Theta > -0.075$ (see insert in figure 5a). At $-0.18 < \Theta < -0.075$ there are two non overlapping, unstable modes and at $\Theta < -0.18$ only the outer mode remained amplified (see also Fig. 3a). The high frequency extent of the amplified region (e.g. $\omega > 1$) and its rate of amplification, $-\alpha_i$, are significantly affected by Θ. One may thus deduce that the amplification of the inner mode, which is correlated with the instability at large ω, is very sensitive to the temperature differential between the ambient fluid and the surface while the outer mode is not. This effect is also very obvious at larger Re where stronger cooling is needed to suppress the inner mode. For example: at Re = 957 & Θ = -0.2 both modes are unstable in the range of $0.55 < \omega < 1$ while the jet is unstable to either mode between $0.2 < \omega < 1.05$. At Re=300 & Θ = -0.2, the wall jet is unstable to a single mode and only a narrow band of frequencies between $0.2 < \omega < 0.6$ is amplified (Fig. 5). Heating

enhances the amplification rate of the inner layer and broadens the range of the amplified, high-frequency perturbations in the flow (compare the neutral curves for $\Theta = 0$ and $\Theta = 0.3$ at large ω in figures 3 & 5). At a moderate Reynolds number, the heated wall jet at $\Theta = 0.3$ becomes unstable to two distinct modes because a decaying mode having a frequency $\omega \approx 0.45$ crossed the $-\alpha_i = 0$ axis at Re = 777 and thus became amplified. The single mode existing at lower Re "cusped" and split into two amplified overlapping modes. generating a new $Re_{cnt,II}$ (see insert in figure 5b). A similar "cusping" occurs when the surface is cooled to $\Theta < -0.075$ at Re = 300 (insert in figure 5a). The influence of cooling or heating on the stability of the flow was expected in view of the experience accumulated in boundary layers but the generation or the suppression of secondary modes is novel.

At a high Reynolds number and for a highly cooled surface (e.g. Re=2000 & $\Theta = -0.3$) the "boundary layer" mode is eniterly embedded inside the unstable "outer mode". Both modes are amplified at dimensionless frequencies ranging from $0.41 < \omega < 0.77$ while the outer mode is amplified between $0.1 < \omega < 1.04$. The amplitude distributions of $|\bar{u}|$ corresponding to the neutral amplification points "A" & "B" of the "boundary layer" mode and to the amplified points "C" & "D" of the "inviscid mode" occuring at the same ω as "A" & "B" (i.e. at $\omega = 0.41$ & 0.77), are also plotted on Fig. 5c. The distributions of $|\bar{u}|$ corresponding to each pair of points are similar. Maximum amplitude occurs either next to the surface (for "A" & "B") or close to the outer inflection point.

(c) Stability of wall-jet having a constant heat flux from the surface.

The linear stability of the wall jet with a constant heat flux from its surface was also investigated. The method of analysis is similar to the isothermal case for whch $\Theta \neq 0$. The coordinate stretching parameters appearing in Eq. (3.1) are $\lambda = 3/4$ and $\Theta = Q$ (see also Eq. 2.21), thus, the self-similar shape of the velocity and temperature profiles depends on the streamwise distance $\bar{x}$. At constant value of Q the stability diagrams also depend on $\bar{x}$ and therefore, the neutrally-stable curves shown in Figure 6 were plotted for constant products of $Q \cdot \bar{x}^{3/4}$. The values of $Q \cdot \bar{x}^{3/4} = -0.04; -0.03; -0.02; 0$ & 0;0.6 were chosen because they correspond to the values of the local wall temperature deficit Θ (-0.2, -0.15, -0.1, 0.0 & 0.3) calculated for the isothermal wall shown in Fig.3. Qualitatively the two flows behave alike, heating the fluid destabilizes the layer near the surface and cooling it enhances its stability. It appears, however, that the effect of heat transfer on the flow is more significant when a constant heat flux condition to or from the surface is maintained.

5. SOME EXPERIMENTS ON PLANE, WAVE INTERACTION

The results presented are but a small part of an investigation whose main purpose is to understand and control the turbulent wall jet at high Reynolds numbers. The experimental exploration of resonance in laminar flow was carried out in support of observations made in the turbulent flow by Zhou et al. (1993). Although the data is incomplete, it validates the hypothesis proposed in conjunction with the calculations presented in Fig. 4. The experiments were carried out in the absence of temperature gradients by ensuring that the temperature in the wind tunnel and in the jet were identical (i.e. that $\Theta = 0$). This also eliminated the need for instantaneous compensation for temperature fluctuations when hot-wire anemometers were used.

Periodic excitation was introduced in the settling chamber of the jet and the input signal provided phase-reference data acquisition. The amplitude of the ensuing velocity perturbation was calibrated at the nozzle, the velocity distributions elsewhere in the flow were phase-locked to the input perturbation and ensemble-averaged. Fourier transforms were used to obtain the specific amplitudes at the frequencies of interest.

Placing the wall jet in a close-loop wind tunnel induced in the test section a slow, uniform stream which did not exceed 5% of the jet velocity. The induced "free stream" velocity was excluded from the data by subtracting it from the outer part of the normalized profiles using the following relation:

$$\overline{U} = \frac{U - U_\infty}{U_{max.} - U_\infty}$$

which enabled us to compare the measured $\overline{U}$ with Glauert's theoretical profile. The normalized mean velocity profiles for the unperturbed flow are plotted in Fig. 7 together with the profile calculated by Glauert and the agreement between the two is excellent. Forcing the flow at frequencies corresponding to the outer, shear-layer mode did not distort the velocity profiles provided the initial forcing level did not exceed 1% of the jet efflux velocity. The spreading rate of the jet was hardly affected by this type of forcing. At forcing frequencies corresponding to the inner eigenmodes, the forcing level had to be curtailed to 0.5% in order to reduce the distortion caused to the mean flow. Even so, the spreading rate of the jet was increased by the external excitation.

Triad resonance may occur when: $\omega_1 + \omega_2 = \omega_3$ and $\alpha_1 + \alpha_2 = \alpha_3$. A sufficient condition, therefore, is to find three waves having the same phase velocity. After

examining the calculations shown in Fig. 4 it became clear that around Re = 380, two linearly amplified waves, belonging to different modes would have undergone the maximum spatial amplification possible. The approximate dimensionless-frequencies, $\omega = fY_{m/2} / U_m$, of these waves are $\omega_i \approx 0.5$, and $\omega_j \approx 1.5$ and their common phase velocity is around $c = \beta / \alpha_r \approx 0.54$. We have, thus initiated a series of experiments in which the wall jet was excited by two frequencies (15 Hz and 45 Hz) having a ratio of 1:3. The jet was initially excited by each frequency independently (Fig. 8) in order to verify that the excitation corresponds to the two modes discussed in section 4 (see also Tumin and Zhou 1995) in the range of 300 < Re< 450. It was also verified that the velocity distribution in the jet was not distorted and that each of the excited modes had undergone the maximum linear amplification possible around Re = 380. The jet was then excited by the same two frequencies simultaneously and the results were also plotted in figure 8. The rate of spread of the wall jet changed somewhat under the combined amplitude of forcing but the results were not materially different provided Re < 410.

Power spectra of the ensuing waves were measured at various distances from the nozzle in search of a frequency corresponding to the difference between the two input modes (i.e. for $\omega_2 \approx 1$). A successful result is shown in Fig. 9. In this case a strong peak in the spectrum appeared at 30 Hz in the inner layer (i.e. at $y=0.3Y_m$) and it prevailed over a fairly long streamwise distance (up to x/b = 30 or Re $\approx$ 600, see figure 9b.) . Only the lower forcing frequency of 15 Hz was observed in the outer region of the jet around $y= 0.8 \ Y_{m/2}$ (Fig. 9a). When the jet was excited simultaneously by two incommensurate frequencies of 15Hz and 50Hz a subharmonic frequency of 25Hz and a difference frequency of 35Hz appeared briefly in the inner and outer regions respectively, around Re=350.

To check that the resonance conditions were actually satisfied, the wave lengths and phase velocities of the traveling disturbances of all the three frequencies involved were measured. This was done by moving a hot-wire probe in the streamwise direction and recording the phase-locked velocity signals at short streamwise intervals (Fig. 10a). The three waves satisfied the resonance conditions in the inner region of the flow by propagating at the same phase velocity of 0.64 m/s., which corresponds to c = 0.55 (Fig. 10b). In the outer region of the flow (i.e. at $y > y_{m/2}$) the same three waves propagated at different speeds and did not resonate.

The most important feature of the resonance is the abrupt amplification of all the three waves involved, inspite of the fact that at least one of them should decay according to the linear stability calculations. The amplitudes plotted in Fig. 11 represent

the filtered, phase-locked portion of the streamwise velocity component integrated across the flow. The actual levels of the periodic motion of each of the three waves participating in the resonance is shown in Fig. 11a. The amplitude of all three waves increased quite suddenly around x/b=16. The amplitude of the 45 Hz wave stopped increasing thereafter, while the amplitude of the 15 Hz wave resumed its natural growth after a short hiatus.

The results shown in Fig. 11b represent the spatial amplification of the 30 Hz wave relative to its base location at x/b=10 when the flow was forced either by the 45 Hz wave, or by the 15 Hz wave, or by both of them simultaneously. The energy contained in the 30 Hz wave was amplified by a factor of 28 between x/b=10 and x/b=20 due to the resonance caused by forcing the flow at the other two frequencies simultaneously. It did not undergo any amplification when the wall jet was forced at 45 Hz but it did benefit from the excitation at 15 Hz. In the latter case, the 30 Hz wave was amplified by a factor of 12. This amplification indicates that the excited wave at 15 Hz attained a finite amplitude around x/b=15 and generated its own hamonic component.

The simultaneous gain of kinetic-energy by all three waves involved in the resonance could only have come from the mean motion. Thus the streamwise development of the energy thickness, representing the loss of energy in the mean motion, was calculated from the mean velocity profiles. Once again the data were normalized by the conditions at x/b=10 which was considered as a reference cross section for these observations. There was an abrupt increase in the energy thickness $\delta_3 = \int\limits_0^\infty \dfrac{u(u_j - u)^2}{u_j^3} dy$ based on the jet efflux velocity at the nozzle around x/b=16. This proved that energy was extracted from the mean flow to the three coherent waves involved in the triad resonance (Fig. 12). There was a concomitant loss of normalized, mean momentum in the jet but hardly an increase in its displacement thickness.

The amplitude distributions of the disturbances measured across the flow at x/b=16 are plotted in Fig. 13. The normalized distribution of the amplitude of the 15 Hz wave was not affected by the presence or absence of the of the 45 Hz wave and vice versa (Figs. 13a & b). The 15 Hz wave has its maximum amplitude near $y/Y_{m/2} = 1$ while the 45 Hz wave has it near $y/Y_{m/2} = 0.2$, suggesting that the former represents the shear layer instability of the outer flow while the latter resembles the boundary layer type of instability. The amplitude distribution of the 30 Hz wave (Fig. 13c) has two equal maxima, one occuring at $y/Y_{m/2} = 0.2$ while the other at $y/Y_{m/2} = 0.8$, suggesting that it is not a linearly evolving mode of instability. The amplitude

distribution of the 30 Hz which was generated by finite amplitude forcing at either 15Hz or 45Hz was different.

CONCLUSIONS

The present analysis indicates that the velocity distribution in a wall jet and its sensitivity to small disturbances are affected by the temperature differential across it. Thus, the flow in a non isothermal wall jet is tied to heat transfer. Two kinds of unstable eigenmodes are present in the flow, one is associated with the outer flow and resembles a free, shear-layer instability while the other is associated with the inner flow region and resmbles a boundary layer instability. However, these modes can not be separated in a clear way since both of them are affected by the no-slip-condition at the surface. The effects of heating or cooling the surface are first and formost felt in the inner layer where the wall jet is sensitive to the high frequency, periodic perturbations. One may state that heating a wall jet in air destabilizes the region near the surface while cooling stabilizes it. However, since the first critical Reynolds number is determined by the instability of the outer region, it is insensitive to the temperature differential prevailing across the wall jet.

Linear stability theory can be used to chart possible routes to transition by providing the basis for secondary instabilities and resonant interactions between plane and oblique waves (Craik, 1971) or between different plane waves as was considered presently. We investigated the possible effect of Θ on the plane, intermodal resonance mechanism and proved its existence experimentally for $\Theta = 0$. In this case the most probable interaction anticipated was to occur between waves having a frequency ratio of 1:3 generating a wave of 2ω as a result. Heating the surface broadend the range of the high frequencies at which the flow was unstable thus shifting the possible resonance conditions to higher frequency ratios. Calculations show that the most probable interaction for $\Theta = 0.2$ might occur between waves having a frequency ratio of 1:4. at Re $\approx$ 600. This makes the probability of such interactions less likely because the disparity of scales involved. Cooling, on the other hand, quenches the range of frequencies to which the jet is unstable and favors the occurance of a subharmonic resonance at lower Reynolds numbers. Expansion of the analysis to slightly divergent flows may make the prediction of resonant interactions more deterministic. One may also find it attractive to replace the traditional, dimensionless frequency ω which changes rapidly with Re$_x$ by one which is independent of x (i.e. $\hat{\omega} = f v^3 / J^2$ where J is the kinematic jet momentum).

We have also considered the possible existence of resonant triads between two-dimensional and oblique waves (see Craik, 1971) in the wall jet and the effect of Θ on them. The results of these calculations were not discussed in the present manuscript because of the lack of an appropriate experiment, however the effect of Θ on this mode of nonlinear interaction is significant. Among the many possibilities considered theoretically, there are also intermodal interactions between plane and oblique waves and those may lead to ejections in the form of Λ - type vortices observed in boundary layers (Saric ...). In the immediate future we plan to concentrate our efforts to document the effects of Θ on the evolution of instabilities in laminar wall jets and on the evolution of coherent structures in turbulent ones. The construction of two experimetal apparati was recently completed: one for the investigation of the flow over a heated or cooled surface which is maintained at a constant temperature while the other provides a constant heat flux to or from the surface. The experimental techniques required to analyze these two boundary conditions are very different and necessitated the construction of separate experimental rigs. We hope to examine the validity of the "Reynolds analogy" so widely used in predicting turbulent, convective heat transfer and to indicate ways for a possible control of the process.

ACKNOWLEDGMENTS

APPENDIX

Non-zero elements of the matrix H_s

The general case of three-dimensional disturbances propagating in 3D boundary layers was presented by *Nayfeh* (1980). In this context, we were interested only in a two-dimensional flow and in the non-zero elements of the matrix H_s defined by the equations below. We denote the ratio of the second viscosity to the first one as e and introduce $r = 2(e+2)/3$; $m = 2(e-1)/3$; $D = d/dy$; γ - specific heat ratio. The subscript s denotes the profile of the base flow (in this case the extended Glauert's solution). $\mu'_s = d\mu_s/dT_s$. H^{ij} denotes an i,j-th element of the matrix H. We denote

$\hat{\omega} = \omega - \alpha U_s; \quad \chi = \left(R/\mu_s - ir\gamma M^2 \hat{\omega} \right)^{-1}$. Thus, non-zero elements of the matrix H_s are written as:

$$H_s^{12} = H_s^{56} = 1;$$

$$H_s^{21} = \alpha^2 - i\hat{\omega} R/(\mu_s T_s);$$

$$H_s^{22} = -D\mu_s/\mu_s;$$

$$H_s^{23} = -i\alpha(m+1) DT_s/T_s - i\alpha D\mu_s/\mu_s + RDU_s/(\mu_s T_s);$$

$$H_s^{24} = i\alpha R/\mu_s + (m+1)\gamma M^2 \alpha\hat{\omega};$$

$$H_s^{25} = -\alpha(m+1)\hat{\omega}/T_s - D(\mu_s' DU_s)/\mu_s;$$

$$H_s^{26} = -\mu_s' DU_s/\mu_s;$$

$$H_s^{31} = -i\alpha;$$

$$H_s^{33} = DT_s/T_s;$$

$$H_s^{34} = i\gamma M^2 \hat{\omega};$$

$$H_s^{35} = -i\hat{\omega}/T_s;$$

$$H_s^{41} = -i\alpha\chi(rDT_s/T_s + 2D\mu_s/\mu_s);$$

$$H_s^{42} = -i\alpha\chi;$$

$$H_s^{43} = \chi\left[-\alpha^2 + i\hat{\omega} R/(\mu_s T_s) + r D^2 T_s/T_s + r D\mu_s DT_s/(\mu_s T_s) \right];$$

$$H_s^{44} = -ir\gamma\chi M^2 \left[\alpha DU_s - \hat{\omega} DT_s/T_s - \hat{\omega} D\mu_s/\mu_s \right];$$

$$H_s^{45} = i\chi\left[r(\alpha DU_s)/T_s + \alpha\mu_s' DU_s/\mu_s - r\hat{\omega} D\mu_s/(\mu_s T_s) \right];$$

$$H_s^{46} = -ir\chi\hat{\omega}/T_s;$$

$$H_s^{62} = -2(\gamma-1)M^2 \Pr DU_s;$$

$$H_s^{63} = -2i(\gamma-1)M^2 \Pr(\alpha DU_s) + R\Pr DT_s/(\mu_s T_s);$$

$$H_s^{64} = i(\gamma-1)M^2 \Pr R\hat{\omega}/\mu_s;$$

$$H_s^{65} = \alpha^2 - iR\Pr\hat{\omega}/(\mu_s T_s) - (\gamma-1)M^2 \Pr\mu_s'(DU_s)^2/\mu_s - D^2 \mu_s/\mu_s;$$

$$H_s^{66} = -2D\mu_s/\mu_s;$$

REFERENCES

***

?????

A-1. Zhou,M.D.;Elsberry,K. & Wygnanski,I.: The forced turbulent wall jet in an external stream. Proc.APS, Albuquerque,1993.

A-2. Tumin,A. and Zhou,M.D.: Eigenmode analysis in the laminar wall-jet. Submitted to J.Fluid Mech.

***

Chun, D.H. and Schwarz, W.H. 1967 Stability of the plane incompressible viscous wall jet subjected to small disturbances. *Phys. Fluids.* V. 10, pp. 911-915.

Cohen, J., Amitay, M. and Bayly, B.J. 1992 Laminar-turbulent transition of a wall jet flows subjected to blowing and suction. *Phys. Fluids A*, V. 4, pp. 283-289.

Craik, A.D.D. 1971 Nonlinear resonant instability in boundary layer. *J.Fluid Mech*, V. 50, pp. 393-413.

Gaster, M. 1974 On the effects of boundary-layer growth on flow instability. *J.Fluid Mech*, V. 66, pp. 465-480.

Glauert, M.B. 1956 The wall jet. *J.Fluid Mech*, V. 1, pp. 625-643.

Kelly, R.E. 1967 On the stability of an inviscid shear layer which is periodic in space and time. *J.Fluid Mech*, V. 27, pp. 657-689.

Mele, P., Moganti, M., Scibila, M.F. and Lasek,A. 1986 Behaviour of wall jet in laminar-to turbulent transition. *AIAA J.*, V. 24, pp. 938-939.

Nayfeh, A.H. 1980 Stability of three-dimensional boundary layers. *AIAA J.*, V. 18, pp.406-416.

Tsuji, Y., Morikawa, Y., Nagatani, T. and Sakou, M., 1977 The stability of a two-dimensional wall jet. *Aeronautical Quarterly.* V.XXVIII, pp. 235-246.

Zhou, M.D., Rothstein, J. and Wygnanski, I. 1992 On the hydrodynamic stability of the wall jet. *11th Australasian Fluid Mech. Conference*, pp. 407-410.

Zhou, M.D.and Wygnanski, I. 1993 Parameters governing the turbulent wall jet in an external stream. *AIAA J.*, V. 31, pp. 848-853.

FIGURE CAPTIONS

Fig. 1 Dimensionless velocity $u/(u_m)_{iso}$ and temperature $(T-T_0)/(T_w-T_0)$ profiles for different values of the wall temperature deficit $\Theta = (T_w - T_0)/T_0$.

Fig.2 Dimensionless velocity $u/(u_m)_{iso}$ and temperature $(T-T_0)/(T_w-T_0)$ profiles normalized by their own scales for values of Θ ranging from -0.2 to 0.3.

Fig.3 Neutral stability diagrams for a wall-jet flowing over a constant temperature surface. The various curves correspond to different values of $\Theta = (T_w - T_0)/T_0$.

Fig.4 (a) Contours of constant amplification and phase velocities when $\Theta = 0$.

(b) The variation of the phase velocities with ω at constant Re

Fig.5 Amplification rates of the disturbances for different values of the parameter Θ at three Reynolds numbers: a) - 300, b) - 957, c) - 2000

Fig.6 Neutral stability diagrams for the jet flowing over a constant flux surface.

Fig.7 The mean velocity distribution in a laminar wall jet comparison with experiment

Fig.8 The occurance of resonancebetween inner and outer modes at $\Theta=0$.

Fig.9 Some measured spectra in the jet indicating a possible resonance

Fig.10 The wave length and the phase velocity of a resonating triad.

Fig.11 The integrated energy contained in the various waves participating in the resonance.

Fig.12 The variation of the energy thickness in the direction of streaming

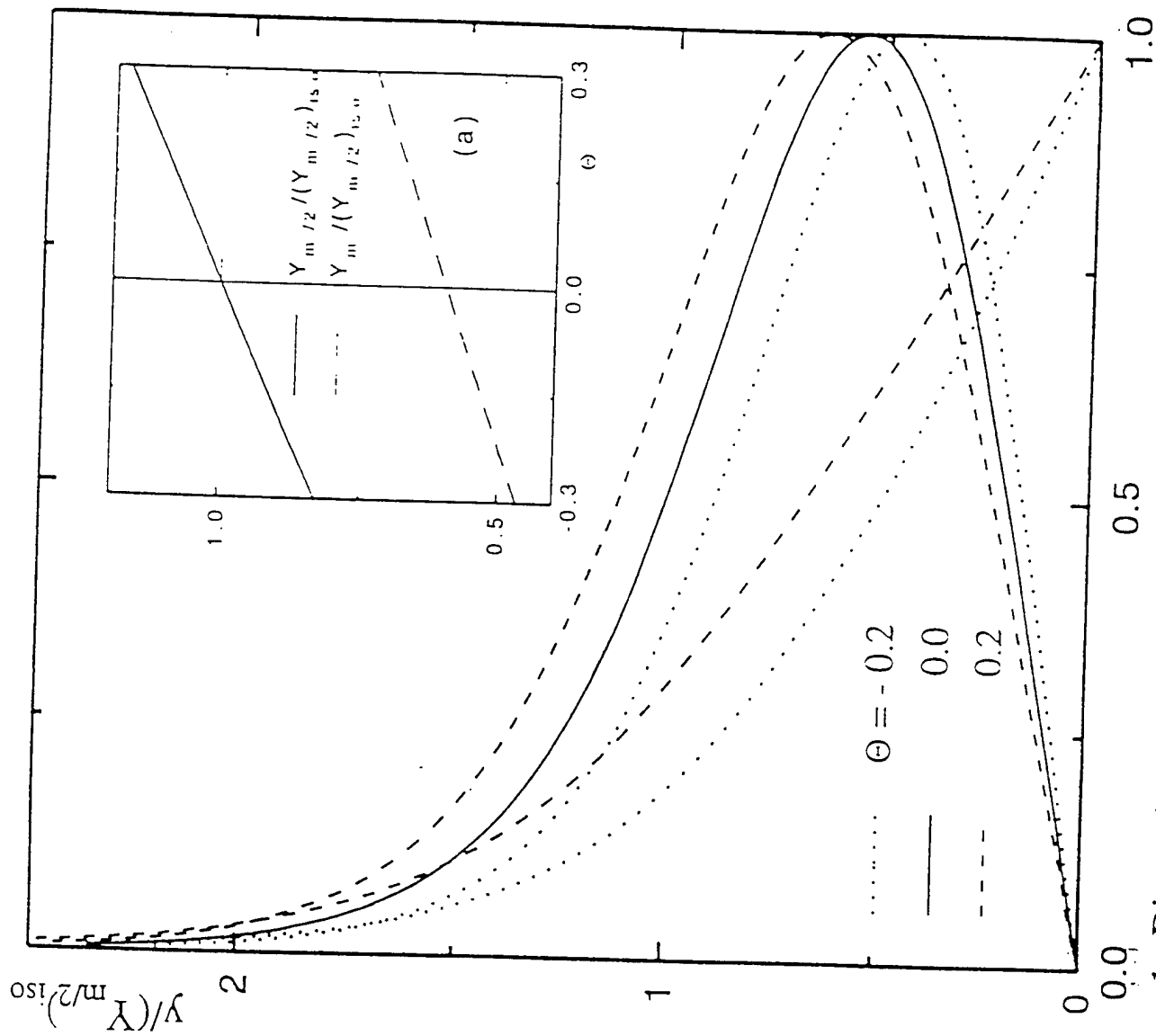Fig.13 The amplitude distributions of the waves participating in the resonance accross the wall jet .

Figure1. Dimensionless velocity $U/(U_m)_{iso}$ and temperature $(T-T_0)/(T_w-T_0)$ profiles for different values of the wall temperature deficit $\Theta=(T_w-T_0)/T_0$
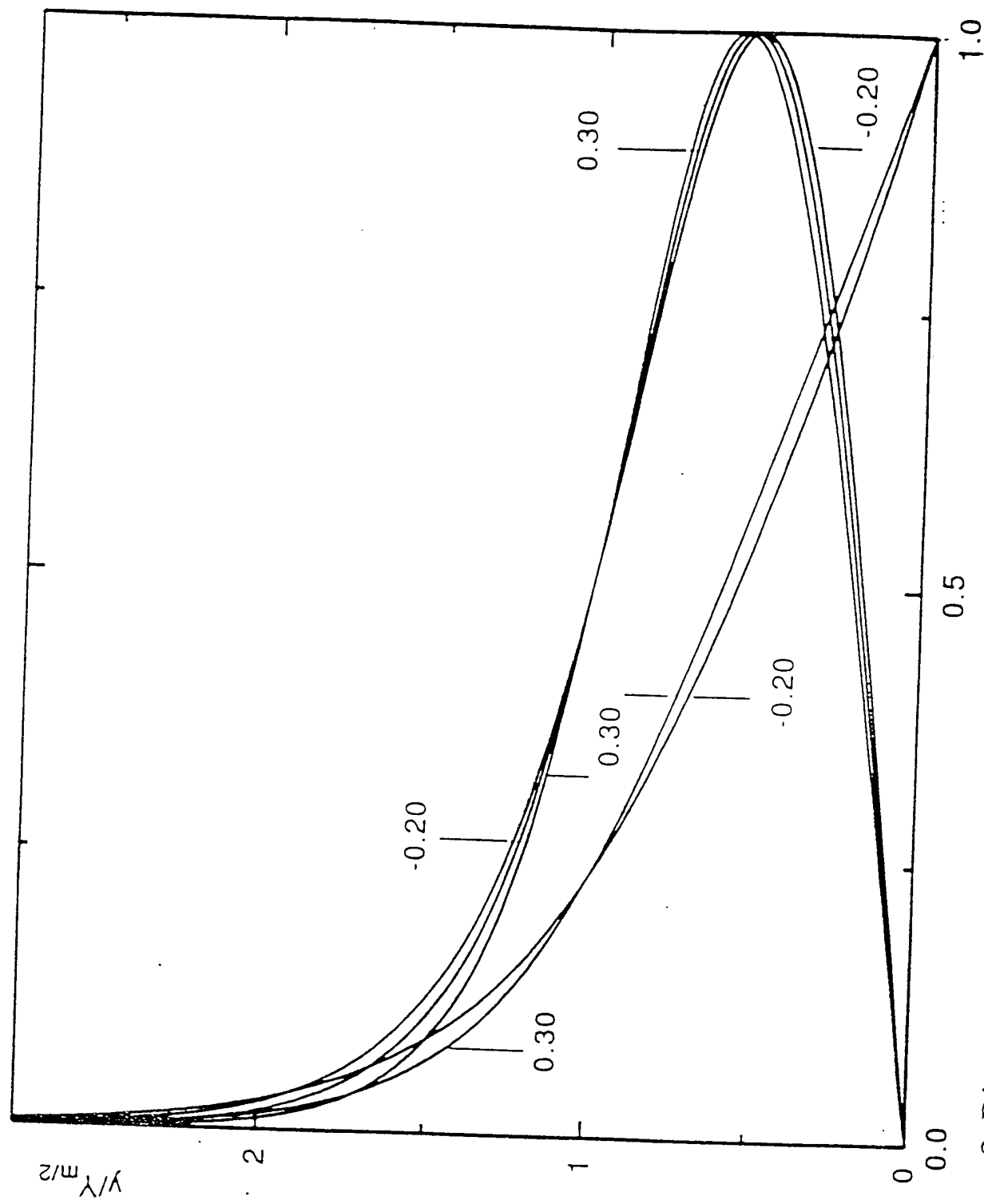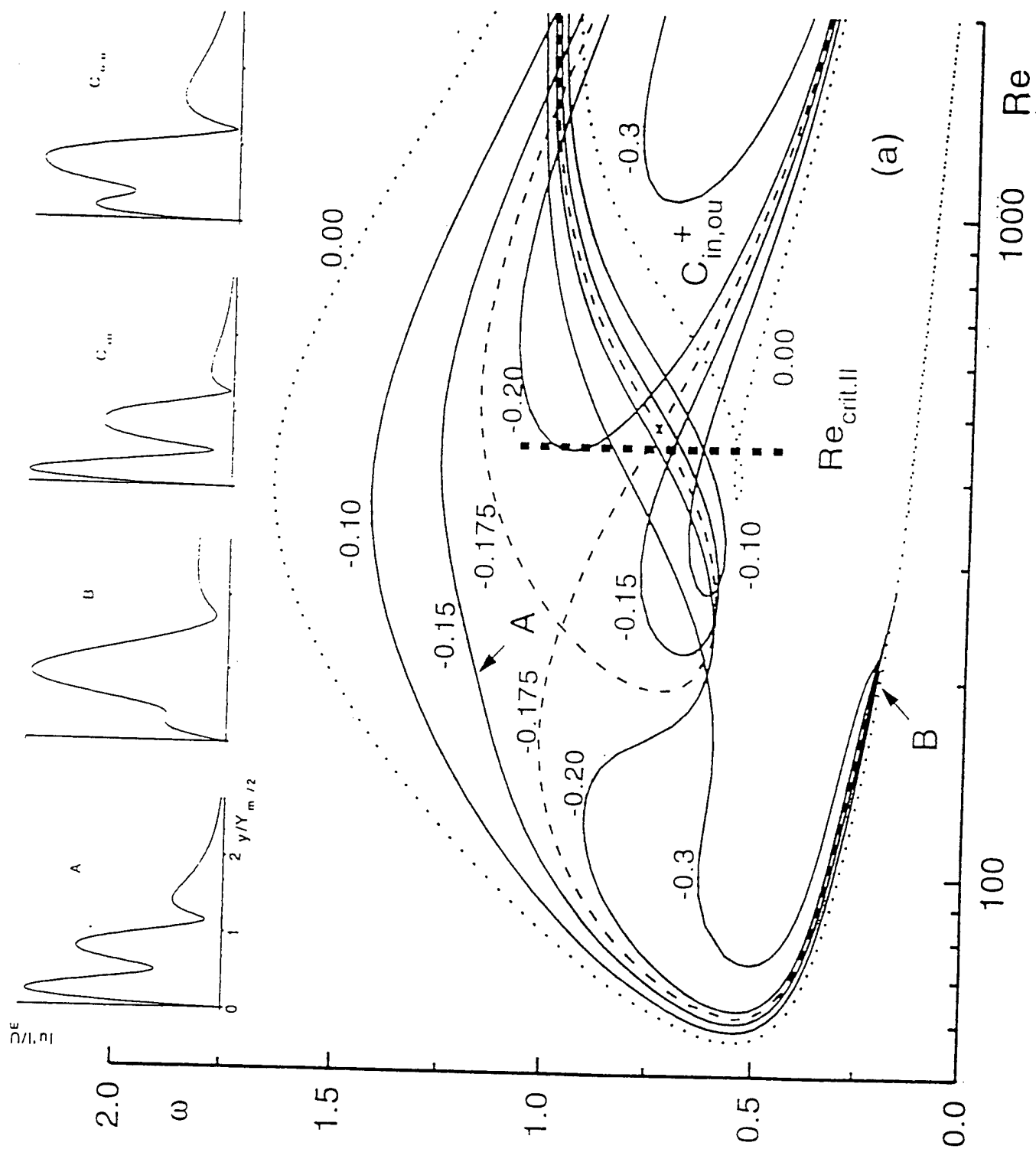
Figure2. Dimensionless velocity U/U_m and temperature $(T-T_0)/(T_m-T_0)$ profiles normalized by their own scales for different values of $\Theta = (-0.2, 0, 0.3)$
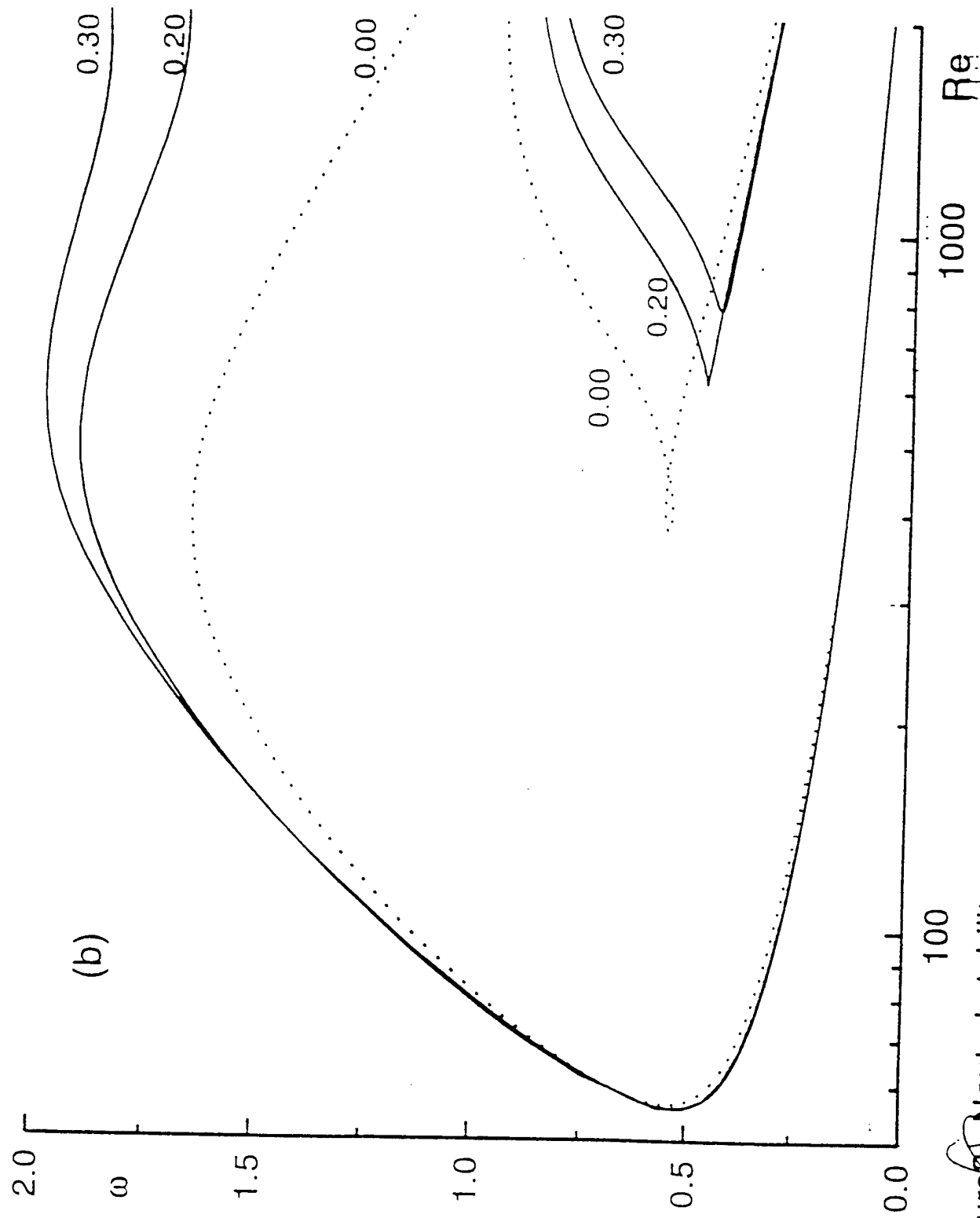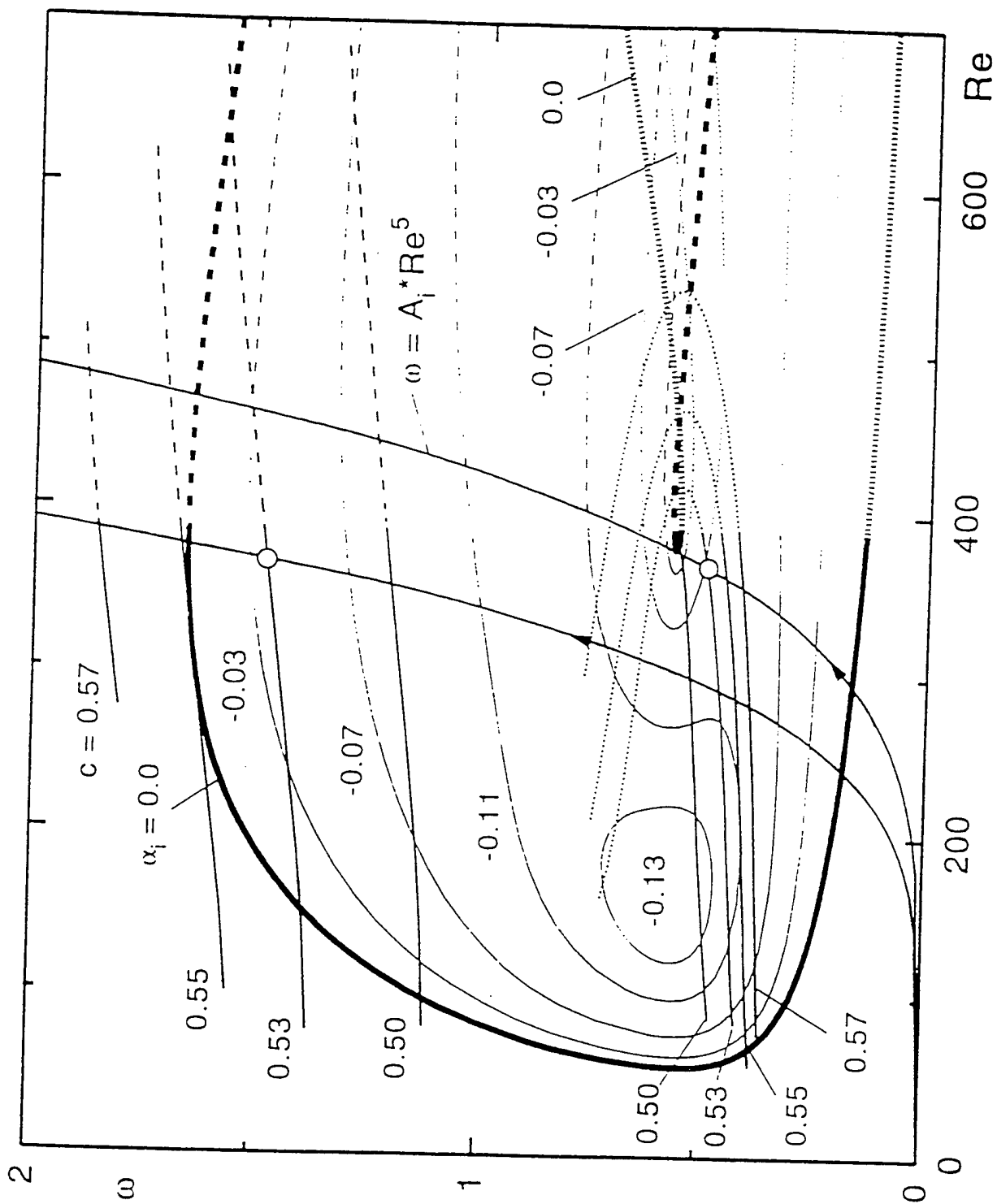
(a)

Figure 3. Neutral stability curves and amplitude distributions in a wall-jet flow over a constant temperature wall. The curves correspond to different values of $\theta = (T - T_\infty)$
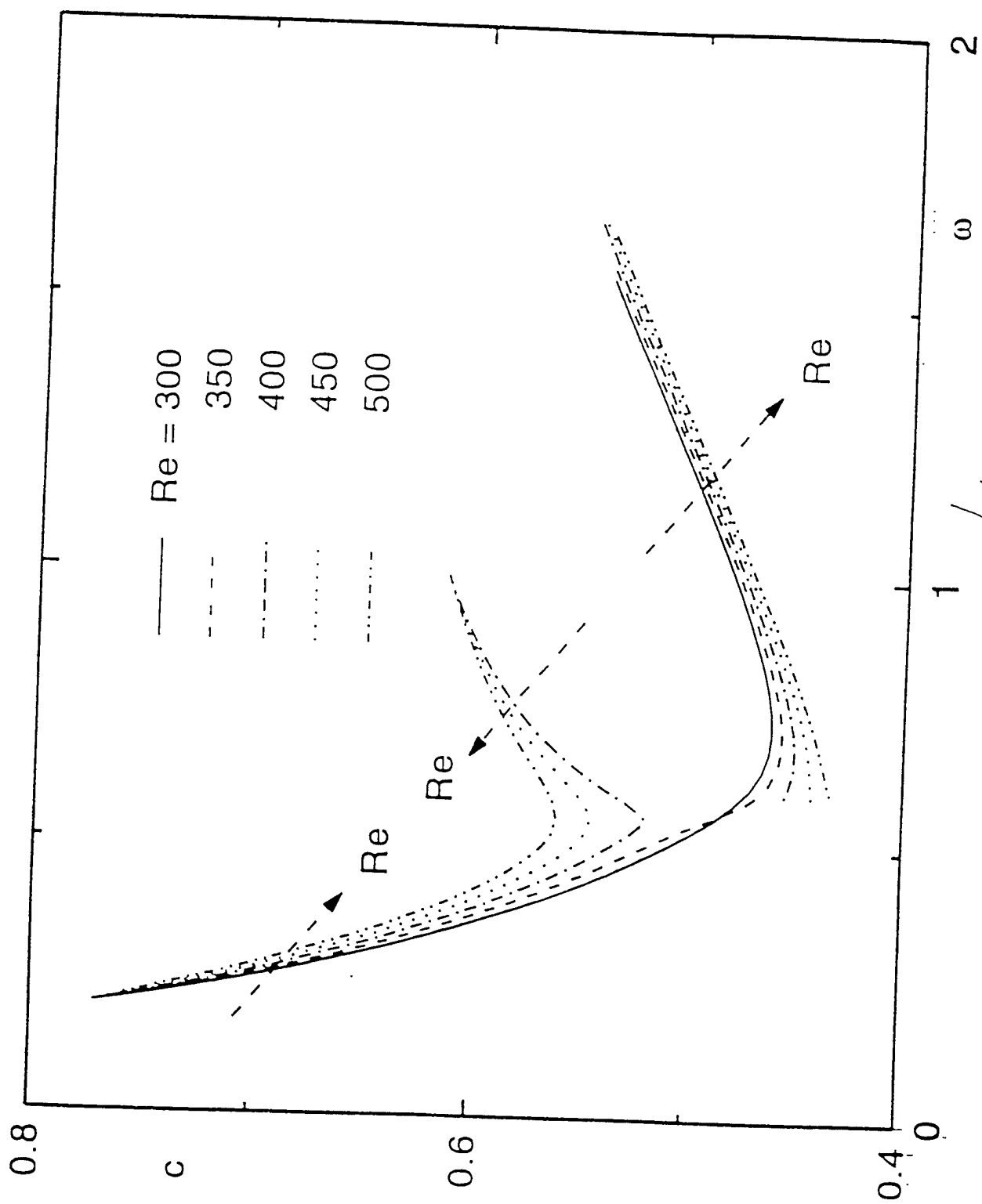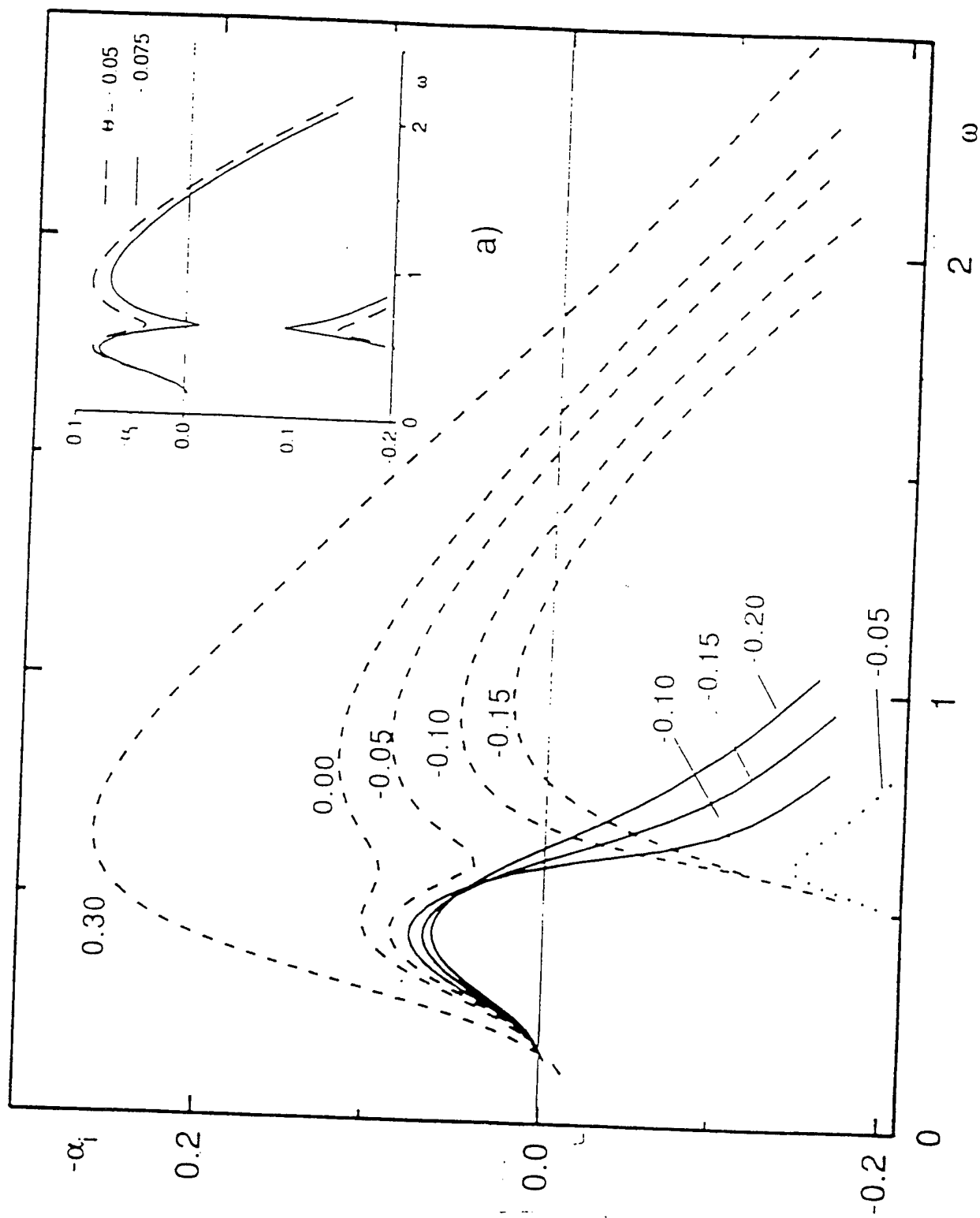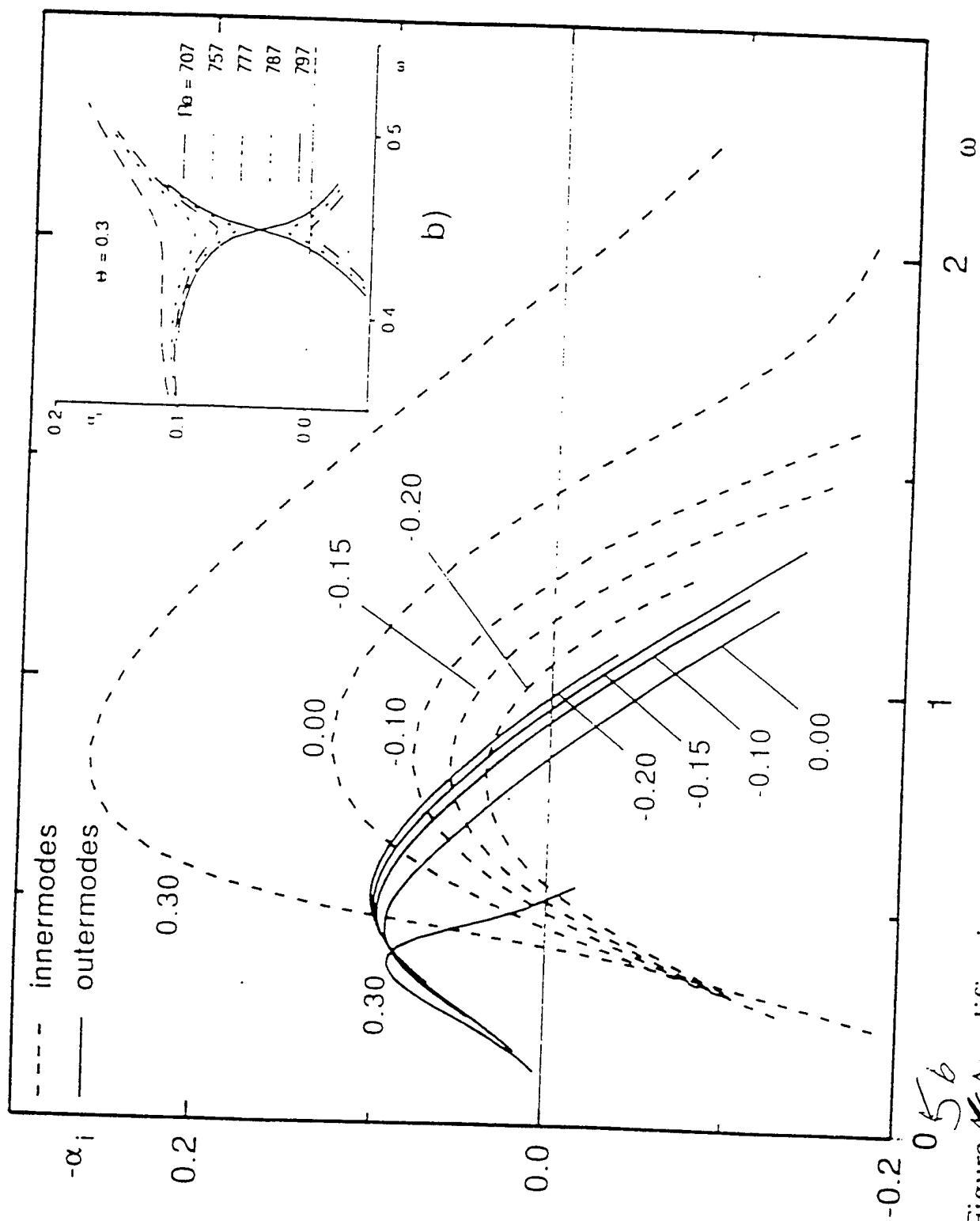
a)

0.30

0.00
-0.05
-0.10
-0.15

-0.10
-0.15
-0.20

-0.05

$-\alpha_i$

0.2

0.0

-0.2

0

1

2

ω

S_q

.05
-.075

Figure 4. Amplification rates of the disturbances for different values of the parameter Θ at three values of the Reynolds number a) - 300, b) - 657, c) - 2000

c)

$-\alpha_i$

0.1

0.0

-0.1

0.0   0.5   1.0   ω

-0.30

-0.30

A   B   C   D

$2 \, y/Y_{m/2}$
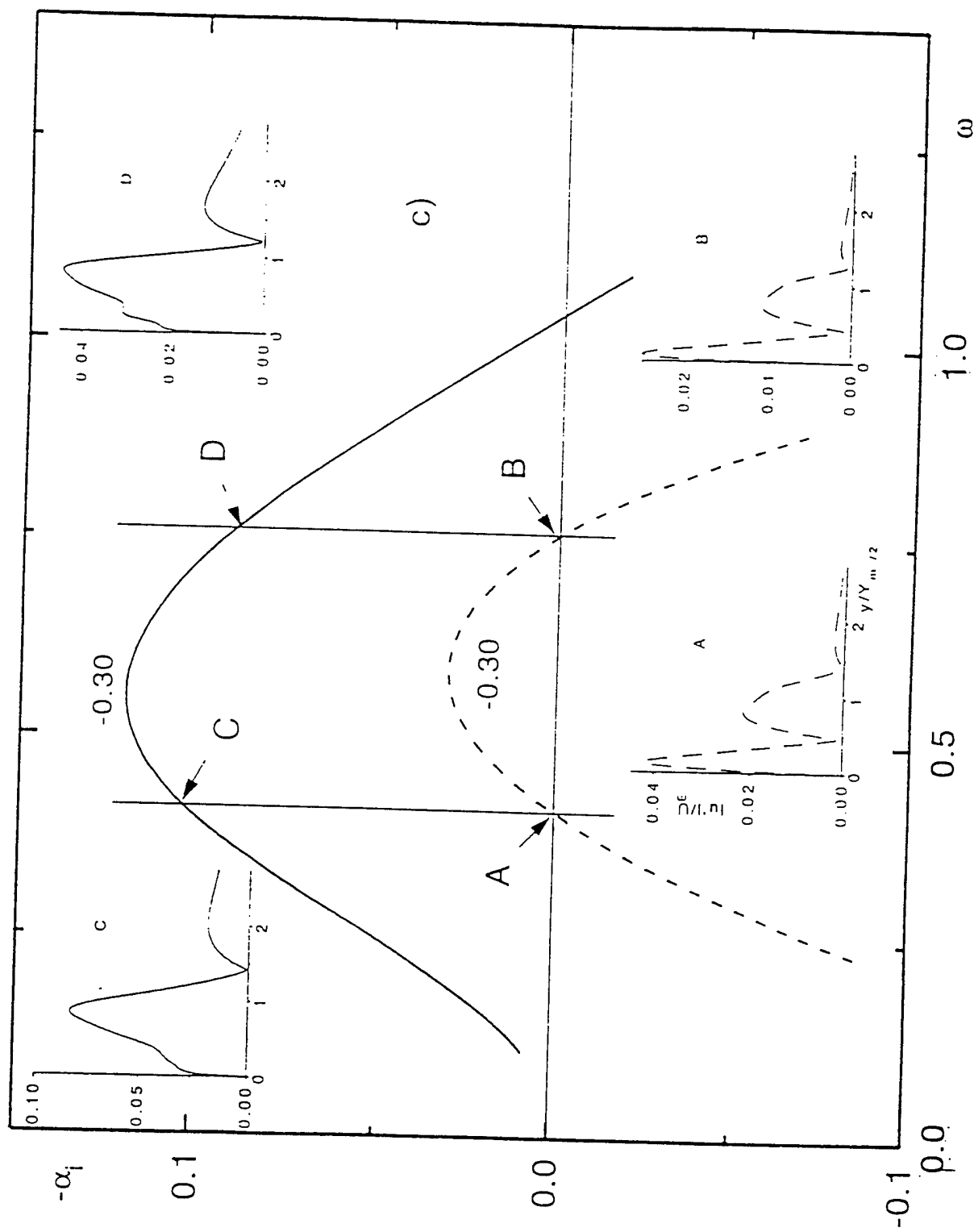
5C
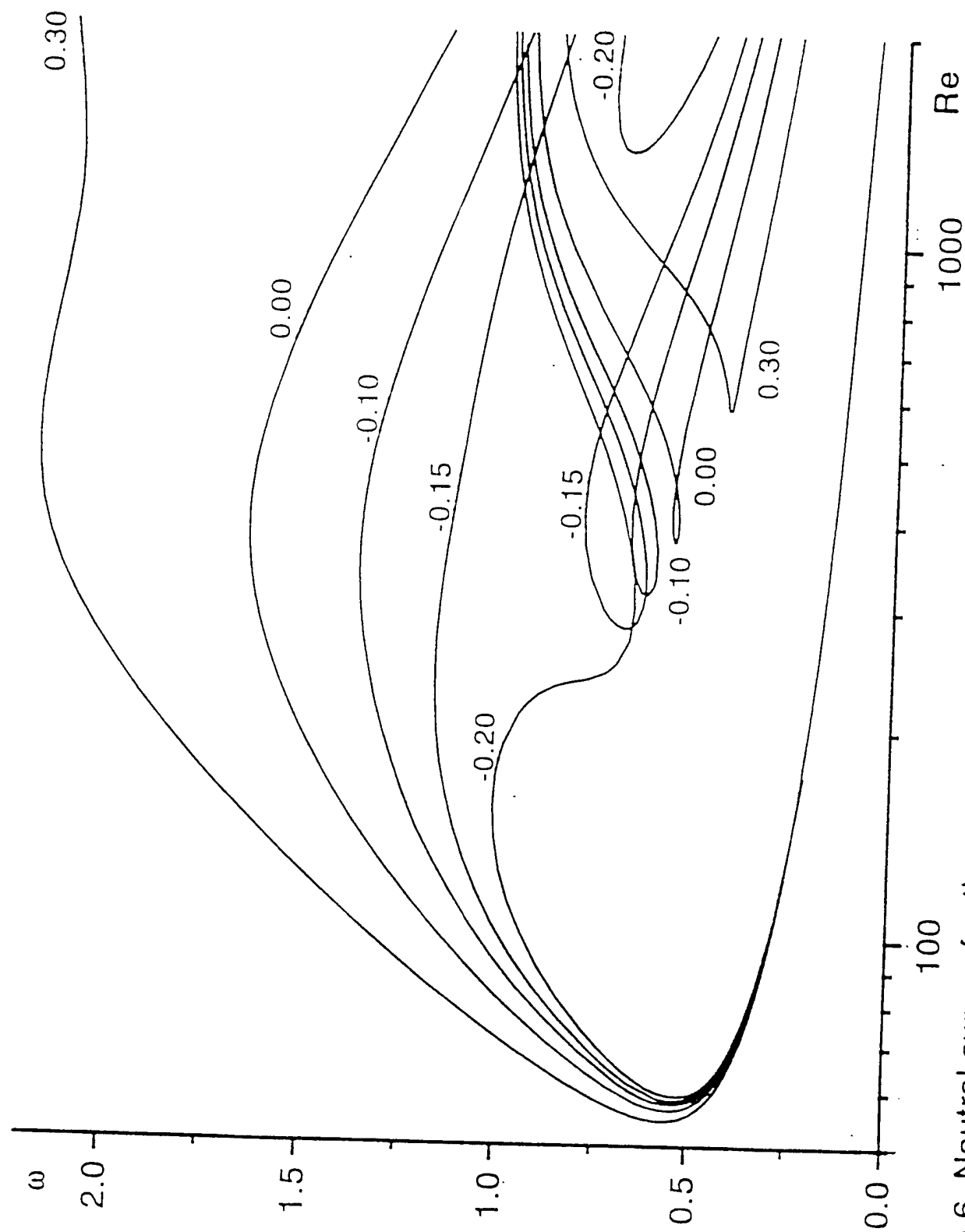
Figure 6. Neutral curves for the case of a wall jet flow over the wall with a constant heat flux to or from a wall. The curves correspond to different values of a local wall temper...

Fig.7 The normalized mean velocity profiles.

(b)

$\omega = A_i \cdot Re^5$

$\alpha_i = 0.0$

$\alpha_i = 0.0$

$c = 0.57$

0.55

0.53

15 Hz ○
45 ●
15 (&45) ×——
45 (&15) +——

ω

3

2

1

0

200   400   600   Re
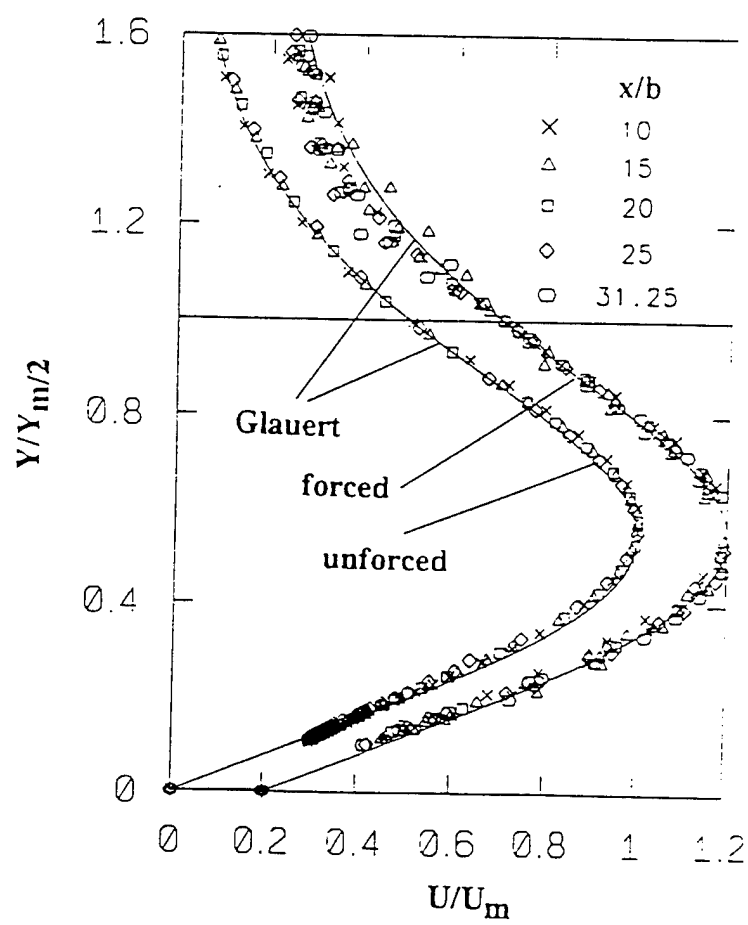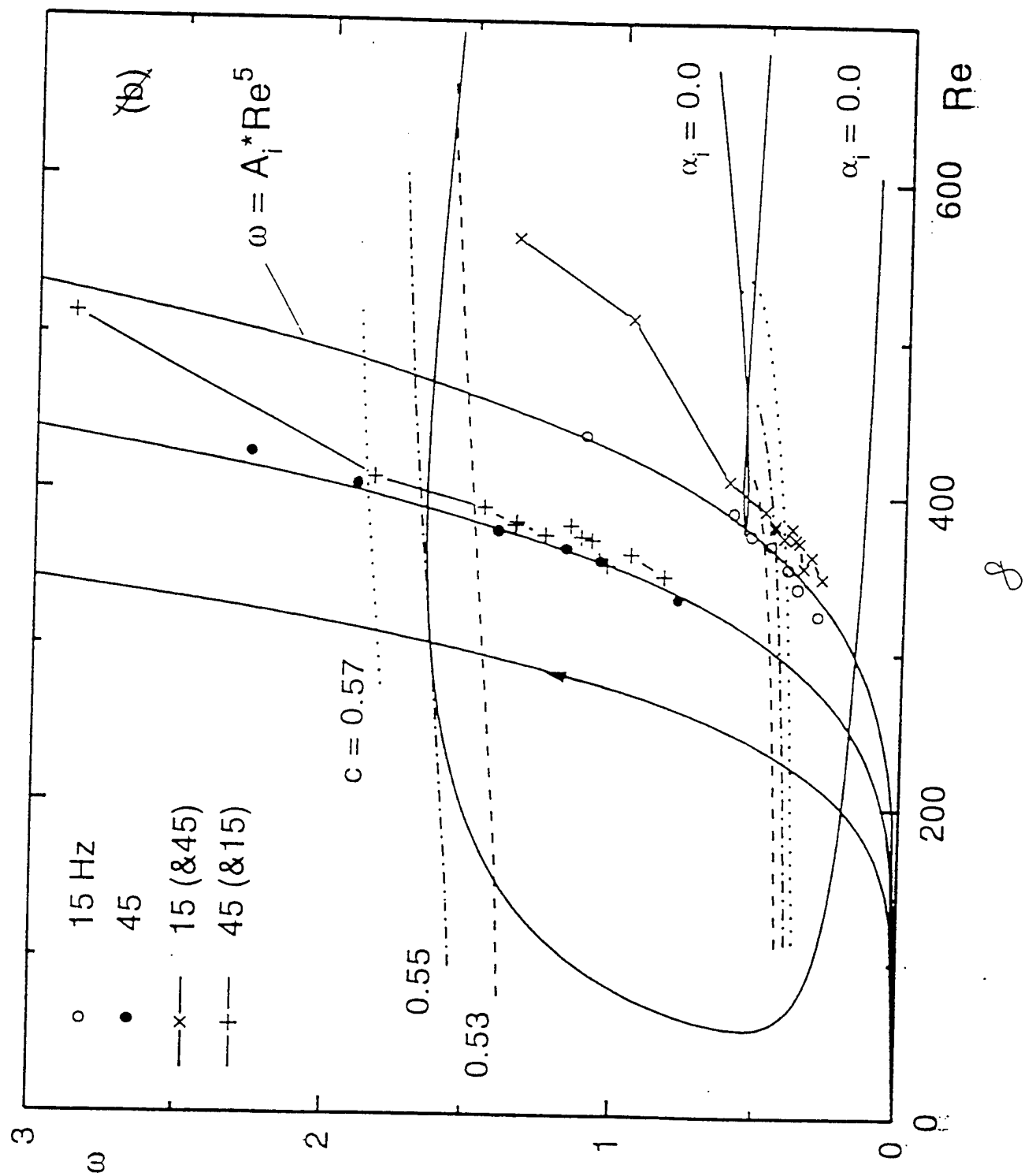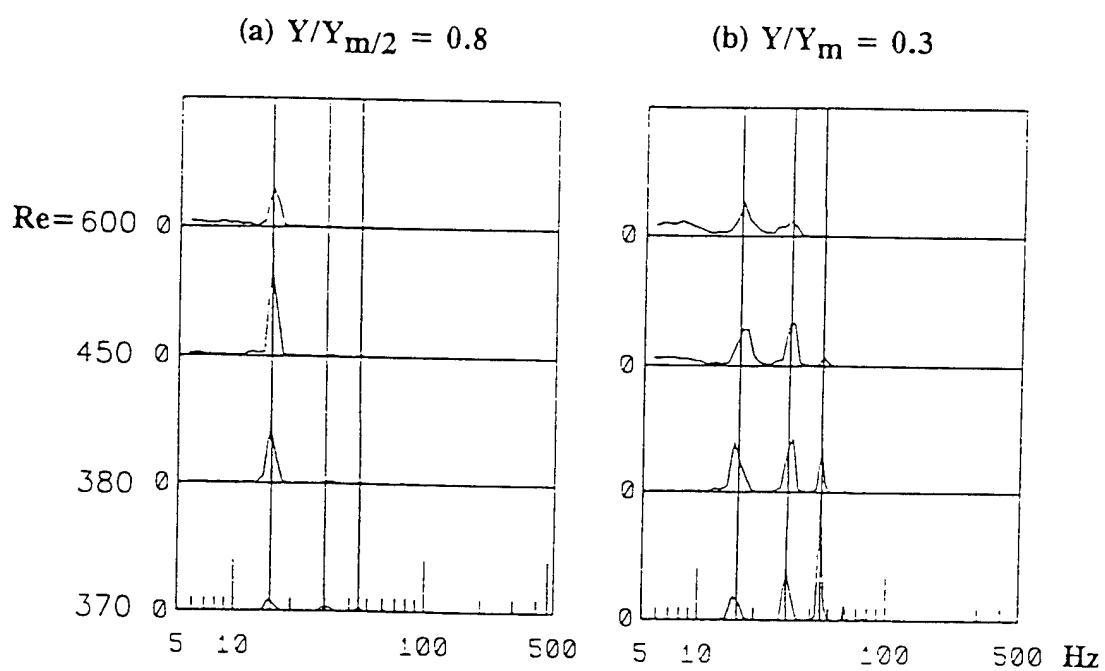
Fig.9 Spectra taken in the outer and inner regions.
Forcing at 15 and 45 Hz simultaneously.

(b) Inner region: $Y/Y_m = 0.3$

(a)

16.75

x/b

f=15Hz
λ=42.1mm
Vph=0.632m/s

f=45Hz
λ=14.4mm
Vph=0.648m/s

f=30Hz
λ=21.6mm
Vph=0.648m/s

14.75

0   180 0   180 0   180

(c) Outer region: $Y/Y_{m/2} = 1.2$

16.75

x/b

f=15Hz
Λ=37.3mm
Vph=0.559m/s

f=45Hz
λ=20.2mm
Vph=0.909m/s

f=30Hz
λ=23.7mm
Vph=0.711m/s

14.75

0   180 0   180 0   180

phase

$Re_j = 320$

$Re = 376$ at $x/b = 16$

Fig.10 Determination of the phase velocities by experiments.

Fig.11 The streamwise developement of the energy
contained in the components of disturbances.

Fig.12 Streamwise developement of energy thickness.

Forcing frequencies:

△ 15 Hz   ◇ 45 Hz   ○ 15 Hz & 45 Hz

Fig.13 Normalized amplitude distribitions of the disturbances.

HEAT TRANSFER IN THE FORCED LAMINAR WALL JET

Donald L. Quintana, Michael Amitay, Alfonso Ortega[1] and Israel J. Wygnanski
Department of Aerospace and Mechanical Engineering
The University of Arizona
Tucson AZ 85721
USA

ABSTRACT

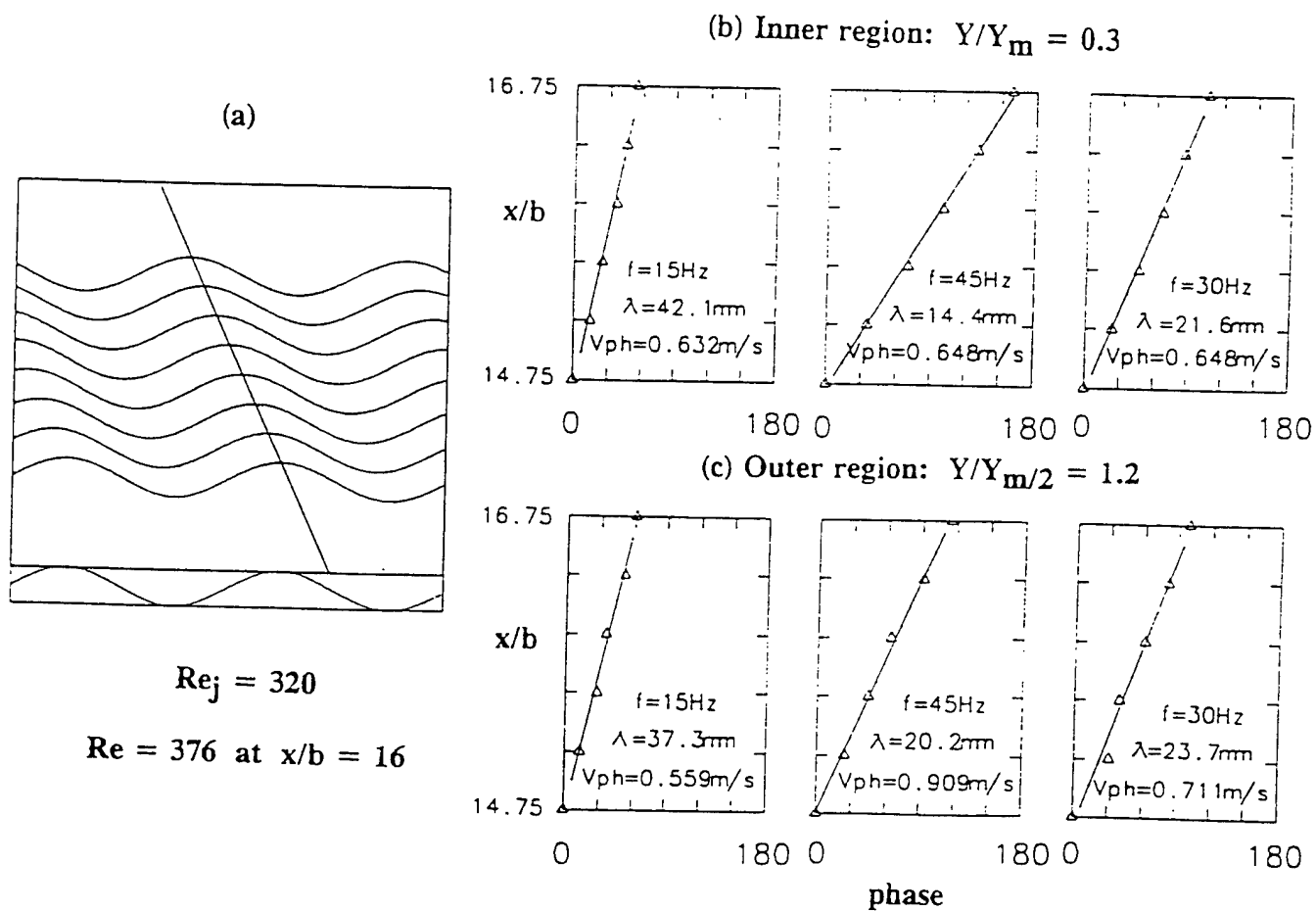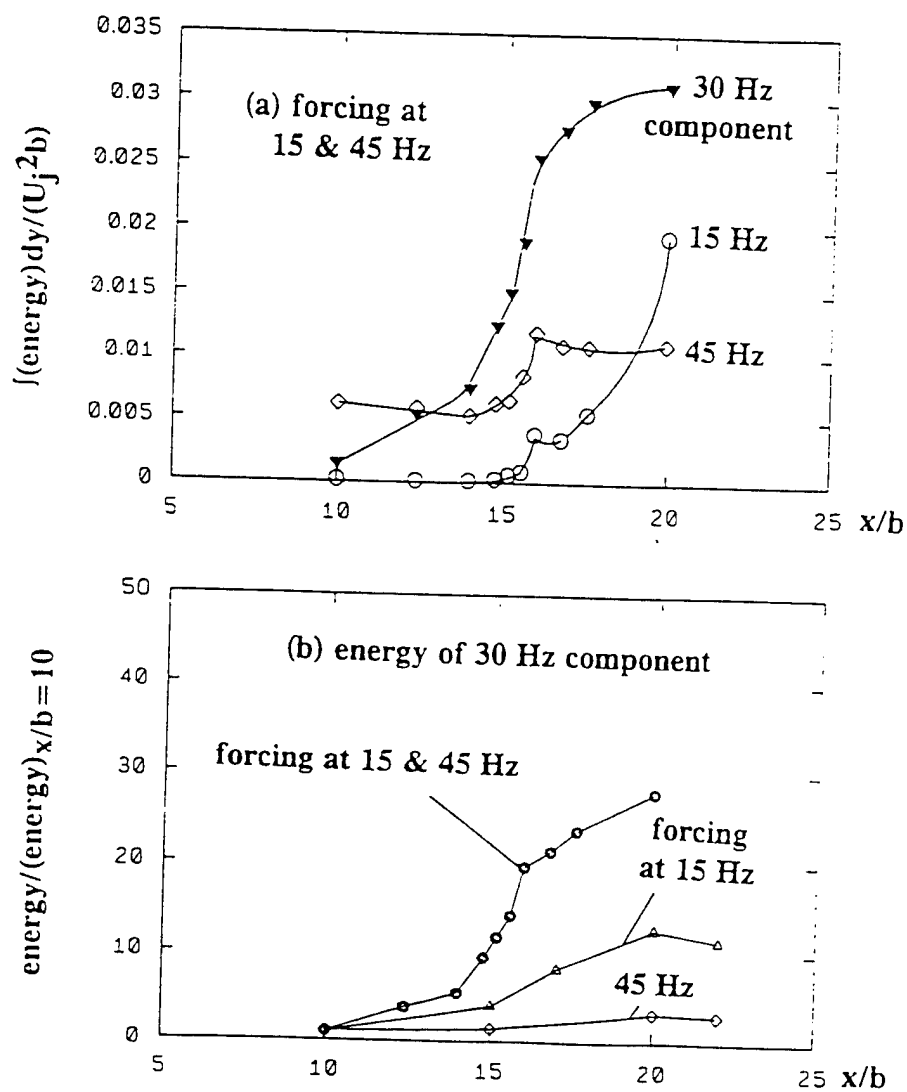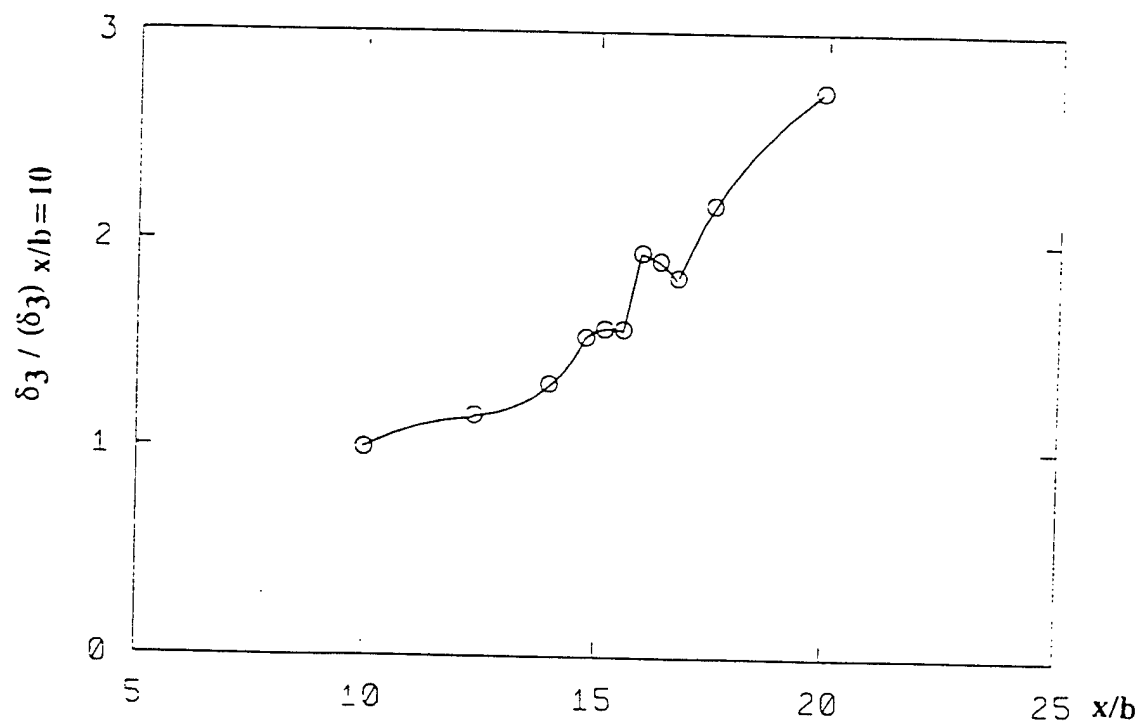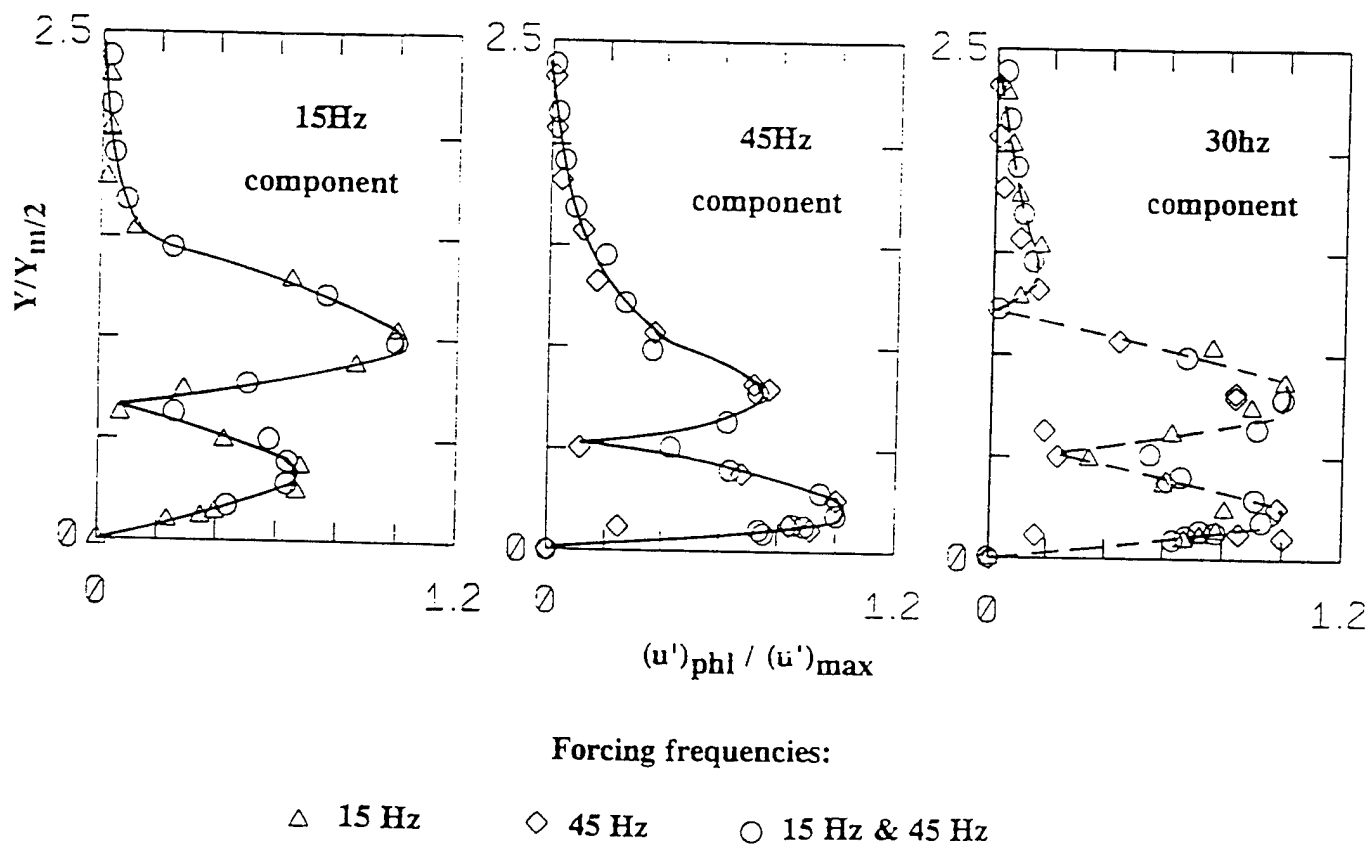The mean flow and stability characteristics of a plane, laminar wall jet were investigated experimentally for a constant wall temperature boundary condition. The streamwise mean velocity and temperature profiles and the downstream development of the hydrodynamic and thermal boundary layer thicknesses were obtained through simultaneous hot and cold wire measurements. Even at relatively low temperature differences, heating or cooling of the surface sufficiently altered the mean velocity profile in the inner region to produce significant effects on the jet stability. Selective forcing of the flow at the most amplified frequencies produced profound effects on the velocity and temperature fields and hence the time-averaged shear stress and heat transfer. Large amplitude excitation of the flow at high frequencies resulted in a reduction in the maximum skin friction by as much as 65% with an increase in the maximum wall heat flux as high as 45%. The skin friction and wall heat flux were much less susceptible to low frequency excitation.

---

[1] Corresponding author: Prof. Alfonso Ortega / University of Arizona / Dept. of Aerospace and Mechanical Engineering / Tucson, AZ 85721 / 520-621-6787 / fax: 520-621-8191 / e-mail: ortega@ccit.arizona.edu

NOMENCLATURE

E_T Thermal energy deficit $= \dot{m}c_p(T_w - T_j)/d$, W/m

J Jet exit momentum $= \rho d U_j^2$, N/m

Re_j Reynolds number measured at exit plane $= \rho U_j d/\mu$

T local mean temperature, K

T_o free-stream temperature, K

T_w wall temperature, K

U local streamwise mean velocity, m/s

U_j jet exit velocity, m/s

U_m local maximum streamwise velocity, m/s

U_o free-stream velocity, m/s

Y_m maximum normal distance from the wall (for the integration domain), m

c_p specific heat of air at free-stream, J/kg-K

d wall jet slot width, m

k thermal conductivity, W/m-K

$\dot{m}$ mass flow rate, kg/s

t' fluctuating temperature, K

u' fluctuating streamwise velocity, m/s

x,y coordinates, m

Greek symbols

δ denotes boundary layer thickness, m

δ_v local hydrodynamic boundary layer thickness, m

δ_t local thermal boundary layer thickness, m

μ free-stream dynamic viscosity, N-s/m^2

ρ free-stream density, kg/m^3

Subscripts

j jet exit plane

m maximum

o	free-stream
t	thermal
v	hydrodynamic
w	wall

INTRODUCTION

A wall jet is a thin jet of fluid blown tangentially along a surface. The free-stream can either be co-flowing or quiescent. The wall jet is a fascinating flow; it provides an example of a flow field consisting of two primary unstable shear layers which are associated with two different kinds of instability modes, the viscous (inner) mode associated with the inner near-wall region, and the inviscid (outer) mode associated with the inflection point in the outer region (see Mele et al. (1986)). Turbulent wall jets have important technological applications in heat transfer such as de-icing or de-fogging of windshields. Another application is in film-cooling where a turbulent wall jet is used to shield turbine blades and other surfaces exposed to either hot or corrosive gases in the free-stream.

In previous explorations of the wall jet, Katz et al. (1992) and Zhou et al. (1993) found that among other effects, significant reductions in average skin friction can be obtained in a turbulent wall jet by excitation of the flow at its dominant mode. Given the importance of the wall jet in the transport of heat and mass to or from surfaces, it is equally important to determine the related effects of forcing on the convective heat transfer. The possibility of augmenting or reducing the wall heat transfer, with minimal energy expenditure for excitation, is the subject of an ongoing investigation. Although most of the examples listed above incorporate turbulent wall jets with or without a free-stream it was decided to begin this research with a simple case to understand some of the physical mechanisms associated with externally excited wall jet flows. The first part of this investigation, the heat transfer in a laminar wall jet with and without external excitation and in the absence of a free-stream, is reported in this paper.

The first theoretical investigation of the incompressible, isothermal, laminar wall jet was done by Tetervin (1948). He predicted that the boundary layer thickness of the wall jet grows and the local maximum of velocity decays with downstream distance as $x^{3/4}$ and $x^{-1/2}$, respectively. Glauert (1956) obtained the solution in a closed form and his results were substantiated by the hot wire measurements of Bajura and Szewezyk (1970). Cohen et al. (1992) theoretically investigated the effects of subjecting an incompressible laminar wall jet to small amounts of blowing or suction. They found a new family of self-similar solutions in which

Glauert's solution is a member. These self-similar solutions were later confirmed experimentally by Amitay & Cohen (1993).

The self-similar solutions of the temperature field for a low speed, laminar, incompressible wall jet with constant physical properties were obtained by Schwarz & Caswell (1961) for the special cases of constant wall temperature, varying wall temperature, and constant wall heat flux. Temperature profiles and heat fluxes were evaluated for a variety of Prandtl numbers. Mitachi & Ishiguro (1974) performed a theoretical investigation of the laminar wall jet with different wall boundary conditions, however, they addressed the thermal entry length problem by using a coordinate transformation. These investigations were carried out with the assumption that there is no property dependence on fluid temperature. Riley (1958) theoretically investigated the compressible, radial wall jet assuming the dynamic viscosity was linearly dependent on temperature. He showed that a similarity solution for the velocity distribution exists which is expressible in terms of the corresponding incompressible wall jet solution. The energy equation was also studied for different Prandtl numbers and for different wall temperatures.

The first linear stability analysis on the wall jet was a temporal study performed by Chun & Schwarz (1967). By solving the Orr-Sommerfeld equation, they predicted that the critical Reynolds number for which small amplitude disturbances become unstable is 57 (Reynolds number based on local maximum velocity and local boundary layer thickness). They were also the first to reveal the existence of a second unstable mode (the viscous mode) at relatively high Reynolds numbers. Bajura & Szewezyk (1970) subjected the wall jet to two-dimensional excitations and showed that the disturbance amplitude distribution contains two large peaks and another small peak. One peak is located in the near-wall (inner) region where the local velocity is equal to 0.5 of the local maximum. The second peak, which is larger, is located in the vicinity of the inflection point in the outer region where the velocity is equal to 0.8 of the local maximum velocity. An additional weak peak was observed in the outer region where the velocity equals 0.06 of the local maximum velocity. They claimed that the existence of this peak was attributed to convective air currents in their laboratory.

Bajura & Catalano (1975) investigated the transition to turbulence in two-dimensional plane wall jets, using flow visualization in a water tunnel. They showed that the initial stages of transition are two-dimensional in nature, and are dominated by the mechanism of vortex pairing, which is commonly observed in free shear flows. A clarifying physical explanation of the existence of the two modes was given by Mele et al. (1986). They demonstrated theoretically that the low frequency mode (inviscid mode for large-scale disturbances) is associated with the outer inflection point while the high frequency mode (viscous mode for small-scale disturbances) is related to the mean velocity gradient in the vicinity of the wall. These results were theoretically and experimentally verified by Amitay & Cohen (1996) who also investigated the effects of blowing and suction on the stability of the wall jet. They found that blowing stabilizes the inviscid (outer) mode and destabilizes the viscous (inner) mode, while suction destabilizes the inviscid mode and stabilizes the viscous mode. Furthermore, blowing and suction tend to increase and decrease, respectively, the ratio between the outer and inner amplitude maxima of the streamwise fluctuation of velocity.

An investigation of the effects of low and high excitation levels on the velocity and temperature fields of a two-dimensional, laminar wall jet flowing over a constant temperature surface is presented in the current paper. The steady, unforced wall jet was examined first, in order to qualify the experiment against existing theories for constant property flow. This was followed by an examination of the effects of forcing on the time-averaged wall shear stress and heat transfer and on the fluctuating components of streamwise velocity and temperature. In the present investigation, the free-stream was quiescent and isothermal with respect to the jet exit temperature. The forced wall jet with heat transfer is currently under analytical, numerical and experimental investigation in the authors' research group in a long term effort to gain a broader understanding of the control of heat transfer in laminar and turbulent wall jet flows with and without a free-stream.

APPARATUS AND INSTRUMENTATION

Experimental Apparatus

The experiments were performed in a thermally controlled, closed return, low speed, air wind tunnel. The test section was 711 mm wide, 165 mm high and 2,362 mm long. A slot type wall jet apparatus was used which essentially duplicates the design of Zhou et al. (1993) which was used in the study of a turbulent wall jet with forcing. This apparatus consisted of a 0.5 HP centrifugal blower, acoustic muffler, air-water heat exchanger, diffuser, a plenum chamber fitted with an acoustic speaker, three screens of 30, 40 and 50 mesh size and a contraction nozzle having a variable area ratio. In these experiments the area ratio was 28:1 resulting in a jet slot width of 3.2 mm and a jet exit velocity of 1.5 m/s. The apparatus was designed to fit in the test section floor of an existing closed return wind tunnel which will provide the free-stream flow in future experiments (see fig 1).

Test Surface

The flow exited the wall jet apparatus tangentially over an isothermal heat transfer surface. The surface consisted of a 19 mm thick highly polished aluminum tooling plate which was held at constant temperature by means of cooled/heated water from a recirculating chiller that counter flowed through milled slots inside the plate. Surface temperatures were measured with Type K thermocouples that were potted into the surface with an aluminum epoxy. A two inch thick sheet of honeycomb was placed beneath the plate and served as an insulator and as a rigid support for the top plate. Another plate with uni-directional cooled/heated water was placed beneath the honeycomb to prevent any backside thermal losses. This experimental configuration allowed for independent variation of surface, jet, and free-stream temperatures. In the present investigation, the surroundings were quiescent, and the jet exit temperature was equal to the free-stream temperature.

Instrumentation

The measurements of the streamwise velocity and temperature were conducted using two side-by-side (7 mm apart) standard Disa Model 55P11 single hot and cold wire probes with a 5 μm diameter tungsten sensor having length-to-diameter ratio of 300. The hot wire was kept at an over-heat ratio of 1.6 and had a maximum frequency response of 30 kHz. The frequency

response of the cold wire was 600 Hz. The cold wire was calibrated against a NIST traceable lab standard thermistor probe (Thermometric Model ES210). The hot wire was calibrated in the exit plane of a thermally controlled vertical axisymmetric jet against a standard Pitot tube used in conjunction with an MKS Baratron (Model 398HD) pressure transducer. Seven velocities, at a constant temperature, were used for calibration and a fourth order polynomial fit was used to generate the calibration curve. Due to temperature gradients in the flow field the hot wire output voltage required temperature compensation. The hot wire output voltage was thus calibrated at different velocities for the range of temperatures which were used in the experiment. This produced a linear relationship between voltage and temperature for each velocity. The slope was averaged for the range of velocities, and thus used to find the temperature compensated voltage. Using this method, the error between the compensated velocity and the actual velocity (obtained by the Baratron) was less than 0.5%. The raw data from the hot and cold wire anemometers and the pressure transducer were acquired using LabVIEW software on a PC.

In order to observe the effects of external forcing on the velocity and temperature fields, the wall jet was artificially excited using acoustic perturbations. These perturbations were generated by a 12 inch speaker cone (a "woofer") that was placed in the diffuser of the wall jet apparatus shown in figure 1. A digital-to-analog converter was used to generate the forcing signal which was passed through an amplifier before it was used to activate the speaker. The forcing frequencies were determined from linear stability theory, and the excitation level measured at the jet exit plane was incrementally varied from 0.6 to 2.0 %. In this investigation the forcing frequencies were fixed at 43.9 Hz and 21.1 Hz corresponding to the inner and outer modes of instability. It can be shown from linear stability theory that when the wall is significantly heated or cooled, these frequencies will vary, however, the small temperature differences used in this experiment (6-8 °C) produced negligible effects on these forcing frequencies. All aspects of the experiment, including the introduction of disturbances into the flow with the speaker, were controlled with LabVIEW software.

In order to retain phase information, the phased locked technique was used in which the hot wire, the cold wire and the function generator records, consisting of 256 points each, were digitized simultaneously and saved. At each measuring point, up to 800 events were recorded.

The amplitude and phase of the fluctuating velocity and temperature components were obtained in the following manner. First, the local mean velocity and temperature were subtracted from the time dependent signals, then a direct Fourier transform was performed on each period. The amplitude and phase could then be calculated by averaging over all the periods.

Experimental Uncertainty

The relative uncertainty in each of the variables and in any calculated variables or parameters was determined by methods outlined by Kline and McClintock (1953). The relative uncertainty in the surface temperature is $\pm 5\%$. The uncertainty in the fluid temperature measurements, based on the cold wire which was calibrated against a NIST traceable lab standard thermistor probe with an uncertainty of $\pm 0.02\%$, and by sampling 256 points at a scan rate of 300 Hz for over 100 loops, was $\pm 1\%$. The free stream temperature was kept constant within $\pm 4\%$ by the air-conditioning in the laboratory. Mean velocity measurements were calibrated against a Baratron pressure transducer and 256 points were sampled at a sampling frequency of 300 Hz for over 100 loops to obtain an uncertainty of $\pm 1\%$. The fluctuating temperature and velocity were measured at a sampling rate which was 35 times higher than the frequency of the excited wave, giving a cyclic resolution of $10°$ relative to the fundamental component of the phase-locked signal. The sampling time, defined by the sampling frequency and the number of points, was chosen so that the uncertainty in the amplitude was less than $\pm 1\%$. The uncertainty in the near wall velocity and temperature gradients was estimated to be less than $\pm 10\%$. The normal distance from the wall was obtained by extrapolating the near wall velocity gradient, giving an uncertainty of less than $\pm 2\%$.

RESULTS

Undisturbed Mean Flow

Three sets of experiments were conducted corresponding to three temperature ratios denoted by T_w / T_o (measured in Kelvin, where T_w is the wall temperature and T_o is the free-

stream temperature): wall cooling with $T_w / T_o = 0.98$, wall heating with $T_w / T_o = 1.03$ and the neutral case with $T_w / T_o = 1$, in which the surface, jet exit, and free-stream temperatures were all the same. Throughout the experiments, the jet exit Reynolds number, $Re_j = \rho U_j d / \mu$, remained fixed at 320. The normalized mean profiles of the streamwise velocity measured for the three cases above and at three normalized streamwise locations ($x / d = 12$, 16, and 20) are shown in figure 2. Here, x is the streamwise distance measured from the wall jet exit plane and y is the normal distance measured from the wall. The local maximum velocity, U_m, and the local thickness of the hydrodynamic boundary layer, δ_v (where the mean velocity is equal to $U_m / 2$ in the outer region), were used to render all variables dimensionless. Figure 2a shows full velocity profiles for all cases, while figures 2b, 2c, and 2d present the inner region in more detail for the cooling, neutral, and heating cases, respectively. The symbols represent the experiments while the solid line corresponds to Glauert's (1956) theoretical prediction. Solid, center-dot and center-cross symbols correspond to the cases of $T_w / T_o = 1$, 0.98 and 1.03, respectively, while squares, circles and triangles correspond to $x/d = 12$, 16 and 20, respectively. The agreement between the experiments and the theory for the neutral case is good except in the inner region where the velocity gradient of the experimental data is higher, figure 2c. This may be due to the relatively high turbulence level (0.5%) of the jet. When cooling is applied, figure 2b, the inner velocity gradient increases and the maximum velocity is shifted closer to the surface. Heating the surface, figure 2d, appears to have the opposite effect, but the differences in the heated case compared to the neutral case cannot be claimed to be outside of the range of experimental uncertainty. As will be shown, despite very small changes in the mean velocity due to heating and cooling, a more significant effect is observed on the fluctuating streamwise velocity distribution.

The effects of temperature on the velocity profile can be evaluated by observing the downstream development of the hydrodynamic and the thermal boundary layers, as plotted in figure 3. Here, δ_t is defined as the distance from the wall to the place where the normalized temperature is equal to 0.5. Figure 3a presents the dimensional form in order to observe the relative magnitudes of the boundary layer thicknesses, while figure 3b displays the boundary

layer thickness normalized by the first measurement point displaying the spread rate of the two scales. As can be seen from figure 3a, heating and cooling have no significant effect on the hydrodynamic boundary layer, however, heating produces a thicker thermal boundary layer. As shown in figure 3b, the growth rate of the thermal boundary layer is greater than the hydrodynamic boundary layer, consistent with existing theories for Pr less than 1.

The temperature profiles for different scaling lengths and at three downstream stations are shown in figure 4, non-dimensionalized as shown on the plot. The hydrodynamic boundary layer thickness δ_v was used as the normalizing scale in figures 4a and 4b while the thermal boundary layer thickness δ_t in figures 4c and 4d. Figures 4a and 4c present the full temperature profiles, while 4b and 4d show the inner region near the wall in more detail. The symbols represent the experimental data and the solid lines correspond to the theory developed by Mitachi & Ishiguro (1974). As can be seen, using δ_v as the length scale causes the data to collapse on two curves, corresponding to two different unheated starting lengths, one for the cooling case and one for the heating case. As is shown in figure 3b, the spread rate for the thermal boundary layer thickness is the same for heating and cooling but the magnitude is different (figure 3a). The virtual origin for the heating case therefore is shifted farther upstream and thus the corresponding unheated starting length is larger. This results in a thicker temperature profile for wall heating as is evident in figures 4a and 4b. On the other hand, scaling on δ_t collapses the two cases onto one curve, shown in figures 4c and 4d. These are not surprising results since the ratio between the thermal and the hydrodynamic boundary layers is different for the two cases above mainly because the changes in δ_t are more significant than the changes in δ_v as was shown in figure 3.

Mean Flow Field Subjected to External Forcing

The mean velocity and temperature fields were also investigated under actively controlled conditions. Disturbances were introduced into the flow by a speaker at various frequencies and amplitudes. Three cases, corresponding to the above three values of T_w / T_o,

were studied. In this section only the results for the heating case are presented, however, similar results were obtained for the other cases mentioned.

The dimensional mean profiles of the streamwise velocity measured for the heating case and at three normalized streamwise locations ($x/d = 12$, 16, and 20) are shown in figure 5. Figure 5a presents the case in which the flow is excited with a high frequency disturbance (approximately 44Hz for inner mode forcing), while figure 5b corresponds to a low frequency disturbance (21Hz for outer mode forcing). The solid, dashed and dotted lines correspond to the unforced, 1% excitation level and 2% excitation levels, respectively. The excitation level is defined at $x/d = 0$ as $100 \cdot u'_m / U_j$, where, u'_m is the maximum fluctuating streamwise velocity (measured by using the phase-locked data technique) and U_j is the jet mean exit velocity. As is shown in figure 5a, when inner mode forcing is applied the velocity field is dramatically altered. The effects become more pronounced as the downstream distance increases. The effect of outer mode forcing is not as dramatic because the growth rates associated with the outer mode are smaller than the inner mode growth rates, as predicted by the theory (see Amitay & Cohen (1996)). In order to see the effects of forcing on the wall shear stress, the near wall region of the velocity field was plotted and is presented in figure 6. Seven cases, corresponding to the unforced case, inner and outer mode forcing with 0.6%, 1% and 2% excitation levels, are presented. Figures 6a, 6b and 6c represent the experimental data taken at $x/d = 12$, 16, and 20, respectively. The solid line corresponds to the velocity gradient for the unforced case. For low levels of excitation, the velocity gradient near the wall is negligibly affected. As the excitation level is increased up to 2% the velocity gradient near the wall is decreased by up to 15% (with respect to the unforced case) for the outer mode forcing, and by up to 65% for the inner mode forcing.

The normalized mean temperature profiles measured for the heating case and at $x/d = 16$ are shown in figure 7a and 7b for inner and outer mode forcing, respectively. As was observed for the velocity field, for low excitation levels the effect of forcing on the temperature profile is negligible. As the excitation level is increased, surprisingly, the temperature gradient near the wall *increases* until an inflection point is formed on the temperature profile. Again, the effect of

the inner mode forcing is much more significant. In order to understand the formation of the inflection point in the temperature profile, measurement of the normal component of the fluctuating velocity is needed. However, since in the reported experiments the boundary layer thickness was on the order of 5 mm, it is extremely difficult to measure it using conventional X-wire techniques. The effect of forcing on the near-wall region of the temperature profile (which corresponds to the heat flux at the wall) is presented in figure 8. Profiles measured at three normalized streamwise locations ($x/d = $ 12, 16, and 20) are shown in figures 8a, 8b and 8c, respectively. Low excitation levels do not alter the temperature gradient near the wall, while increasing the excitation level causes an increase in the temperature gradient. Outer and inner mode forcing at 2% excitation level increases the temperature gradients by up to 20% and 45%, respectively. As was mentioned above, the augmentation in the heat transfer is accompanied by a net reduction in the time-averaged wall drag, a result which could not be anticipated.

The integrated effect of different forcing frequencies and amplitudes on the normalized total skin friction drag and the total heat flux is presented in figures 9a and 9b, respectively. Here, x_1 is the first measured downstream station, J is the jet exit momentum defined as $J = \rho d U_j^2$, and E_T is the thermal energy deficit between the jet and the wall defined as $\dot{m}c_p(T_w - T_j)/d$. The total effect of the outer mode forcing is weak and within 5% of the unforced curves. The effect of inner mode forcing is much more significant, with up to 45% reduction of the total skin friction drag and 20% increase of the total heat flux.

As shown in figure 5 high levels of forcing introduce non-linear effects as observed by a dramatic thickening of the boundary layer. large scales associated with the outer region become more significant. As was shown by Bajura & Catalano (1975) and Amitay & Cohen (1996) two rows of counter rotating vortices associated with the two regions of the wall jet are present in laminar to turbulent transition. It is the outer row of vortices (which rotate in the counter-clockwise direction and thus transport momentum away from the wall) that receive most of the energy under high levels of forcing and therefore, decrease the velocity gradient near the wall as shown in figures 5 and 6. It is believed that this same motion is responsible for the increase in the near-wall temperature gradient which was observed in figures 7 and 8. A plausible

explanation may be that the large vortices in the outer region transport fluid away from the wall to the outer region (which is at a different temperature) and also entrain fluid towards the wall. This motion may also explain the large reduction in the temperature gradient, occurring at y/δ_v of about 0.2 as seen in figure 7a, because the unsteady upward advective transport is increased compared to diffusive transport in this region. This enhanced thermal mixing is manifested also in the observed increase in the wall temperature gradient and thus the wall heat flux.

Fluctuating Quantities

Since the evolution of controlled disturbances apparently is a primary factor in augmenting the heat transfer, the structure and evolution of the temperature and streamwise velocity fluctuations were further investigated. In order to obtain phase information, phase-locked data were measured and analyzed for low and high levels of excitation corresponding to the two modes of instability associated with the wall jet flow. These levels of excitation correspond to the linear and nonlinear transitional behavior of the flow. Figure 10 shows the dimensional fluctuating temperature distribution versus the dimensional distance from the wall. The data were taken using the conventional phase-locked technique, and were measured at x/d =16 for T_w/T_o= 1.03 and for three excitation levels of (a) 0.6%, (b) 1%, and (c) 2%. A single peak is present for 0.6% forcing, as is shown in figure 10a. This peak is located at the same distance from the wall for both inner and outer mode forcing. The magnitude of this peak for inner mode forcing is higher due to higher initial growth rates associated with this mode. As the level of forcing is increased, a second peak is formed on the distribution very close to the wall. This second peak occurs at the same location as the inflection point in the mean temperature profile, and is most likely due to a maximum in the unsteady normal velocity v occurring at this location. Also, the width of the disturbed region is much thicker for inner mode forcing due to the increase of the boundary layer thickness (figure 5). Similar trends occurred when the wall was cooled.

Figure 11 shows the normalized distribution of the fluctuating fundamental streamwise velocity for an excitation level of 0.6% and for both heating (a) and cooling (b) for outer mode forcing. The distribution contains two large peaks corresponding to the velocity gradient near

the wall and the inflection point in the outer region, as was explained by Mele et al. (1986). The outer peak is initially larger and has a broader disturbed region than the inner peak because the above mentioned forcing frequency prevails in the outer region. In both cases, as the downstream distance increases, the ratio between the inner and outer peaks is increased which is consistent with linear stability theory. According to the linear stability theory, as the downstream distance is increased smaller scales governed by the near wall region become more dominant. For a fixed downstream location, the ratio between the inner and outer amplitude maxima is larger for the cooling case. Another way to observe the difference between heating and cooling is to plot the integrated energy of the fluctuating velocity as a function of the downstream distance for heating and cooling, as in figure 12. As can be seen, both the magnitude and the growth rate for the cooling case are higher than the heating case. This behavior is related to the apparently small but non-negligible increase and decrease of the slope of the mean velocity profile at the wall when cooling and heating are applied. The same effects were reported by Amitay & Cohen (1996) when wall blowing or suction were applied, in which the ratio between the inner and outer amplitude maxima is larger when suction is applied.

In order to further understand the effect of forcing on the velocity field, the effect of the level of excitation was also addressed. In figure 13, two cases of inner mode forcing corresponding to (a) 0.6% and (b) 2% are presented for three downstream locations. δ_v was used to normalized the normal distance from the wall which is consistent with the stability theory. The inner peak is significantly higher, as expected, because the effect of inner mode forcing is most dominant in the inner region. For the low excitation level of 0.6%, the ratio between the inner to outer maxima increases with the downstream distance as was observed when outer mode forcing was applied in figure 11. This is once again consistent with linear stability theory. However, for the 2% forcing the trend is the opposite, with the ratio between the inner to outer maxima decreasing with downstream location. This is probably due to the fact that for high excitation levels non-linear mechanisms are introduced. At any given x/d, the boundary layer is much thicker and therefore large scales, corresponding to low frequencies, prevail throughout the flow field. As was mentioned before, when the forcing frequency is low,

the outer maxima dominates the fluctuating streamwise velocity distribution since it corresponds to the large scales.

CONCLUSIONS

In order to better understand the heat and momentum transfer associated with complex unsteady film-cooling problems, the plane, laminar, wall jet was investigated experimentally for the constant wall temperature boundary condition. As a simplification, the free-stream was quiescent and isothermal with respect to the jet exit temperature. With this configuration the velocity profile that flows tangentially onto the heat transfer surface contains two primary unstable shear layers which are associated with two different kinds of instability modes, the viscous mode and the inviscid mode. Controlled acoustic disturbances were introduced into the flow in an attempt to influence the wall heat transfer by taking advantage of these two instability modes.

Measured streamwise mean flow velocity profiles for the unforced case for small temperature differences (6-8 °C) were compared to the theoretical predictions. Although the temperature difference between the surface and the jet was small, heating or cooling of the plate changed the mean velocity profile predominately in the inner region. When cooling was applied, the inner velocity gradient was the highest and the maximum velocity was shifted closer to the surface, while heating the surface had the opposite effects. Previous theoretical models require that the thermal and hydrodynamic boundary layers originate at the same location for full similarity, however, as is shown in figure 1, an unheated starting length exists in the experimental apparatus. The solution of Mitachi & Ishiguro (1974), which accounts for the unheated starting length, was employed to compare the experimental results for the temperature field. It was found that using δ_t as the length scale collapsed the data for heating and cooling on a single theoretical solution.

Acoustic disturbances were introduced at excitation levels of 0.6%, 1% and 2% and at two forcing frequencies corresponding to the inner and outer modes associated with the wall jet. It was found that the high levels of forcing (1% and 2%) greatly altered the velocity and temperature profiles. The most significant effects occurred for inner mode forcing where the

total skin friction drag (integrated effect) was *reduced* by 45% and the total heat flux was *increased* by 20%. The skin friction and wall heat flux were less susceptible to outer mode excitation but the trends were not altered. The same results occurred for both heating and cooling of the surface.

In order to obtain phase information, the phase-locked fluctuating temperature as well as fluctuating streamwise component of velocity were measured. It was found that in the fluctuating temperature distribution, a large peak is located at $y/\delta_v = 0.5$. Outer mode forcing increases the width of the disturbed region when compared to inner mode forcing since it is associated with large wavelengths. As the level of forcing is increased, the ratio between the width of the disturbed region and the local boundary layer thickness is increased as well. A second peak is formed on the distribution very close to the wall ($y/\delta_v = 0.2$) for high levels of inner mode forcing. This peak occurs at the same location as the inflection point in the mean temperature profile and is associated with a maximum in the unsteady normal velocity v, which is presently being investigated. The fluctuating velocity distribution contains two peaks associated with the inner and outer regions of the wall jet where the ratio between the inner and outer peaks is greater when cooling is applied due to higher velocity gradients at the wall. From linear stability theory, the ratio between the inner and outer maxima increases as the downstream distance is increased, however, for high levels of forcing, the opposite trends were observed because non-linear effects cause a dramatic thickening of the boundary layer thus causing large scales associated with the outer region to become more significant.

Inner mode forcing had the most significant effects on the velocity and temperature fields. The initial spatial growth rates associated with the inner mode are greater than the outer mode growth rates. It is the outer row of counter-rotating vortices that receive most of the energy under high levels of forcing and therefore, *decrease* the velocity gradient near the wall. These large vortices enhance thermal mixing and produce the observed *increase* in the temperature gradient near the wall.

ACKNOWLEDGMENTS

REFERENCES

Amitay, M. and Cohen, J., 1993, "The Mean Flow of a Laminar Wall Jet Subjected to Blowing or Suction", *Phys. Fluids*, A 5, 2053.

Amitay, M. and Cohen, J., 1996, "Transition in a Two-Dimensional Plane Wall Jet Subjected to Blowing or Suction", submitted to *J.Fluid Mech.*

Bajura, R. A. and Catalano, M. R., 1975, "Transition in a Two-Dimensional Plane Wall Jet", *J. Fluid Mech.*, Vol. 70, part 4, 773-799.

Bajura, R. A. and Szewezyk, A., 1970, "Experimental Investigation of a Laminar Two-Dimensional Plane Wall Jet", *Phys. Fluids*, 13, 1653.

Chun, D. H. and Schwarz, W. H., 1967, "Stability of the Plane Incompressible Viscous Wall Jet Subjected to Small Disturbances", *Phys. Fluids*, 10, 5, 911-915.

Cohen J., Amitay M. and Bayly, B.J., 1992, "Laminar-Turbulent Transition of Wall Jet Flows Subjected to Blowing and Suction", *Phys. Fluids* A 4, 283.

Glauert, M.B., 1956, "The Wall Jet", *J.Fluid Mech*, 1, 625-643.

Katz, Y., Horev, E. and Wygnanski, I., 1992, "The Forced Turbulent Wall Jet", *J.Fluid Mech*, 242, 577-609.

Kline, S. J., and McClintock, F. A., 1953, "Describing Uncertainties in Single Sample Experiments," *Mechanical Engineering*, Vol. 75, Jan., pp. 3-8.

Mele, P., Morganti, M., Scibillia, M. F. and Lasek, A., 1986, "Behavior of Wall Jet in Laminar-to-Turbulent Transition", *AIAA Journal*, 24, 938-939.

Mitachi, K & Ishiguro, R., 1974, "Heat Transfer of Wall Jets", *Heat Transfer: Japanese Research*, 27-40.

Riley, N., 1958, "Effects of Compressibility on a Laminar Wall Jet", *Journal of Fluid Mechanics*, 4, 615-628.

Tetervin, N., 1948, "Laminar Flow of a Slightly Viscous Incompressible Fluid that Issues from a Slit and Passes over a Flat Plate", NACA TN, No. 1644.

Schwarz W. H. and Caswell B., 1961, "Some Heat Transfer Characteristic of the Two-Dimensional Laminar Incompressible Wall Jet", *Chemical Engineering Science*, 16, 338-351.

Schwarz W. H. and Caswell B., 1961, "Some Heat Transfer Characteristic of the Two-Dimensional Laminar Incompressible Wall Jet", *Chemical Engineering Science*, 16, 338-351.

Zhou, M. D., Heine, C. and Wygnanski, I., 1993, "The Forced Wall Jet in an External Stream", *AIAA* 93-3250.
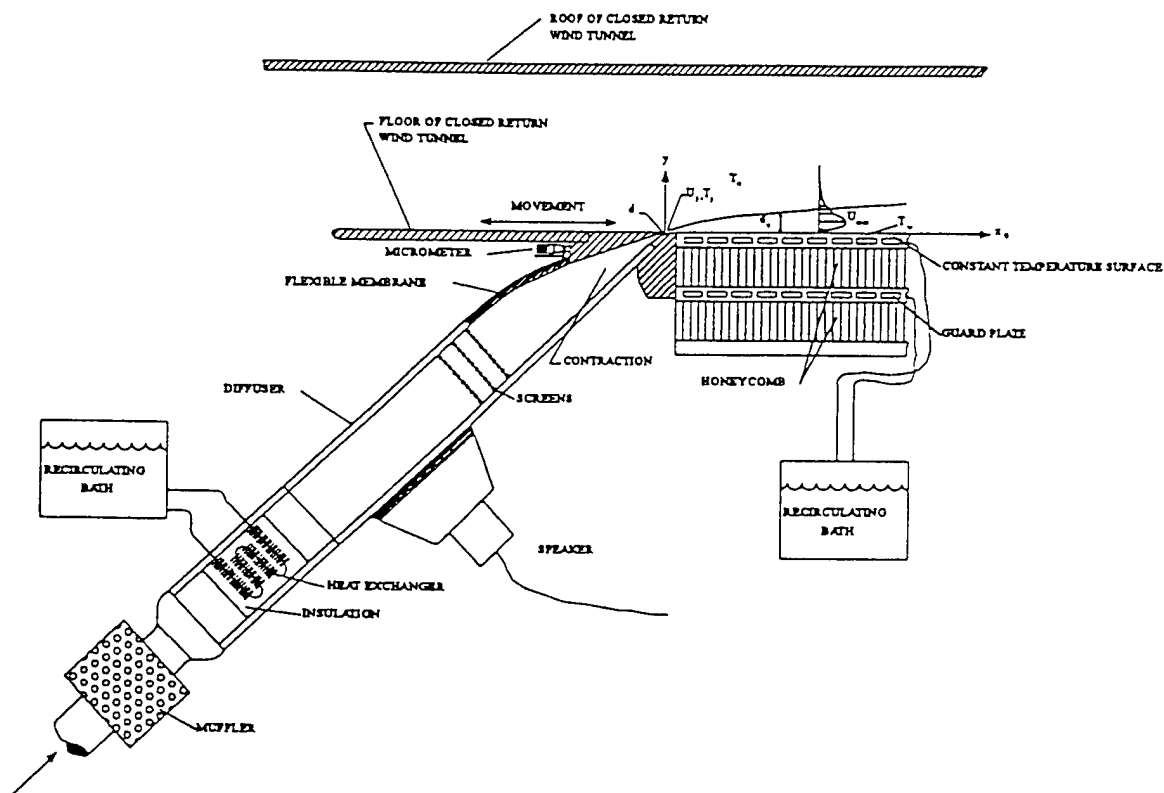
Figure 1: The experiment apparatus.
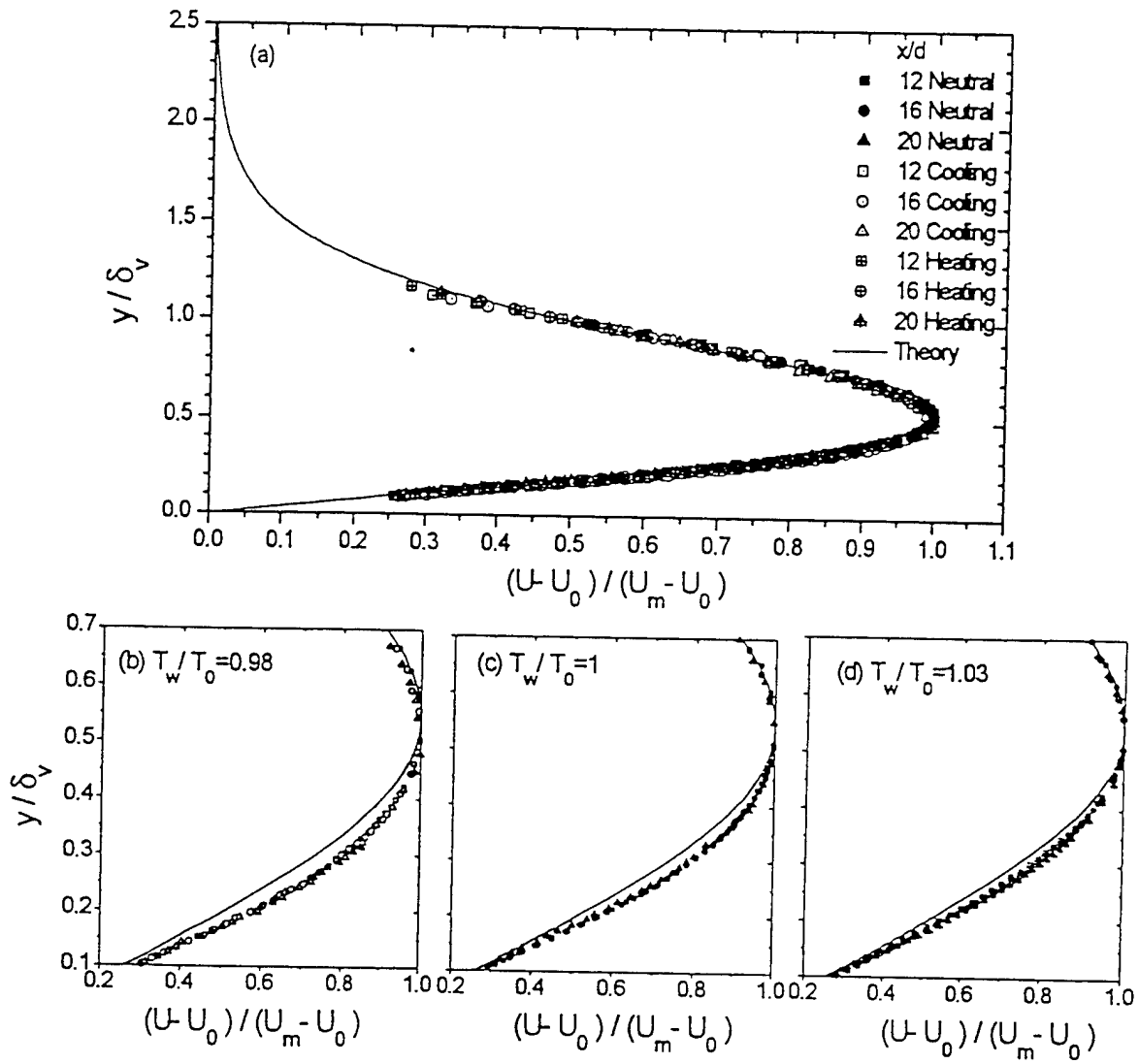
Figure 2: Comparison of normalized velocity profiles at three x/d locations and for T_w/T_o = 0.98, 0 and 1.03 (a) full profile, (b), (c) and (d) near-wall region.
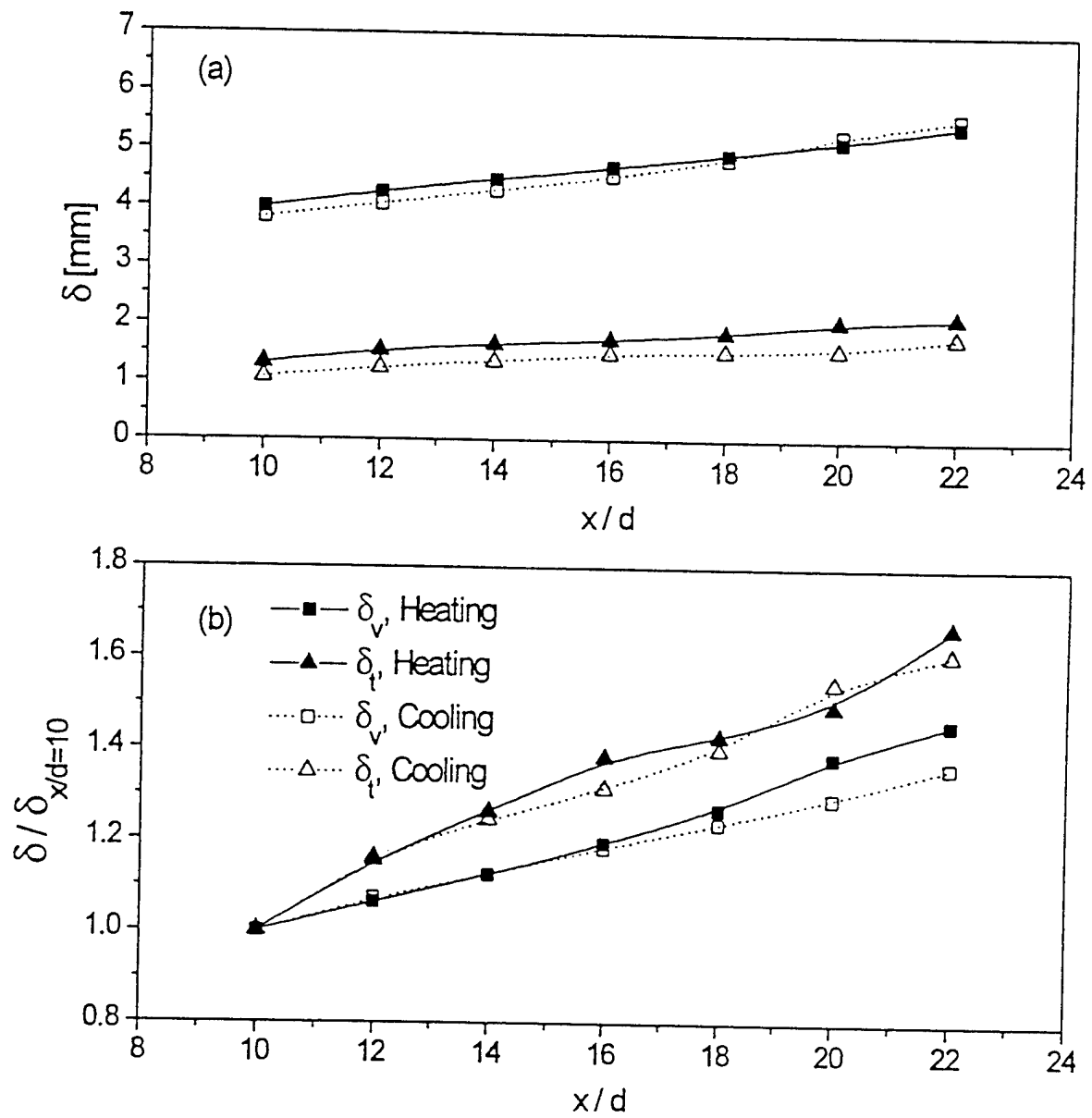
Figure 3: The downstream development of the different boundary layer thicknesses, (a) dimensional and (b) normalized.
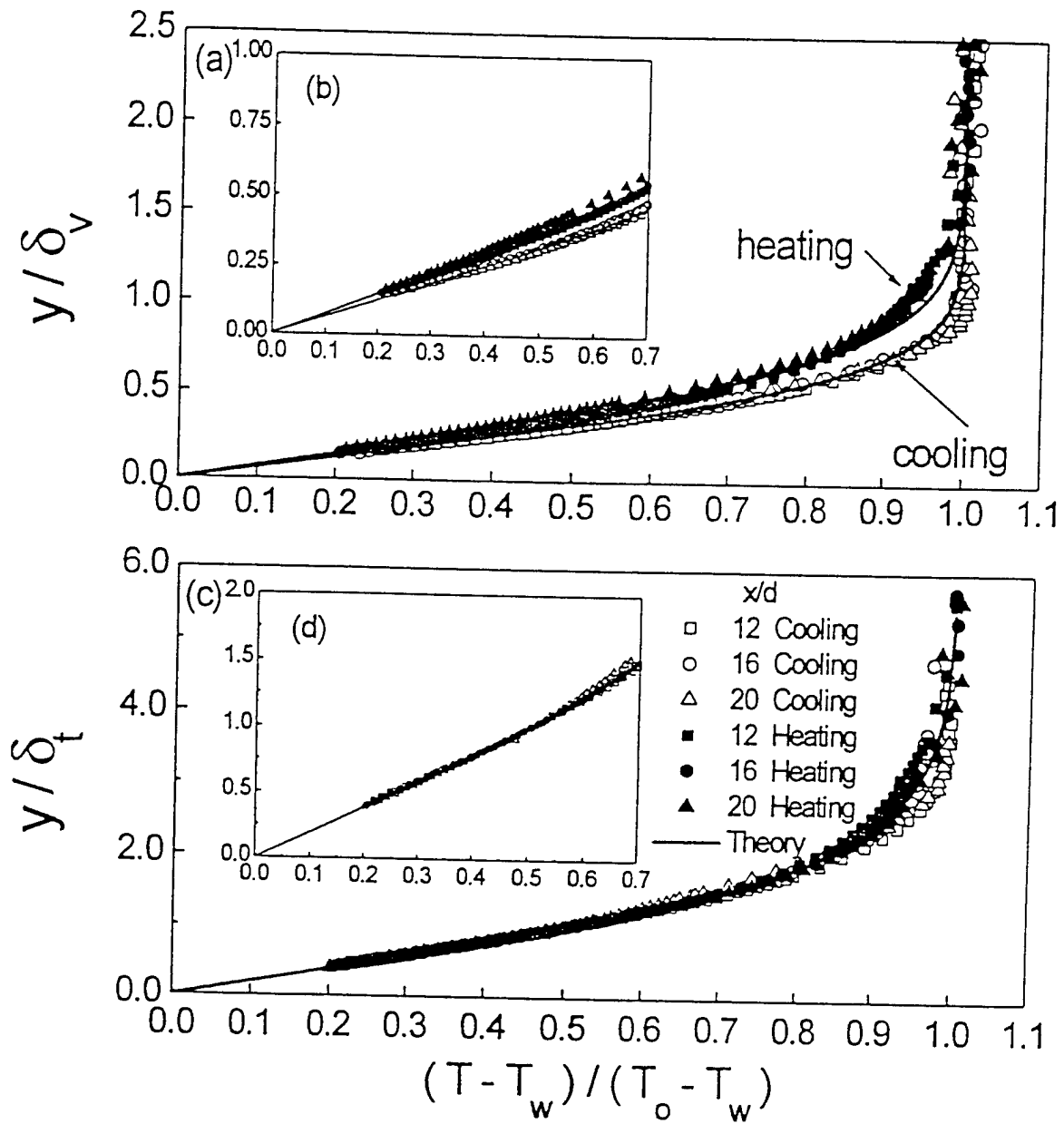
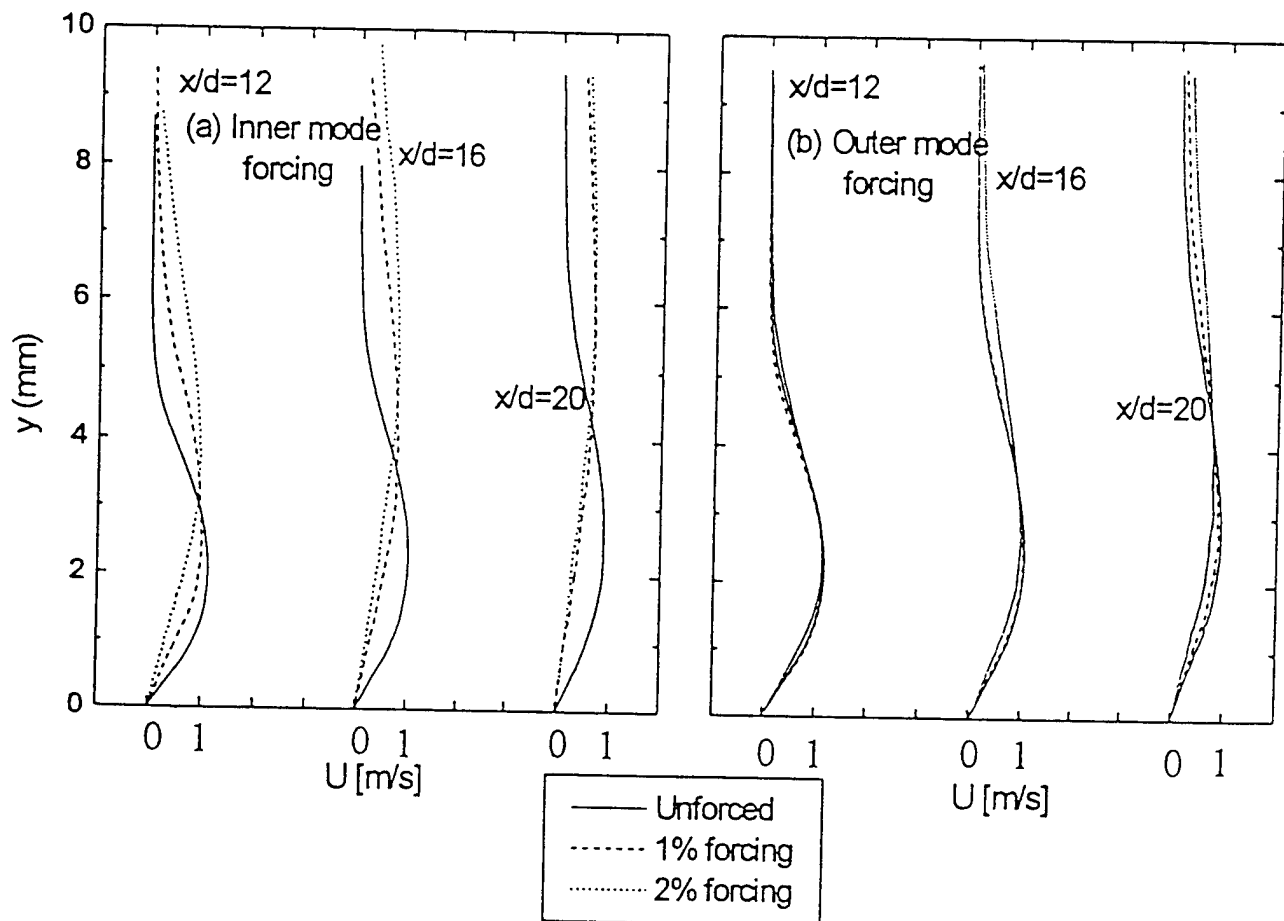Figure 4: Normalized temperature profiles (a) scaled by δ_v and (c) scaled by δ_t, where (b) and (d) are the near-wall regions.

Figure 5: Dimensional mean velocity profiles for various excitation levels and downstream locations (a) inner mode forcing and (b) outer mode forcing for $T_w/T_o = 1.03$.
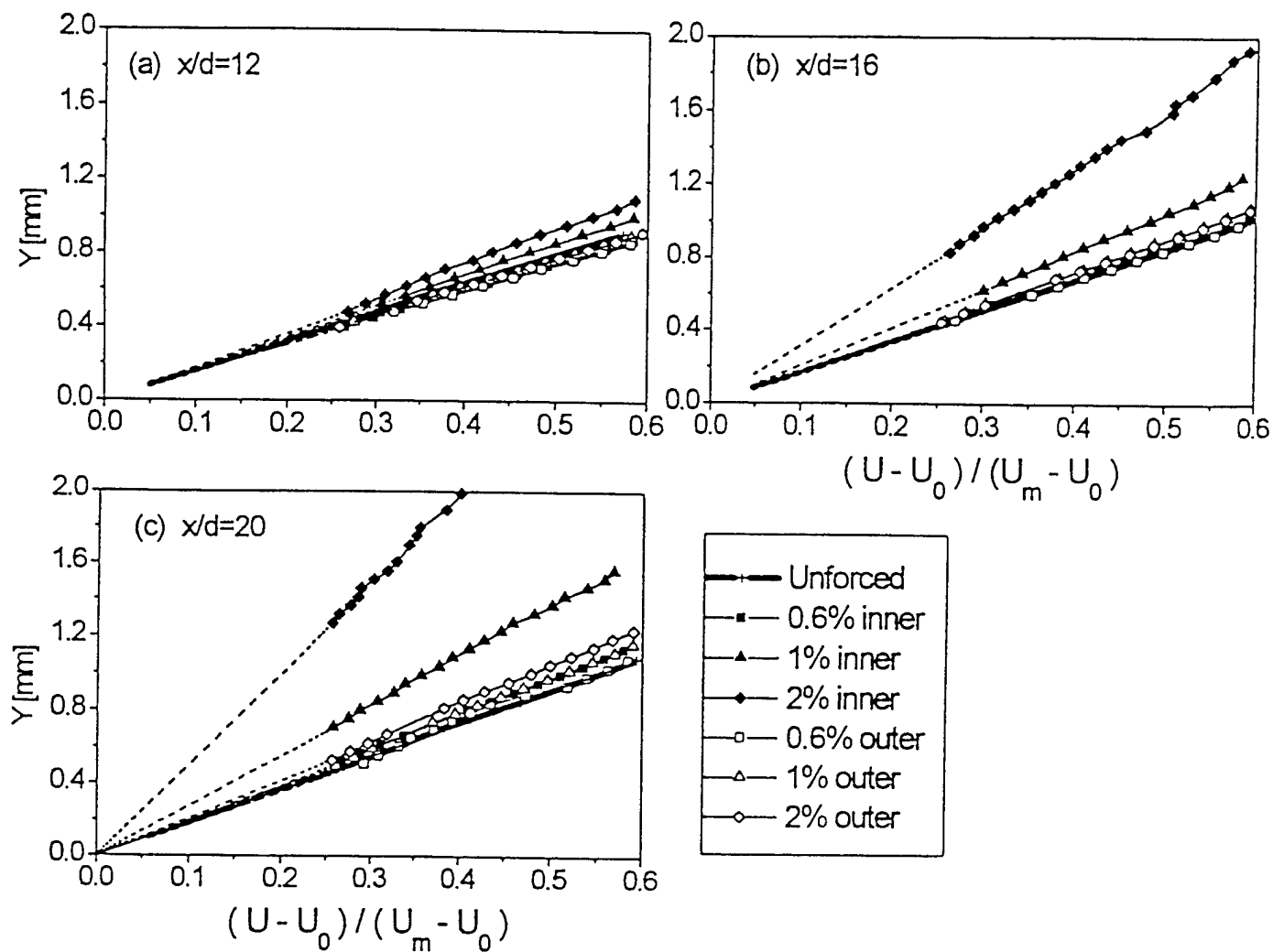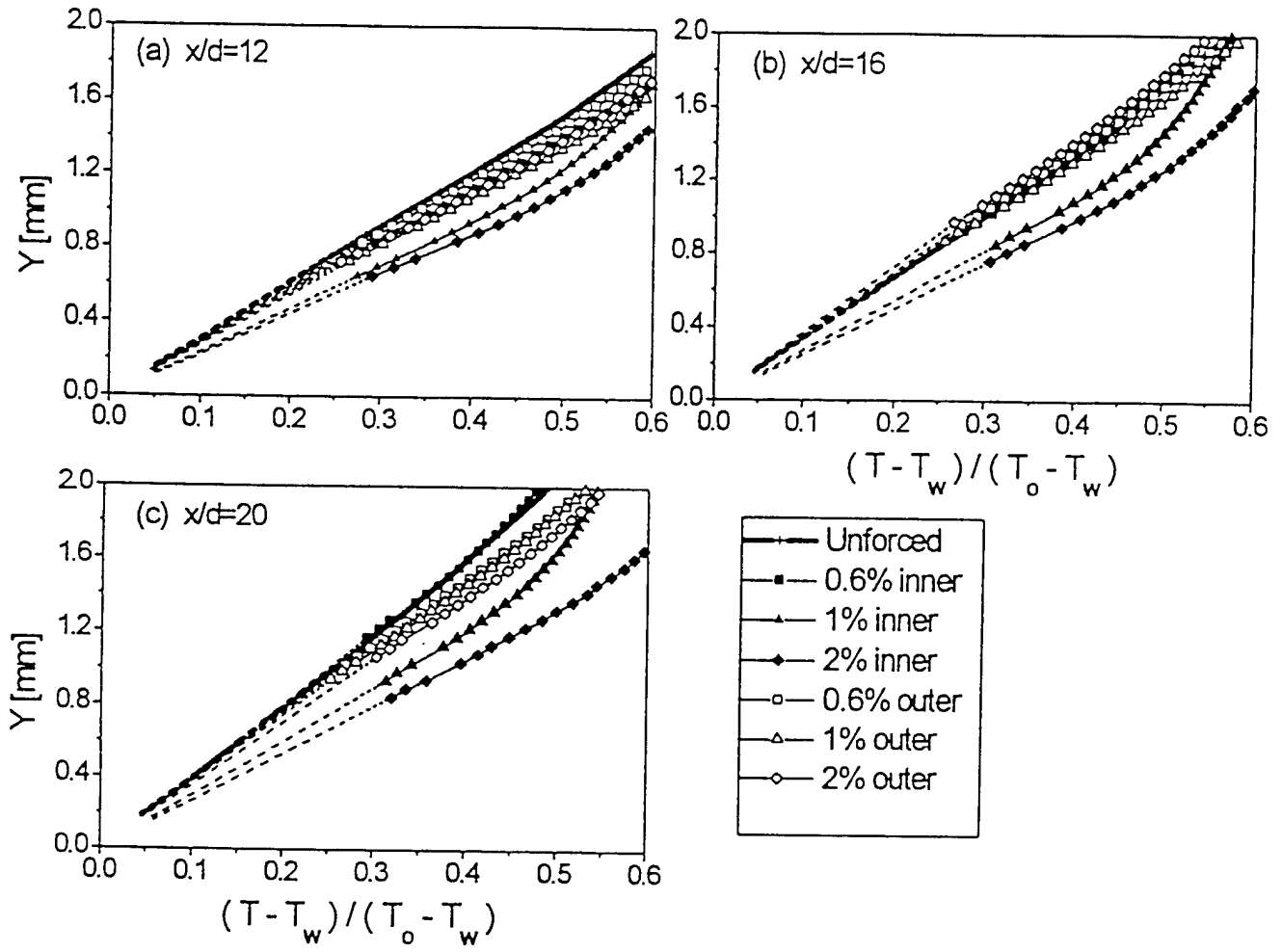
Figure 6: Near-wall velocity gradient comparison for different excitation levels and frequencies at x/d of (a) 12, (b) 16 and (c) 20 and for $T_w/T_o = 1.03$.
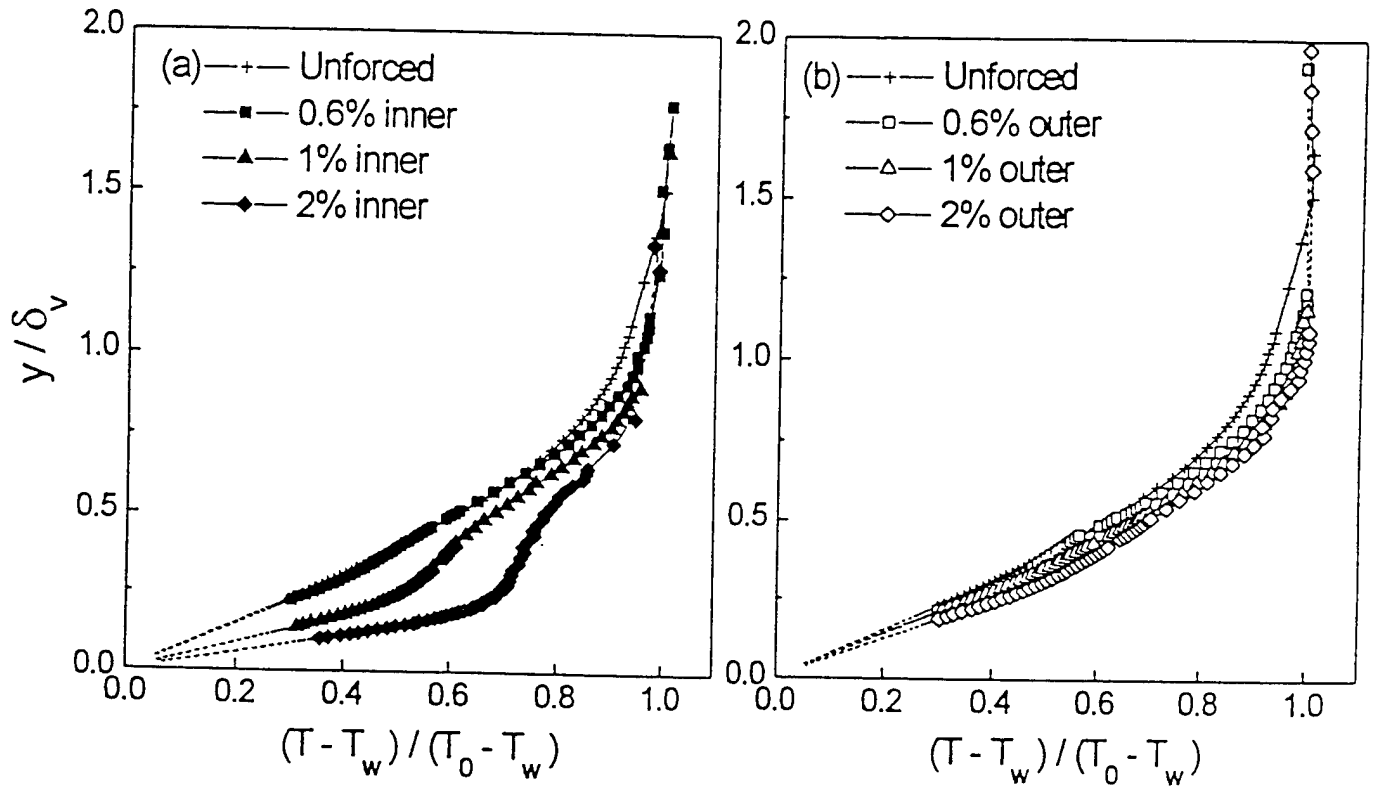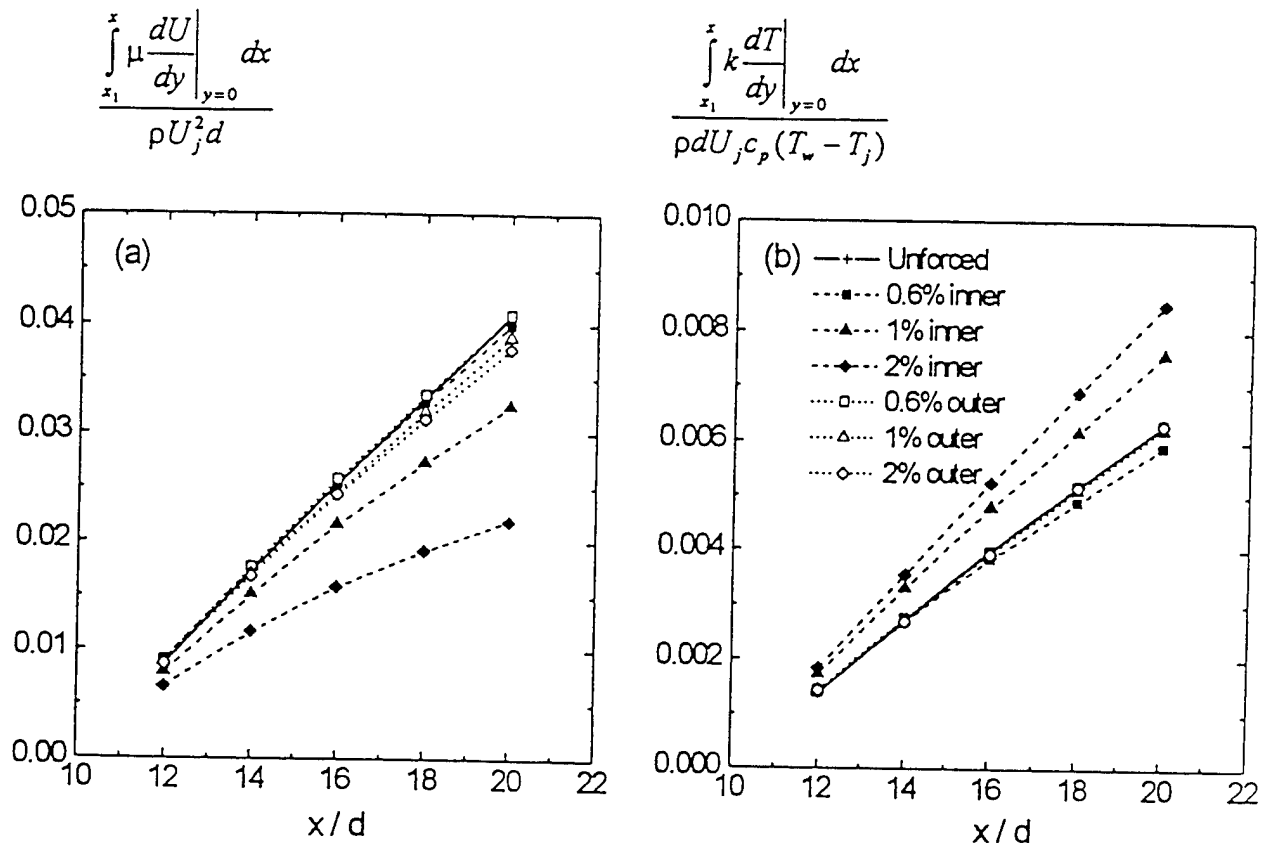
Figure 7: Comparison of normalized temperature profiles measured at $x/d = 20$ and for different excitation levels for (a) inner mode forcing and (b) outer mode forcing for $T_w/T_o = 1.03$.

Figure 8: Near-wall temperature gradient comparison for different excitation levels and frequencies at x/d of (a) 12, (b) 16 and (c) 20 and for $T_w/T_o = 1.03$.

$$\frac{\int_{x_1}^{x} \mu \frac{dU}{dy}\Big|_{y=0} dx}{\rho U_j^2 d}$$

$$\frac{\int_{x_1}^{x} k \frac{dT}{dy}\Big|_{y=0} dx}{\rho d U_j c_p (T_w - T_j)}$$

Figure 9: Integrated (a) skin friction drag and (b) total heat flux for various excitation levels and frequencies and for $T_w/T_o = 1.03$.
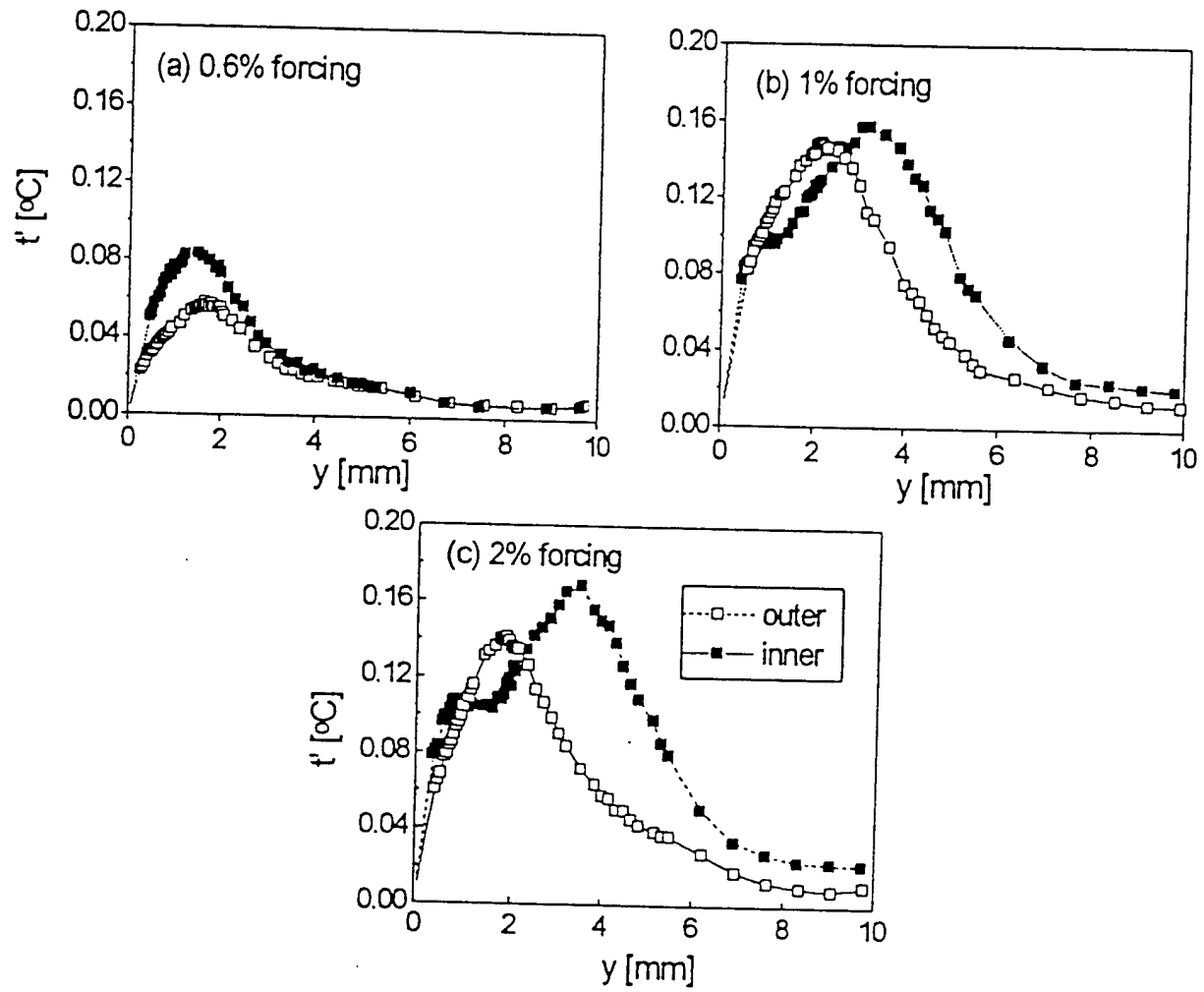
Figure 10: Fluctuating temperature distribution for inner and outer mode forcing for (a) 0.6%, (b) 1% and (c) 2% excitation levels ($x/d = 16$ and $T_w/T_o = 1.03$).
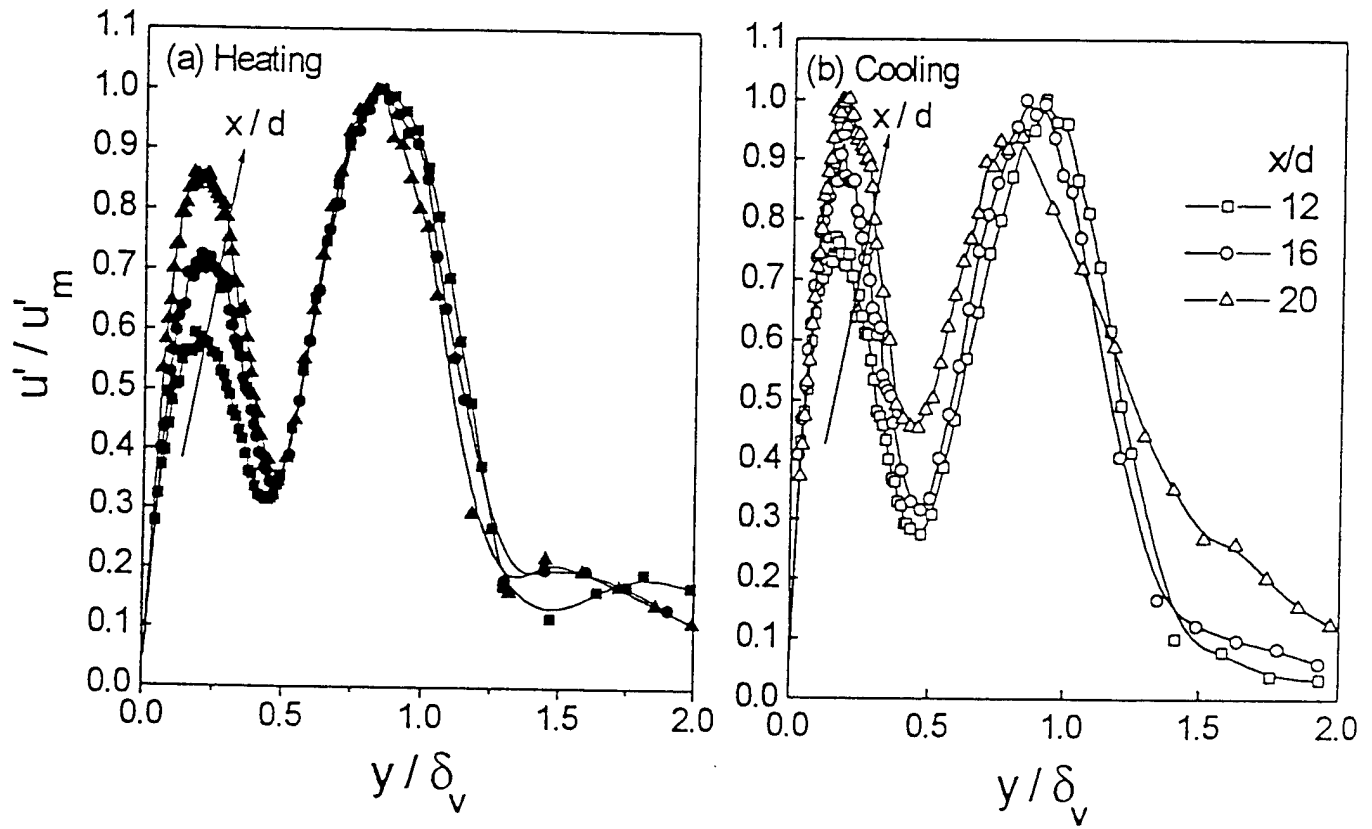
Figure 11: Normalized fluctuating streamwise velocity comparison at three x/d locations and for outer mode forcing at excitation level of 0.6%, (a) wall heating and (b) wall cooling.
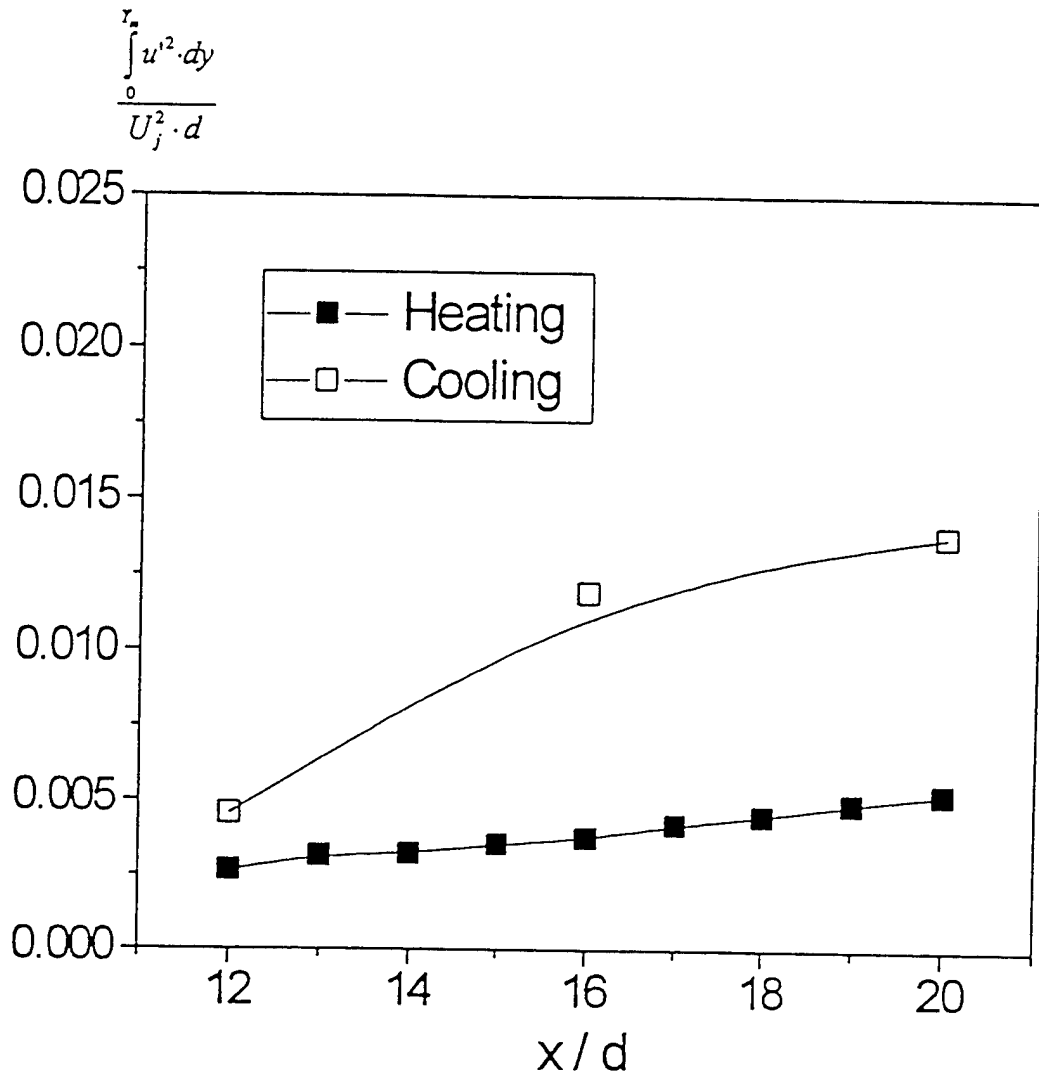
$$\frac{\int_0^{r_\infty} u'^2 \cdot dy}{U_j^2 \cdot d}$$

Figure 12: Downstream development of the integrated energy of the fluctuating for inner mode forcing and 0.6% excitation levels and $T_w/T_o = 1.03$, 0.98.
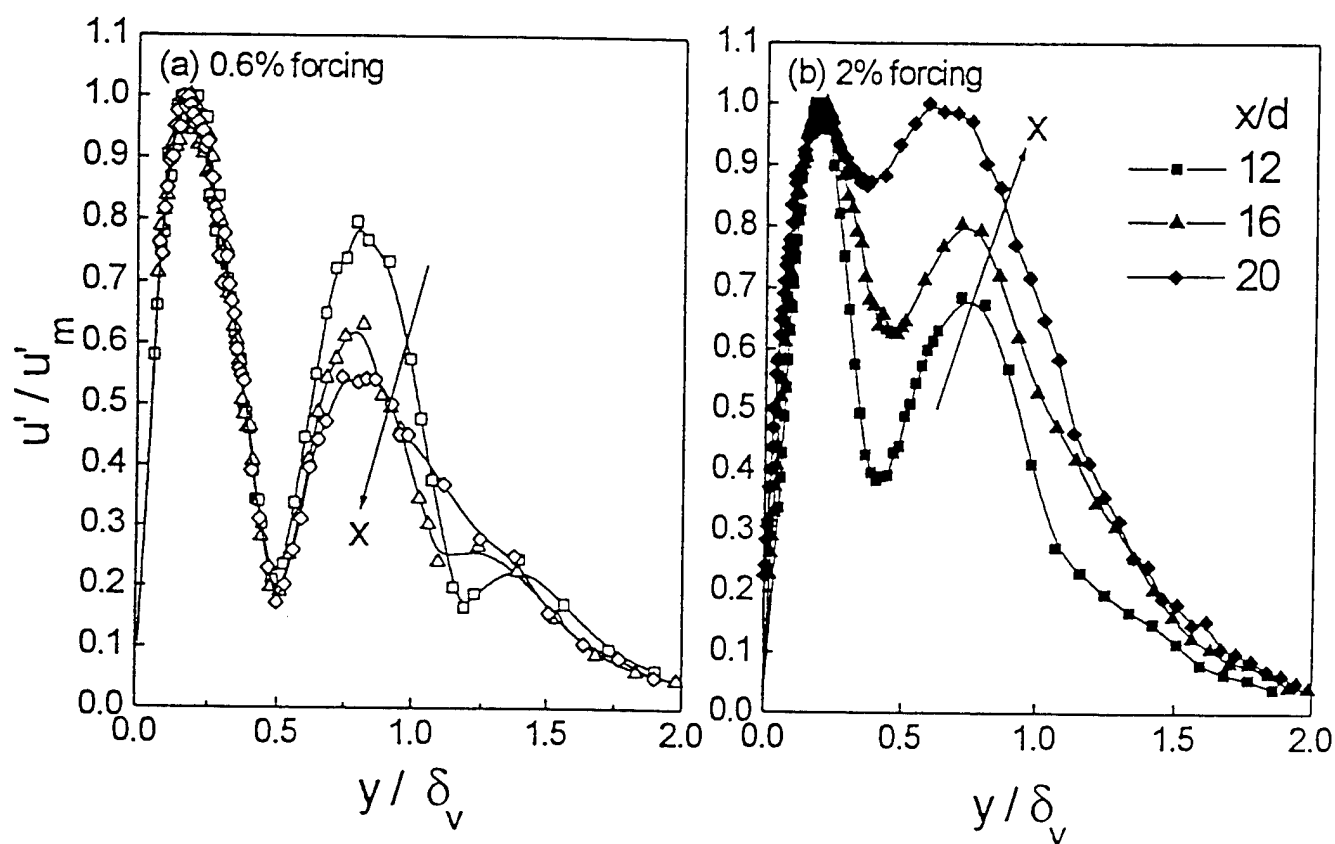
Figure 13: Normalized fluctuating streamwise velocity comparison at three x/d locations and for inner mode forcing, (a) 0.6% and (b) 2% excitation levels and $T_w/T_o = 1.03$.

Numerical Simulation of Wall Jets

H. F. Fasel * and S. Wernz

Department of Aerospace and Mechanical Engineering, University of Arizona, Tucson, Az, 85721, USA

Transitional wall jets are investigated using direct numerical simulations (DNS) based on the spatial model. When forcing the wall jet with large amplitudes, nonlinear mechanisms can cause the ejection of vortex pairs from the wall layer that then can repeatedly interact with the wall jet layer and thus strongly influence the breakdown process.

1. INTRODUCTION

Wall jets, or wall-jet-like flows, are of great technical relevance for numerous aerospace applications. Wall jets can be used as efficient mechanisms to control external and internal boundary layers. For external applications, wall jets can be advantageously employed for circulation control of airfoils and thus can serve as efficient lift-augmentation devices. Such lift augmentation can be accomplished by either tangentially blowing (through the wing section) along the upper surface of airplane wings or by employing multi-segment airfoils (for example, slotted flaps). Wall jets are also highly relevant for modern jet engines, where wall jets occur, for example, in the flow over a cowl of a fan-jet engine or, internally, in the flow over film-cooled turbine blades.

Although wall jet flows were widely investigated in the past, many of the basic phenomena occuring in both transitional and turbulent wall jets are far from being understood. In retrospect, this lack of understanding is due to the fact that the wall jet is a combination of a wall-bounded shear flow and a free shear layer. Therefore, from a stability point of view, the wall jet exhibits viscous boundary layer-type instabilities and free shear layer-type instabilities. However, this conceptual decomposition into these two stability modules, although methodically helpful, cannot provide for the total picture because both instabilities are present simultaneously and thus interact with each other. This is particularly true when amplitudes are sufficiently large, that nonlinear effects become important. In this case linear superposition of the various modes is no longer justified.

An important nonlinear phenomenon that occurs in transitional wall jets, namely vortex ejection from the wall layer, is discussed in the present paper. The investigations were carried out using direct numerical simulation (DNS). The goal of our research was to identify and understand the relevant nonlinear mechanisms during the transition process, in particular with regard to their possible relevance to fully turbulent wall jets.

2. COMPUTATIONAL MODEL

For our direct numerical simulations (DNS), a three-dimensional incompressible Navier-Stokes code, which was developed by Meitz [4] for boundary layer transition, was adapted to the wall jet geometry.

2.1. Governing Equations

The governing equations are a special form of the three-dimensional incompressible Navier-Stokes equations employed in a disturbance flow formulation. They consist of the incompressible vorticity transport equations (VTE),

$$\frac{\partial \omega_x}{\partial t} = -\frac{\partial A}{\partial y} + \frac{\partial C}{\partial z} + \frac{1}{Re}\nabla^2 \omega_x \ , \tag{1}$$

$$\frac{\partial \omega_y}{\partial t} = \frac{\partial A}{\partial x} - \frac{\partial B}{\partial z} + \frac{1}{Re}\nabla^2 \omega_y \ . \tag{2}$$

$$\frac{\partial \omega_z}{\partial t} = -\frac{\partial C}{\partial x} + \frac{\partial B}{\partial y} + \frac{1}{Re}\nabla^2 \omega_z \ , \tag{3}$$

and the velocity Poisson equations

$$\nabla^2 v = \frac{\partial \omega_x}{\partial z} - \frac{\partial \omega_z}{\partial x} \ , \tag{4}$$

$$\frac{\partial^2 w}{\partial x^2} + \frac{\partial^2 w}{\partial z^2} = \frac{\partial \omega_y}{\partial x} - \frac{\partial^2 v}{\partial y \partial z} \ , \tag{5}$$

$$\frac{\partial^2 u}{\partial x^2} + \frac{\partial^2 u}{\partial z^2} = -\frac{\partial \omega_y}{\partial z} - \frac{\partial^2 v}{\partial x \partial y} \ , \tag{6}$$

where the streamwise, wall-normal and spanwise vorticity components are defined as

$$\omega_x = \frac{\partial v}{\partial z} - \frac{\partial w}{\partial y}, \qquad \omega_y = \frac{\partial w}{\partial x} - \frac{\partial u}{\partial z}, \qquad \omega_z = \frac{\partial u}{\partial y} - \frac{\partial v}{\partial x}$$

and the variables A, B, C represent the nonlinear terms

$$A = v\omega_x - u\omega_y + v_B\omega_x - u_B\omega_y \ ,$$
$$B = w\omega_y - v\omega_z - v_B\omega_z - v\omega_{zB} \ ,$$
$$C = u\omega_z - w\omega_x + u_B\omega_z + u\omega_{zB} \ .$$

Quantities of the two-dimensional base flow are denoted by "B".

However, for the results presented in this paper, the code was used only in its two-dimensional version. In this case, only equations (3), (4) and (6) are solved, with $\omega_x = \omega_y = w \equiv 0$.

2.2. Computational Domain and Boundary Conditions

The governing equations (1)-(6) are solved inside the computational domain shown in figure 1. The boundary conditions include the no slip condition and zero normal velocity at the wall (except over the blowing and suction slot), decay of the disturbances at the free stream boundary, and a buffer domain near the outflow boundary which damps out

the disturbances using a technique similar to that proposed by Kloker et al. [3]. At the inflow, the flow properties of u, v, w and $\omega_x, \omega_y, \omega_z$ are prescribed.

The base flow for the computations is given by the two-dimensional similarity solution by Glauert [2] as shown in figure 1. There is no significant difference between disturbance flow solutions calculated using the similarity solution as a base flow and disturbance flow solutions calcuated using the numerical solution of the Navier-Stokes equations as a base flow. Using the similarity solution instead of the numerical steady state solution saves a considerable amount of computer time.

The disturbances are introduced into the flow by blowing and suction through a slot in the wall close to the inflow boundary. This technique is very efficient for producing pure vorticity disturbances while minimizing accoustic disturbances. The form of the disturbance velocity distribution over the blowing and suction slot is shown in figure 3a.
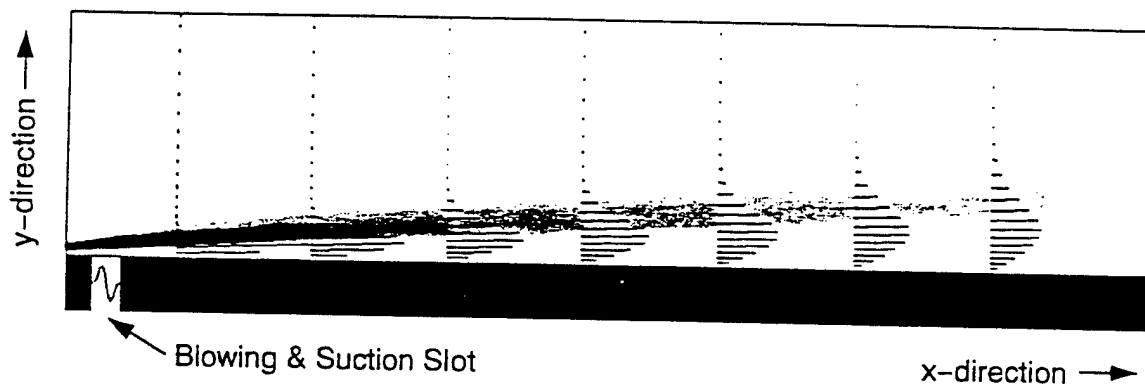

Figure 1. Computational domain with Glauert's similarity solution used as the base flow. The velocity field is represented by vectors, and the spanwise vorticity ω_z by greyscales. White indicates maximum clockwise rotation and black indicates maximum counterclockwise rotation. Disturbances are introduced by blowing and suction through a slot in the wall.

2.3. Numerical Method

The numerical scheme employed in the computations uses a fourth-order Runge-Kutta method for the time integration and fourth-order compact differences in the streamwise and wall-normal directions. For the wall-normal direction a variable step size is used such that the step size decreases near the wall. For three-dimensional calculations, the spanwise direction is treated pseudo-spectrally. At each Runge-Kutta substep, first, equations (1)-(3) are solved explicitly, then the Poisson equations (4)-(6) are solved by a direct method.

2.4. Code Validation

For code validation, results computed with the present code were compared with results obtained from other incompressible and compressible Navier-Stokes calculations. In all cases, very good agreement was found. Calculations with different step sizes were carried out in order to ensure that the spatial and temporal resolution was sufficient.
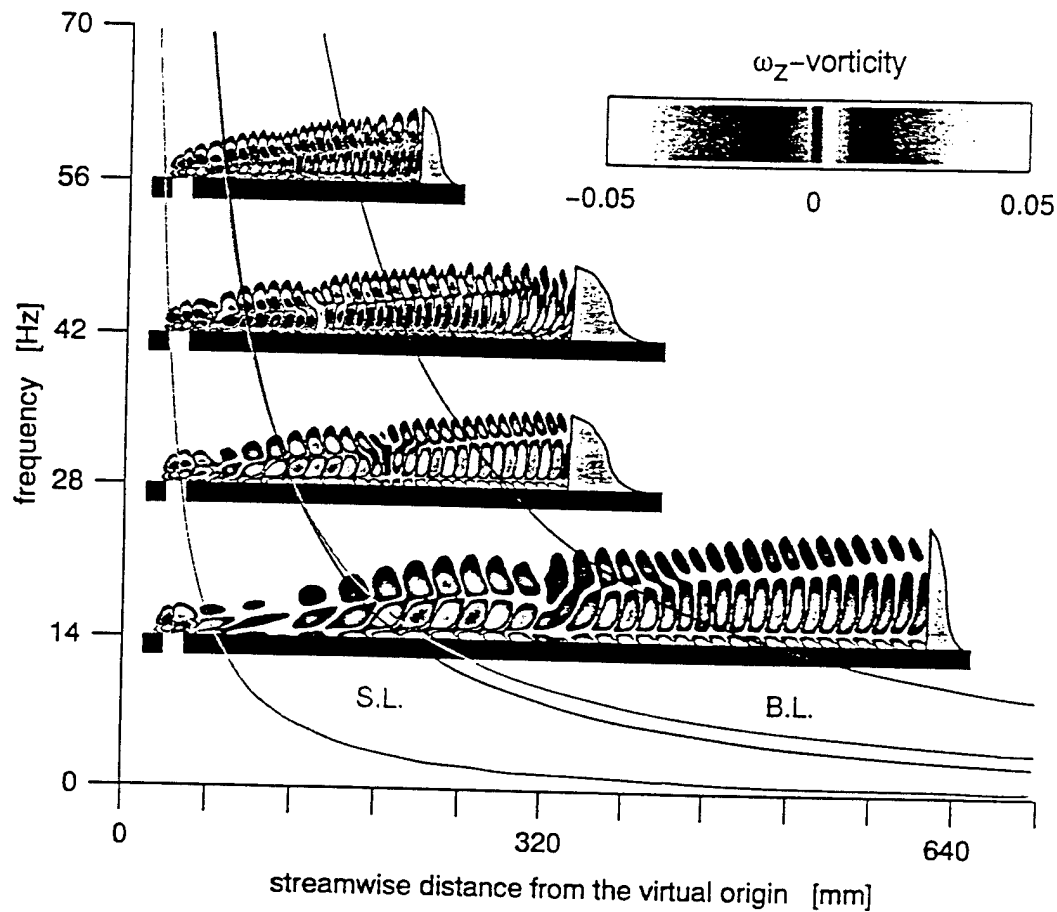
Figure 2. Results from numerical simulations for small disturbance amplitudes shown in the stability diagram of linear stability theory (neutral curves).

Results from calculations of small two-dimensional disturbances were also compared with linear stability theory, as shown in figure 2. The wall jet is forced by small amplitude blowing and suction of various frequencies at one streamwise location. The blowing and suction slot is located such that, according to linear stability theory, low frequencies are damped. Accordingly, the DNS results show that the low frequency disturbances decay first and then start to grow later downstream. For higher frequencies, the blowing and suction slot is in the unstable region of the shear layer mode, and the resulting disturbance waves begin to grow immediately. Since the wall jet is susceptible to two modes of instability (shear layer mode and boundary layer mode), the disturbances have a relatively large wavelength. These disturbances start to decay at the neutral curve of the shear layer mode but dominate up to the middle of the unstable region of the boundary layer mode. Then, the boundary layer mode, which has a shorter wavelength, reaches a large enough amplitude to dominate the disturbance flow, until it starts to decay at the neutral curve. In this region, an excellent agreement with linear stability theory is observed. Upstream, where a combination of both modes exists, a proper decomposition of the total disturbance flow into these modes would be required. As demonstrated by Amitay [1], this is possible, although quite involved.

2.5. Computational Parameters

For the results presented in this paper, the following parameters were used:

flux of exterior momentum flux:
$$F \equiv \int_0^\infty u_B \left[\int_y^\infty u_B^2 d\check{y} \right] dy$$
$$= 1.6875 \cdot 10^{-5} \, m^5/s^3$$

kinematic viscosity: $\quad \nu = 1.5 \cdot 10^{-5} \, m^2/s$

reference velocity: $\quad U_{ref} = 3 \, m/s$

reference length: $\quad L_{ref} = 3.2 \, mm$

distance of the inflow location from
the virtual origin of the wall jet: $\quad x_{in} = 16 \, mm$

forcing by blowing and suction
through a slot in the wall: $\quad v = A_{v_s}(x) \cdot F(t)$

3. RESULTS

When the wall jet is forced at small amplitudes (in the order of 0.1% of the local velocity maximum or less), a time periodic state is reached within twenty to thirty periods corresponding to the forcing frequency. During the startup of forcing the wall jet, after blowing and suction is switched on instantly at time $t = 0$ (figure 3b), the leading edge of the generated disturbance waves propagates downstream through the computational domain.

In contrast, when the wall jet is forced at larger amplitudes (in the order of 1% of the local velocity maximum), the flowfield undergoes a much longer transient stage, and a very complex flow pattern is observed. This phenomenon might be of great technical importance and was therefore investigated in greater detail. Here, results for two types of forcing are discussed, first for the startup with periodic large amplitude forcing, as shown in figure 3b, and second for forcing with a single pulse disturbance, as shown in figure 3c.
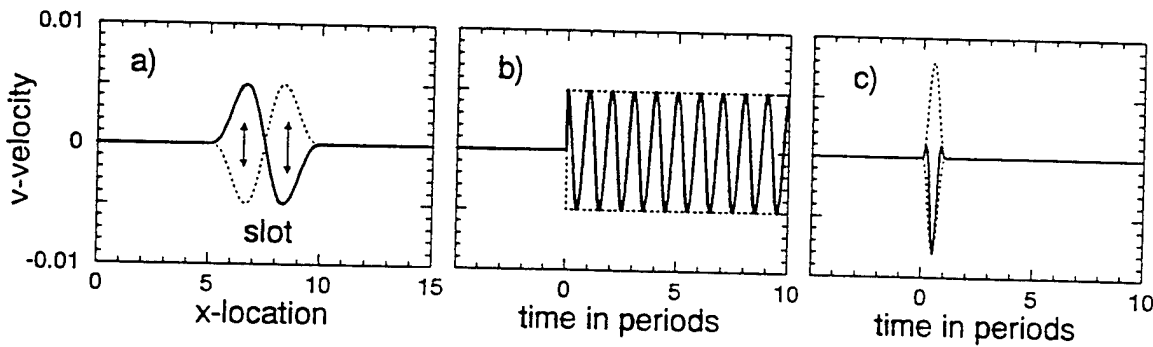

Figure 3. Disturbance generation by blowing and suction in a slot. a) Variation of the wall-normal velocity over the blowing and suction slot $A_{v_s}(x)$, b) time-function $F(t)$ for the startup with periodic disturbances, c) time-function $F(t)$ for a single pulse disturbance.

3.1. Case 1: Startup with Periodic Forcing

In this simulation, the wall jet is periodically forced with a frequency $f = 56Hz$ and an amplitude $A = 0.005 \cdot U_{ref}$ (considered a "large" amplitude). As shown in figure 4a, at an early time during startup, the leading edge of the disturbance wave propagates downstream, as in the case with small amplitude forcing. For the large amplitude forcing, however, merging of subsequent vorticity concentrations ("vortices") within the travelling wave occurs. Merging occurs in such a way that "vortices" in the outer layer of the wall jet predominantly have a counterclockwise rotation, while in the wall-near region they mainly have a clockwise rotation. Repeated vortex merging generates one pair of "vortices" with particularly high vorticity, as shown in figure 4b. The outer "vortex" of this pair (with conterclockwise rotation) has moved further away from the wall where the base flow velocity is low. It has accumulated enough strength to lift the companion "vortex" (with clockwise rotation) away from the inner layer of the wall jet. As shown in figure 4c, the two vortices which form the vortex pair then propel themselves further away from the wall by mutual induction and form a mushroom shaped vortex pair.

The sequence of vortex mergings in the wall jet during startup can be observed nicely in the space-time diagram of the wall vorticity, as shown in figure 5. In the diagram, merging of vortices is indicated by the merging of characteristic lines. When vortex ejection occurs, the "vortices" have undergone a series of mergings (four) while slowing down considerably, as indicated by the steepening slopes of the characteristic lines.

The observed vortex mergings, as discussed above, can also be looked at from a different point of view. The "vortices" are a consequence of the travelling disturbance waves in the wall jet. For large enough disturbance amplitudes, subharmonic disturbances (with half the frequency of the fundamental) can be generated by a secondary instability process. For a periodic disturbance flow, the development of subharmonic disturbance waves can be analyzed easily by performing a Fourier decomposition in time. We found that, for blowing and suction amplitudes larger than $A = 0.003 \cdot U_{ref}$ and a fundamental frequency of $f = 56Hz$, subharmonic disturbances introduced into the flow are greatly amplified. This confirms that, similar to a free shear layer, the wall jet is susceptible to two-dimensional subharmonic resonances. In the transient case here, a simple Fourier decomposition is not meaningful. It can be conjectured, however, that by introducing a whole spectrum of small subharmonic disturbances through the sudden startup a subharmonic cascade is initiated that eventually leads to the ejection of a vortex pair. In fact, subharmonic resonances during startup can be avoided alltogether if the blowing and suction amplitude is ramped up very carefully over a long time duration.

3.2. Case 2: Forcing with a Single Pulse

For the second calculation case discussed here, the wall jet was disturbed by a single pulse (figure 3) with a time duration of one period of the periodic disturbance in the previous case. Thus, the frequency spectrum for this disturbance input has a broad frequency spectrum with a maximum at $f = 56Hz$. This pulse disturbance generates a wave packet that travels downstream, as shown in figure 6a. At the time instant shown, it is obvious that there are fewer "vortices" in the wall jet, compared to the previous case. From the space-time diagram in figure 7, it is apparent that merging of "vortices" occurs much earlier (further upstream) than in the previous case. This can be explained by the fact that pulse disturbances generate subharmonic disturbance waves with a much
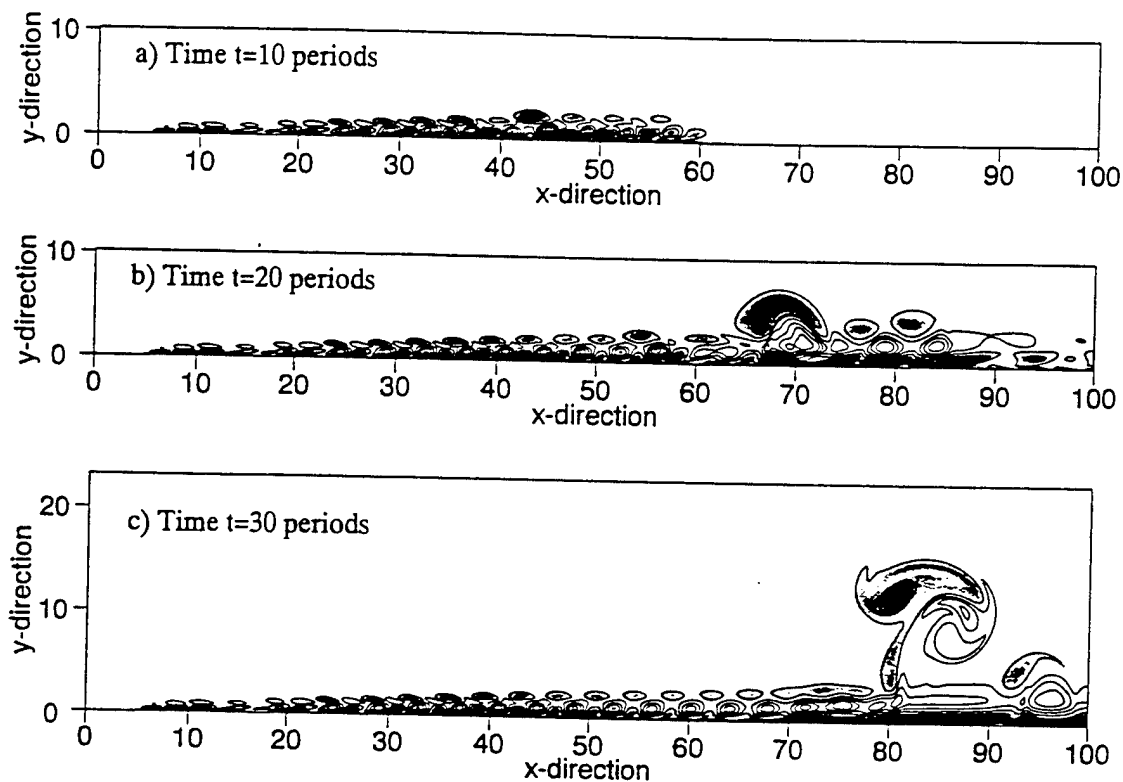
Figure 4. Generation of a mushroom shaped pair of vortices during startup of disturbing the wall jet by periodic blowing and suction. Shown are contours of instantaneous spanwise vorticity (in the x-y plane) at different time instants. The greyscale indicates clockwise rotation (light) and counterclockwise rotation (dark).
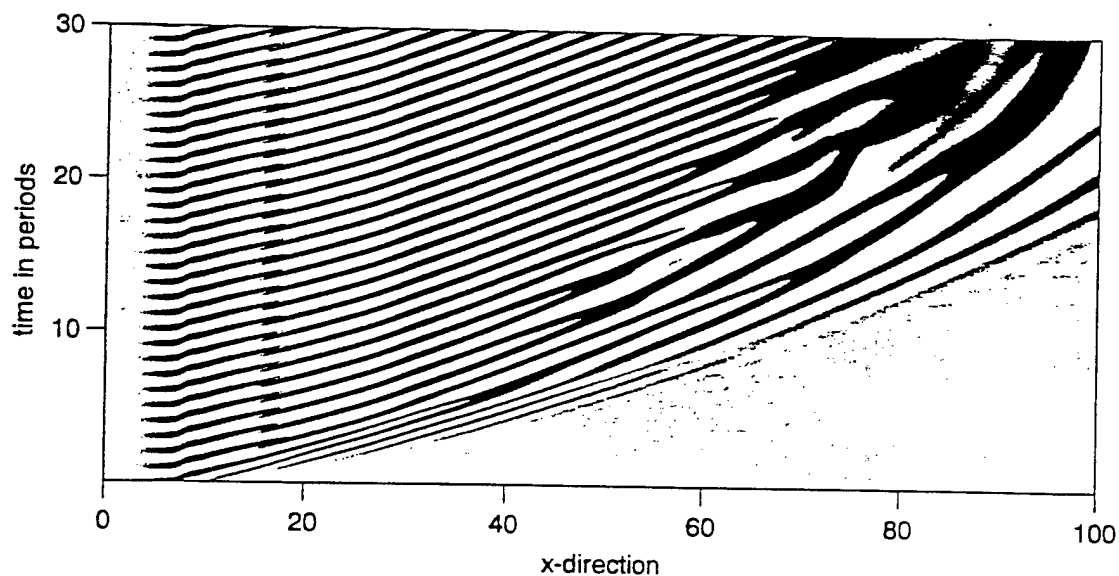

Figure 5. Space-time diagram of the wall vorticity during startup of disturbing the wall jet by periodic blowing and suction.
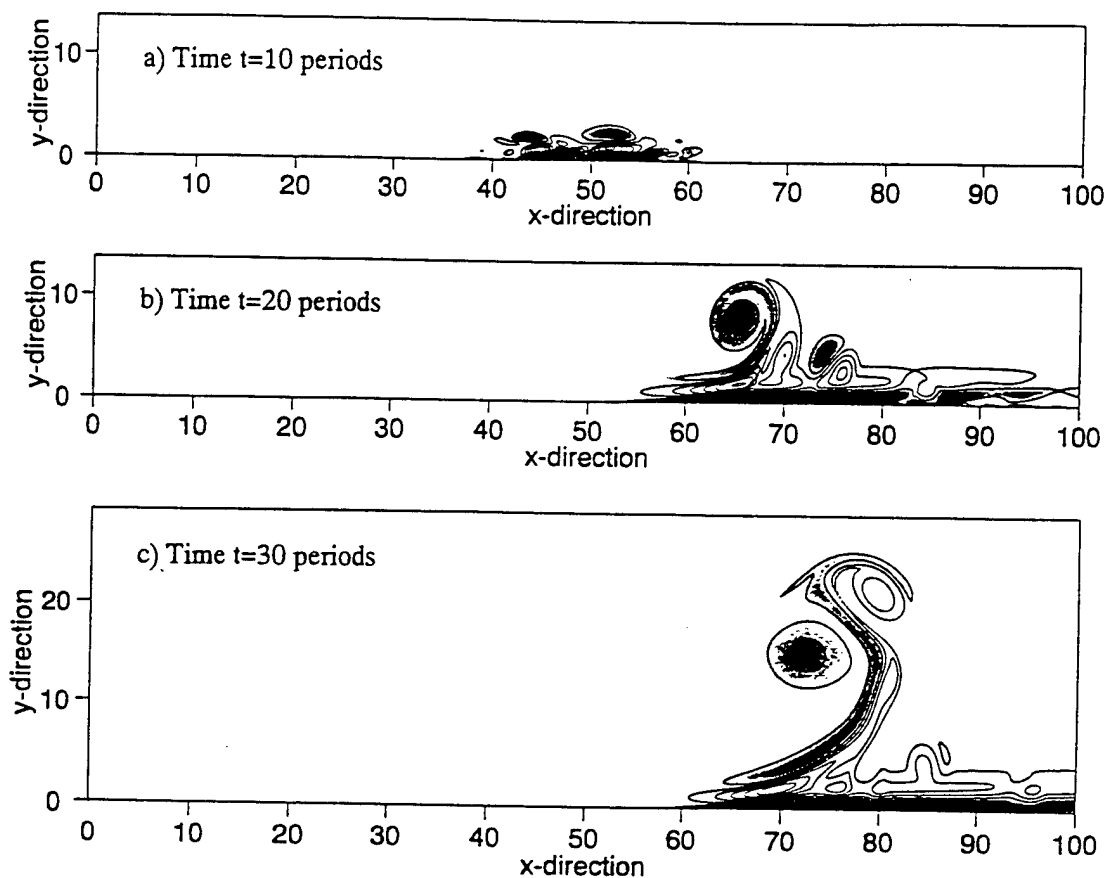
Figure 6. Generation of a mushroom shaped pair of vortices during startup of disturbing the wall jet by a single pulse. Shown are contours of instantaneous spanwise vorticity (in the x-y plane) at different time instants. The greyscale indicates clockwise rotation (light) and counterclockwise rotation (dark).
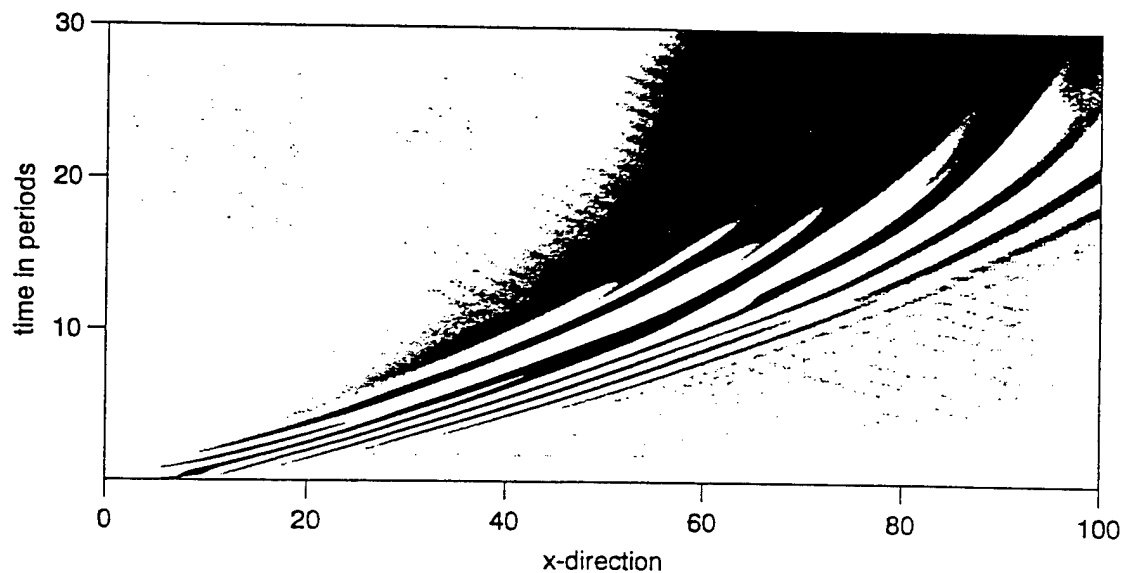

Figure 7. Space-time diagram of the wall vorticity for disturbing the wall jet with a single pulse.

higher initial amplitude than the startup of periodic forcing does. Although only two distinct events of merging can be observed in the space-time diagram. there is a clear trend towards approximately the same wavelength as in the previous case with periodic forcing.

As before, a mushroom shaped pair of strong vortices emerges which lifts up from the wall (figure 6b) and penetrates the ambient fluid in a curved trajectory (figure 6c). This is due to the fact that the counterclockwise-rotating vortex is considerably stronger than the clockwise-rotating vortex. Also. downstream of the vortex pair. the vorticity mean flow distortion of the disturbance flow is approximately equal to the vorticity of the base flow. with an opposite sign. For the total flow, this implies that the wall jet has started to detatch from the wall.

3.3. Long Term Behavior

For the first calculation case. we continued the two-dimensional numerical simulation until the time periodic state was reached. The mushroom shaped vortex pair shown in figure 4 propels itself upstream in a curved trajectory and gets sucked back into the wall jet. Then, as a consequence, more mushroom shaped vortices are generated. At one time instant, the wall jet even starts to detach itself from the wall. as shown in figure S. However, this process is interrupted by newly generated mushroom pairs. Eventually one weak clockwise-rotating vortex remains almost stationary above the wall jet for a long time duration, until it gradually decays by entraining negative vorticity from the wall jet. This is in contrast to the second case shown in figure 9, where the vortex remained detached from the wall for as long as the simulation was continued.

When the simulations for the case with periodic forcing was repeated with a slightly changed initial condition, an essentially similar sequence of events could be observed. However, the position of the ejected vortices and the time when ejections occur could be very different.

This suggests that the startup process with periodic forcing (as well as the response to a pulse disturbance) is of a chaotic nature, with an extreme sensitivity to initial conditions.
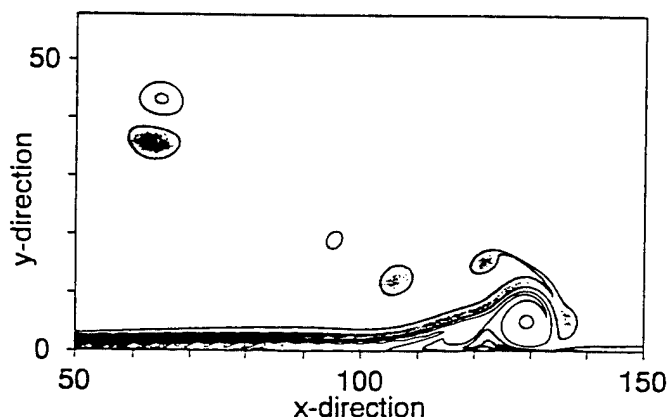

Figure S. Total flow for periodic disturbances after 60 periods corresponding to the frequency $f = 56 Hz$.
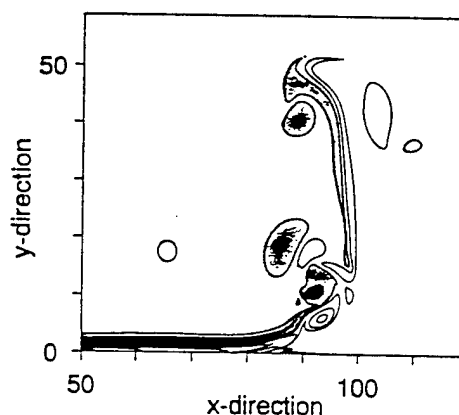
Figure 9. Total flow for a single pulse disturbance after 60 periods corresponding to the frequency $f = 56 Hz$.

4. CONCLUSION

Our numerical simulations have shown that nonlinear mechanisms in a transitional wall jet can give rise to surprising phenomena. During the startup of periodic forcing. mushroom shaped vortex pairs may be generated. These vortices are ejected from the wall layer, propagate upstream, and can interact repeatedly with the wall jet. These vortices are indeed physical, as similar vortex phenomena have also been observed in the experiments by Amitay [1] and Shih et al. [6]. However, in their experiments, breakdown to turbulence takes place very rapidly after the first vortex pair is ejected.

Since this is an intrinsically three-dimensional process, the two-dimensional simulations discussed in the present paper cannot correctly predict the actual breakdown to turbulence.

Therefore, this research is currently being extended to fully three-dimensional numerical simulations. This will allow the capture of the relevant physics after vortex ejection and the associated breakdown to turbulence.

Mushroom shaped vortices have also been observed in experiments involving turbulent wall jets used for turbine blade cooling [5]. Therefore, we also intend to study this phenomenon for turbulent wall jets using large eddy simulations (LES) in the near future.

REFERENCES

1. M. Amitay, "Theoretical and Experimental Investigations of a Laminar Two-Dimensional Wall-jet", Research Thesis, *Israel Institute of Technology*, 1994.
2. M.B. Glauert, "The wall jet", *J. Fluid Mech.* Vol.1, pp. 625-643, 1956.
3. M. Kloker, U. Konzelmann and H. Fasel, "Outflow boundary conditions for spatial Navier-Stokes simulations of transitional boundary layers", *AIAA Journal*, Vol.31. No.4, pp.620-628. 1993.
4. H. Meitz and H. Fasel, "Navier-Stokes Simulations of the Effect of Suction Holes on a Flat Plate Boundary Layer", *AGARD Conference Proceedings*, AGARD-CP-551, 1994.
5. R. Rivir, *Private Communication*, 1995.
6. C. Shih and S. Gogineni, "Experimental Study of Perturbed Laminar Wall Jet", *AIAA Journal*, Vol.33, No.3, 1995.